Dispersion Stability And The Surface Charge Mechanism Of Rutile Titanium Dioxide Dispersions In Low Dielectric Medium.

Order Number 9325938

Dispersion stability and the surface charge mechanism of rutile titanium dioxide dispersions in low dielectric medium

Fluck, David James, Ph.D.

Lehigh University, 1993

U·M·I
300 N. Zeeb Rd.
Ann Arbor, MI 48106

Dispersion Stability and The Surface Charge Mechanism of Rutile Titanium Dioxide Dispersions in Low Dielectric Medium

by

David James Fluck

A Dissertation

Presented to the Graduate Committee

of Lehigh University

in Candidacy for the Degree of

Doctor of Philosophy

in

Chemistry

Lehigh University

1993

CERTIFICATE OF APPROVAL

Approved and recommended for acceptance as a dissertation in partial fulfillment of the requirements for the degree of Doctor of Philosophy.

21 May 1993
Date

John W. Larsen
Dr. John W. Larsen, Professor in Charge

Special Committee Directing
the Doctoral Work of
David J. Fluck

John W. Larsen
Dr. John W. Larsen, Chairman

Daniel Zeroka
Dr. Daniel Zeroka

James E. Sturm
Dr. James E. Sturm

Thomas B. Lloyd
Dr. Thomas B. Lloyd

Dr. Daniel Ou-Yang

This work was carried out under the guidance of Dr. Frederick M. Fowkes, who died on 18 October 1990.

DEDICATION

To my family through which all things are possible.

ACKNOWLEDGEMENTS

I would like to thank my dissertation committee for their effort and time. I am especially grateful to Dr. John Larsen for assuming responsibility as committee chairman when my original advisor (Dr. Frederick Fowkes) died. Drs. James Sturm and Daniel Zeroka have helped me along the way in my course work as well as with my dissertation. Dr. Thomas Lloyd has been especially helpful in my research as well as doing the "leg work" to facilitate my dissertation and defense while I was working at Cabot Corporation (Cab-O-Sil Division) in Tuscola, Illinois.

The important role Dr. Fowkes played in my research and education should not go unmentioned. He showed me how to apply colloidal principles to "real life" problems while letting me work independently.

I am deeply indebted to my family whose help and encouragement made my education possible. My parents imparted a strong work ethic in me, that I cherish greatly. My mother and brother were very influential in my quest to further my education. I would also like to thank my sister Debbie for her support.

I learned a great deal of electrokinetic techniques from Dr. Wen Chen. We had many discussions on nonaqueous charging mechanisms. His emphasis on the desorption portion of the Fowkes acid-base mechanism was found to very important. My discussions on adsorption and calorimetry with Dr. Yan Huang were greatly appreciated. I would like to thank Dr. Stephen Horvath for SEM analysis and Dr. David Dwight and Mary Jo Kulp for ESCA analysis.

I would also like to thank all the graduate students, postdoctors, and faculty members at Lehigh University who helped me along the way, especially Dr. David Cole for assistance with flow calorimetry. I would finally like to thank Dr. Michael Lucarelli for proof reading and Georgette van Buitenen for editing and typing the dissertation. Both are with Cabot Corporation at Tuscola.

TABLE OF CONTENTS

LIST OF FIGURES

LIST OF TABLES

ABSTRACT

Two series of dispersions of each of three types of titanium dioxide in cyclohexane have been prepared with one each of two charging agents. The three rutile pigments vary in acidity and basicity. One of the charging agents is basic whereas the other is amphoteric. The basic agent has an anchoring group that strongly adsorbs to the acidic sites on the rutile pigments, forming a monolayer that is partially responsible for its maximum stability ratio. This maximum stability ratio is attributed to the large negative zeta potential and the presence of the steric barrier formed from the charging agent. The amphoteric agent, by contrast, yields a low, maximum positive zeta potential that occurs at a concentration far exceeding the region of the maximum stability ratio. Further, the stability ratio of the amphoteric agent is low compared to the basic agent. The positive zeta potential is a result of the charging agent interacting through self association with previously adsorbed charging agent on the TiO_2 surface.

A mathematical model based on the Fowkes acid-base mechanism was developed to explain the zeta potential-charging agent concentration profile in these low dielectric medium dispersions. The model can semi-quantitatively explain the zeta potential maximum encountered in the profile by taking into account the significant decrease in Debye length, while the surface charge remains at a plateau.

CHAPTER I

INTRODUCTION TO DISPERSION STABILITY AND ACID-BASE INTERACTIONS IN LOW DIELECTRIC CONSTANT MEDIA

1-1 Introduction

Dispersions of colloidal particles in low dielectric liquid media are useful in the printing, paint, copying and display industries, to name a few(1). All of the above applications require particles to remain dispersed in a liquid medium for some period of time. It is this time period that is important for characterizing colloidal or dispersion stability. For example, a dispersion may be thermodynamically unstable yet could have a shelf-life (remain dispersed) of weeks or years. Therefore understanding dispersion stability or its converse, flocculation (the process whereby small particles clump together to form larger clusters(2)), is important from an industrial as well as an academic standpoint. Flocculation is due to the attractive van der Waals forces (primarily the London or dispersion forces). The van der Waals forces are in opposition to the repulsive electrostatic force that occurs when particles become like-charged. In the case of an electrodeposition device (a device that requires the migration of charged particles to an oppositely charge electrode), the electrostatic charge that develops on the dispersed particles via the use of a charging agent (defined later), is important in two respects: first, it contributes to the

dispersion stability, and second, it allows the particle to migrate in an applied electric field. It should be noted that there are other important factors, which will be discussed later, that lead to dispersion stability.

The object of this research was to study the charging mechanism which contributed to dispersion stability of variously coated rutile titanium dioxide (TiO_2) pigments dispersed in a liquid of low dielectric constant (cyclohexane), using two types of charging agents. This research was industrially funded for the purpose of developing a stable dispersion of highly mobile, highly charged pigment particles for an electrodeposition device. The success of the device depended on several factors, the two most important being the dispersion stability and the electrostatic charge on the particle. Therefore, this research deals with these two factors. Chapter II will deal with the stability of the dispersion and Chapter III is concerned with the charging mechanism. The rest of the present chapter covers the background information necessary to understand dispersion stability and the origin of the charging mechanism in media of low dielectric constant.

1-2 Characterizing the Surface Potential of the Particle

1-2.1 Zeta Potential and the Double Layer

Particles that are dispersed in a liquid medium are known to develop a charge on their surface as a consequence of the dissociation of ionogenic groups or

preferential adsorption of ions(2,3). No matter which mechanism of charging occurs or whether the system is aqueous(4,5) or non-aqueous(1,6), counter-ions will be produced and the largest concentration will be near the particle's surface. A charge concentration gradient or electrical double layer is created (see Figure 1-1) and is characterized by the Debye length, also known as the double layer "thickness"(4,7). The electrical double layer can be divided up into surfaces each having a corresponding potential, as shown in Figure 1-1. The first is the surface itself and its potential is called the surface potential. The surface potential is an important parameter since it can be related to the stability of the dispersion. Unfortunately, it is not measurable by any direct experimental technique(3). The next plane is the Stern layer. This is the layer of surface adsorbed ions and the potential that rises from this is known as the Stern potential (8). The next plane is the shear or slipping plane. Particle motion, whether by random motion or under a force (i.e., mechanical or electrical) in the medium, develops a shear plane such that all adsorbed ions and liquid medium molecules move with the particle as one kinetic unit, leaving behind the bulk ions and medium(9). The potential at this plane is known as the zeta potential,ζ, and is easily measured by various available electrophoretic methods. The zeta potential is often used to help characterize the stability(10) of a dispersion, since in many cases it is approximately equal to and/or reflects the surface potential, ψ_o,(11). This approximation is especially true for dispersions with thick double layers

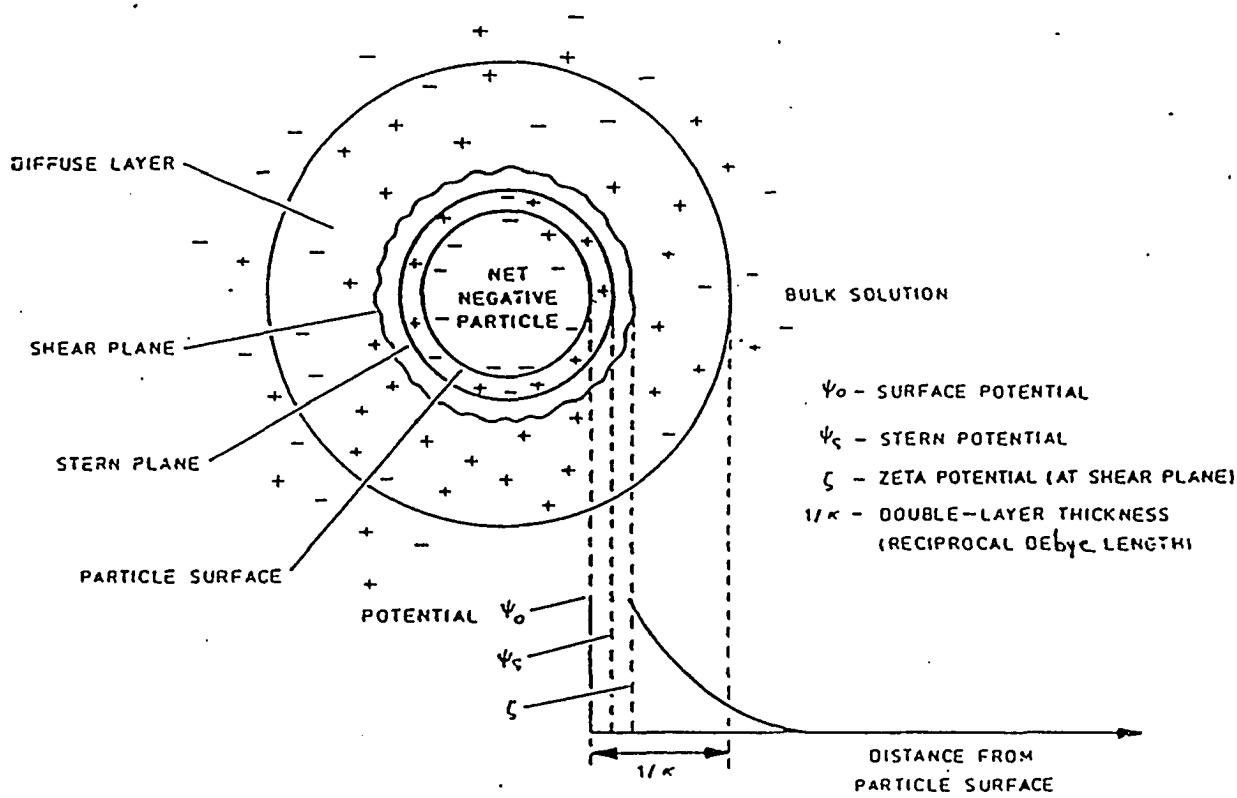

Figure 1-1. Potentials Associated with Colloidal Particles.

as can be demonstrated through the use of Equation 1-1 for a spherical particle with a double layer potential(11,12).

$$\psi(r) = \left\{ \frac{\psi_o a}{r} \exp[-\kappa(r-a)] \right\} \qquad 1\text{-}1$$

where ψ_o is the surface potential of a particle of radius a, r is the distance from the center of the particle, $\psi(r)$ is the potential at r, and $1/\kappa$ is the Debye length where κ expressed in Equation 1-2:

$$\kappa = \left\{ \frac{8\pi e^2 n z^2}{\epsilon_r \epsilon_o kT} \right\}^{1/2} \qquad 1\text{-}2$$

Here e is the electronic charge, n is the ion concentration, z is the valence of the ion, ϵ_r is the dielectric constant of the medium, ϵ_o is the permittivity of free space, k is Boltzmann's constant, and T is the absolute temperature. At low ion concentration the Debye length is large and the exponential term in Equation 1-1 approaches unity. The potential decays in a gradual manner as seen in Figure 1-2 for a non-aqueous dispersion as opposed to an aqueous one, where the potential decays more rapidly(11). Thus the zeta potential is a good approximation of the surface potential in low ionic concentrations, such as those found in low dielectric constant media(11,13,14)). All dispersions used throughout this research use low dielectric liquid media, such as cyclohexane; and so substitution of the zeta potential for surface potential is justified (11,21).

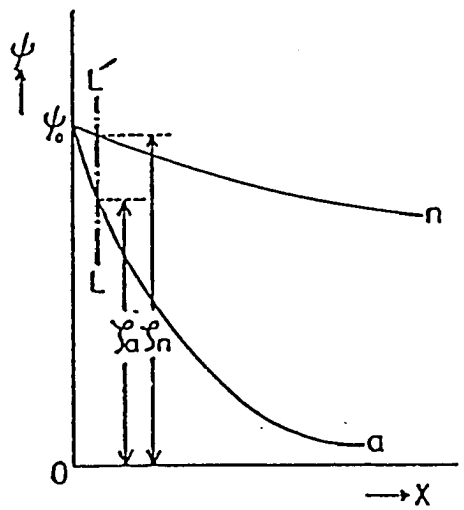

Figure 1-2. Double layer potentials in aqueous and nonaqueous media: a, aqueous; n, nonaqueous (low ϵ_r); LL', slipping plane.

1-2.2 The Measurement and Calculation of Zeta Potential

The zeta potential for long Debye lengths and colloidal sized particles can be calculated via the Hückel equation(15):

$$\zeta = \frac{3U\eta}{2\epsilon_r\epsilon_o} \qquad 1\text{-}3$$

where ζ is the zeta potential, U is the mobility of the particle, and η is the viscosity of the medium. The mobility of the particle is given by Equation 1-4:

$$U = \frac{v}{E} \qquad 1\text{-}4$$

where v is the terminal velocity, and E is the applied electric field(2). Modern light scattering electrophoretic equipment enable quick and reliable measurements of the speed of the particles (at terminal velocity) at various applied electric fields, making possible the calculation of mobility and then zeta potential. Two such instruments, the DELSA 440 and the PEM KEM 3000, that were used in the work are discussed briefly in the following paragraphs.

1-2.3 Doppler Electrophoretic Light Scattering Technique

The DELSA (Doppler Electrophoretic Light Scattering Analyzer) 440 by Coulter Electronics, INC. is an instrument that combines two technologies: electrophoresis

(a technique that characterizes particles by their movement in an applied electric field) and laser Doppler velocimetry (a method for measuring the speed of particles by analyzing the Doppler shifts of light scattered by them)(16). When light is scattered from a charged particle moving in an electric field, the frequency of the light detected is shifted from the incident frequency by an amount proportional to the speed of the particle (16,17). This frequency shift is called a Doppler shift. The Doppler shift is determined using the heterodyne mixing of scattered light with four coherent reference beams at various angles which are split from the same laser source before entering the migrating suspension for mixing. The electrophoretic velocity of the particle is then determined from a damped cosine photon correlation function which was obtained by converting the mixed Doppler shift via an autocorrelator for each angle(16) (Figure 1-3).

The sample cell is comprised of two hemispherical silver electrodes with a sample chamber between them. The hemispherical electrodes ensure that a uniform electric field is maintained. The sample chamber is made of fused quartz with dimensions of 8 mm in length, 1 mm in height, and 2.5 mm in width. The short gap between electrodes allows for high field strength at low voltages and minimizes Joule heating. The stationary layer (the layer where motion is due purely to electrophoresis) was determined to be 16% or 0.16 mm from the top or bottom of the interior of the sample cell(17).

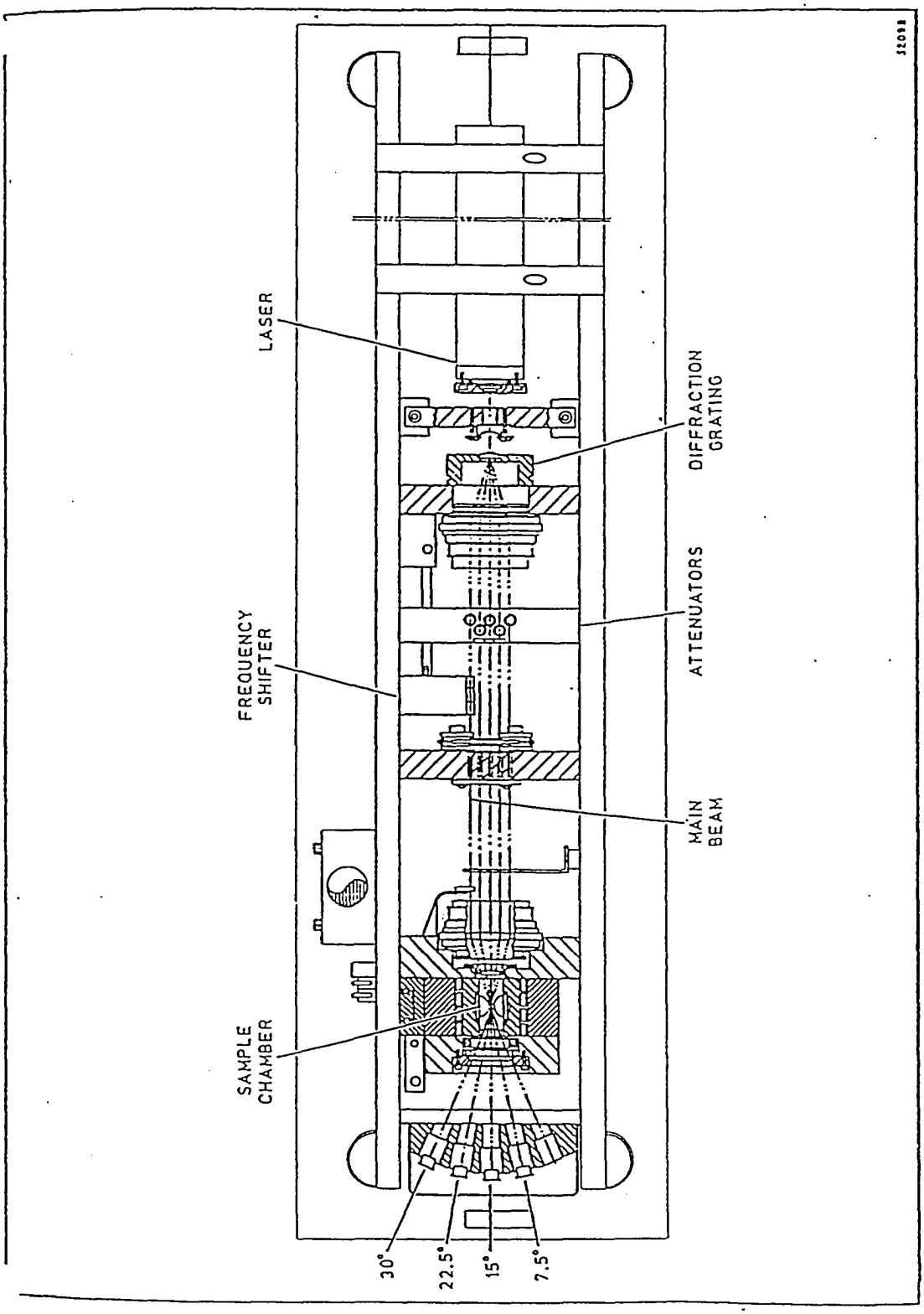

Figure I - 3 Schematic diagram of Coulter DELSA 440.

1-2.4 The Rotating Grating Technique

The PEM KEM 3000 employs a circumferentially arranged grating on a transparent rotating disk to image and then modulate scattered light from migrating particles in a cylindrical electrophoresis chamber. The light (He-Ne laser) beam (which can be focused at any layer) is oreinted at 90 degrees from the rotating disk(18). This modulated image of the particle movement is then transmitted to a photomultiplier tube which in response produces a fluctuating power spectrum (18). A frequency translator receives the output signal which is compared to a reference frequency of 1000 grating lines per second. A stationary particle would have a frequency of 1000 Hz. If the image of a particle moves in the same direction as the grating, a signal of lower frequency will result. If the image of the particle moves in the opposite direction as the grating a higher frequency will occur. In this manner the direction of the particle can be determined relative to the polarity of the electrodes, hence the polarity of the charge on the particle can be obtained. Many particles are measured simultaneously, each particle contributing a signal at a frequency shift determined by its electrophoretic velocity. A frequency spectrum can then be computed from the Doppler signal via a Fast Fourier Transform Analyzer (FFT), which averages all successive spectra to obtain the electrophoretic distribution (18).

The schematic diagram of the PEN KEM 3000 can be seen in Figure 1-4. The cylindrical cell has a diameter of 1 mm and a stationary layer 0.147 mm from the interior of the fused quartz wall. When the laser is focused in this layer only the

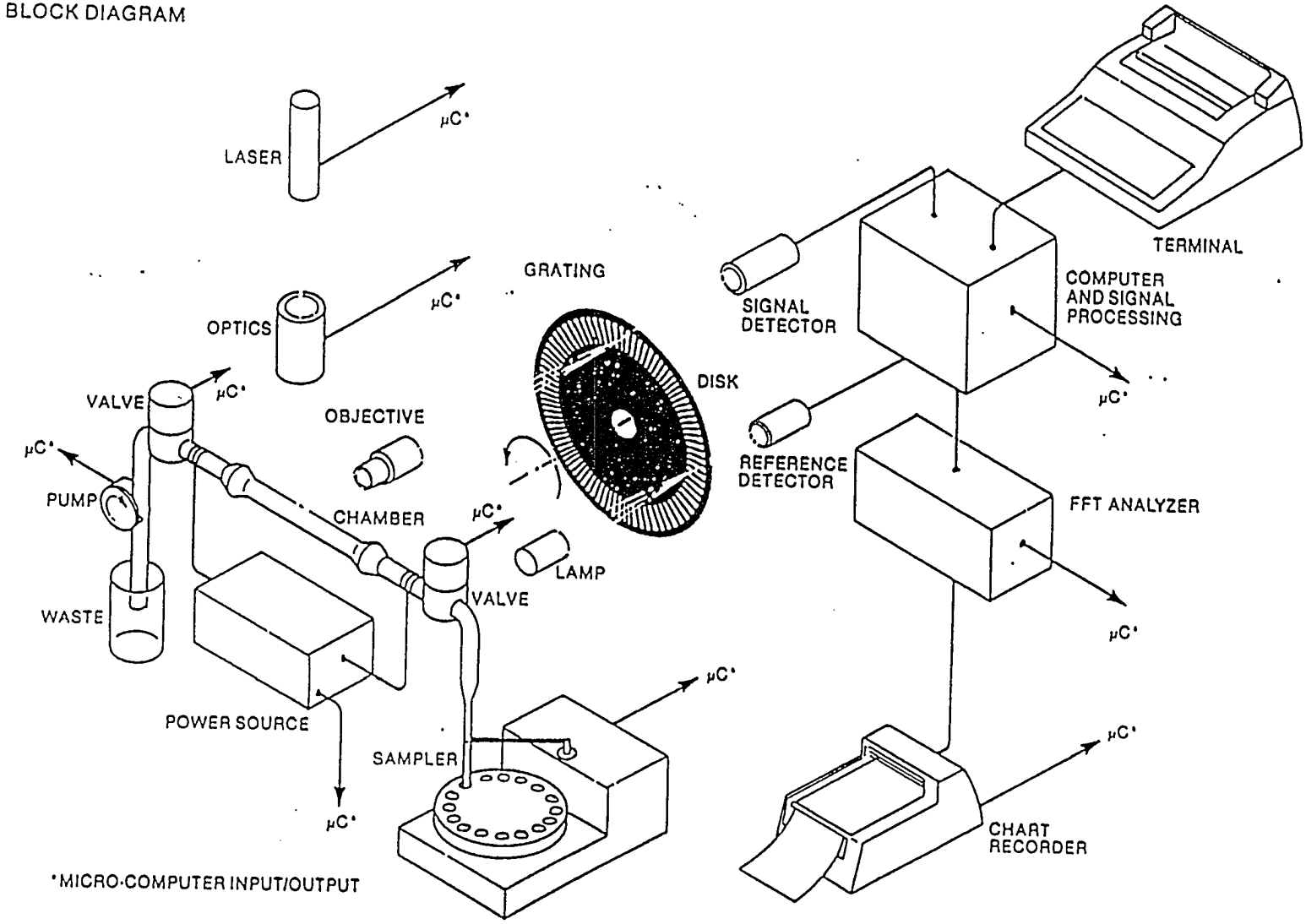

Figure 1-4 Schematic diagram of Pen Kem 3000.

speed due purely to electrophoresis (no electro-osmotic flow) is measured; hence the true mobility is calculated. The PEN KEM has a programed procedure to find this layer. An alternative procedure uses mobility measurements on a standard colloid suspension, at three layers, to calculate the stationary layer (19). This calculation is based on the parabolic flow that is obtained when the dispersion moves in the cell during electrophoresis. If the cell position (the position where a measurement takes place) is plotted as a function of mobility, the resulting plot would look parabolic. The stationary layer would be found at 147 μm from the cell wall. A van Gils plot (Figure 1-5), which linearizes the parabolic profile, was used as a check of this procedure. A van Gils plot is made by plotting mobility versus a parameter for the cell position being observed, this parameter being the square of the difference of the cell radius and measurement position divided by the square of the cell diameter(20). At an abscissa value of 0.5 the stationary layer is found (Figure 1-5). The mobility value found at the stationary layer should be the same as that of the standard.

It has been shown by the author(21) and others(22,23) that data obtained by the two above mentioned electrophoretic techniques agree within 5%. Both techniques are employed in this thesis to obtain mobilities from which the zeta potential is calculated via the Hückel equation.

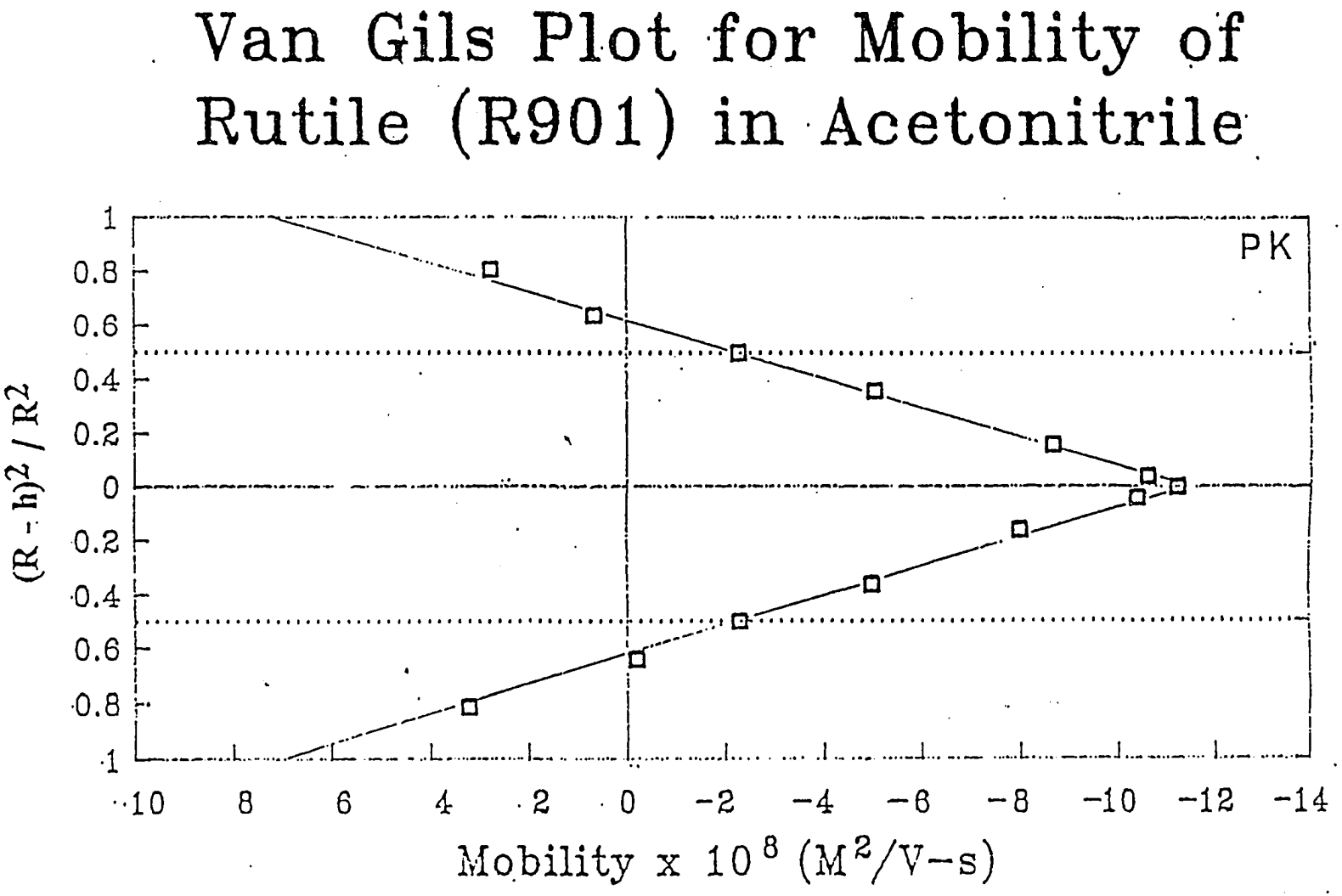

Figure I -5 Van Gils plot for velocities of rutile (901) dispersed in acetonitrile measured in a cylindrical cell of Pen Kem 3000.
R is the cell radius and h is the distance from the wall.

1-2.5 Mobility measurements in Low Dielectric Constant Media

It is considerably more difficult to establish a uniform electric field in low dielectric media than in aqueous media. An uniform electric field is necessary to obtain a parabolic flow profile so that the stationary layer can be found. A problem arises at low conductivity where current can leak down the cell wall(24,25). For instance, when trace amounts of water (as well as other contaminants) are adsorbed on the cell wall, the applied electric field can be distorted. A non-uniform electric field distorts the parabolic flow across the cell which is necessary to measure the mobility(25). One way to preserve parabolic flow is to condition the electrophoretic cell before use by rinsing in a series of solvents of decreasing polarity(18,26,27). For example, one could use ethanol, then acetone, followed by dry cyclohexane. The cell should also be conditioned when any additives, such as polymeric charging agents, are used. When a series of dispersions are measured at varying concentrations of additives, the solution at the lowest concentration of the additive should be allowed to soak in the cell for several hours to days to effect adsorption. Then, when measurements are made with increasing amounts of additive, only a short time is necessary for equilibration since the surface area of the capillary cell is small and a monolayer should have formed(26,28). By conditioning the cell wall in such a manner, a uniform wall is produced which will not distort the electric field(29).

Another problem that occurs in low conductivity dispersions (less than 1×10^{-10} S/cm) is the time delay of the particles to reach terminal velocity(18,30).

This time delay can be seconds to hours depending on the conductivity(27,30). Thus the conductivity must be measured in order to set the delay time.

Other problems of which any experimenter should be aware when using the above techniques to measure mobility we pointed out in this paragraph. The velocity is proportional to the applied field, but since it is divided by the field to calculate mobility (equation 1-4), the mobility should be field independent(30,31). In addition, the particle should reverse direction when the polarity of the cell is switched. If a van Gils plot is made (Figure 1-5) the flow pattern should be rectilinear and superimposable around the center of the cell (a mirror image around the center)(2,20,28,31). If not, cleaning the cell usually solves the problem.

1-3 DLVO Theory

Two particles of the same material dispersed in a liquid medium will undergo an attractive force mainly due to the dispersion or London component of the van der Waals forces(32,33,34). This force can be offset by an electrostatic repulsion which occurs when two charged particles approach each other and their electrical double layers overlap(34,35). The sum of these two potentials, described in DLVO theory (named after B. V. Derjaguin, L. Landau, E. J. W. Verwey, and J. Th. G. Overbeek) indicates whether a dispersion can remain stable(36). A positive potential value means a repulsive or favorable (stable) potential is reached. On the other hand, a negative potential means an attractive potential (unstable) is encountered.

There is one more potential that will be considered in this thesis and that is the steric potential that arises from the overlap of adsorbed polymer chains. These adsorbed chains can act like springs in moderate concentration(37). In most non-aqueous dispersions the combination of the electrostatic and steric potentials enables a dispersion to remain stable, as illustrated in Figure 1-6 (38). In this figure(a), the adsorbed layer that gives rise to the steric potential is not thick enough to eliminate the attractive potential altogether, since a shallow attractive well (known as a secondary minimum) exists at a short distance from the approaching particles. While this secondary minimum can be overcome, from an energy standpoint the system still remains unstable. It is the addition of the electrostatic potential that can eliminate this shallow well, effecting a stable suspension. The combination of the electrostatic and the steric potentials is very important in non-aqueous dispersions where much higher surface potentials are required to achieve a stable dispersion than for aqueous ones(39).

A quantitative measure of dispersion stability is necessary in order to make full use of DLVO theory. One way to quantify dispersion stability is to calculate a stability ratio. The stability ratio (to be discussed later) is the ratio of the fast flocculation rate constant (calculated) over the slow flocculation rate constant (measured or apparent). The slow or apparent rate constant will be obtained by measuring the particle (flocculate) size as a function of time. Particle size as a function of time will be measured by photon correlation spectroscopy which will be discussed in the next section.

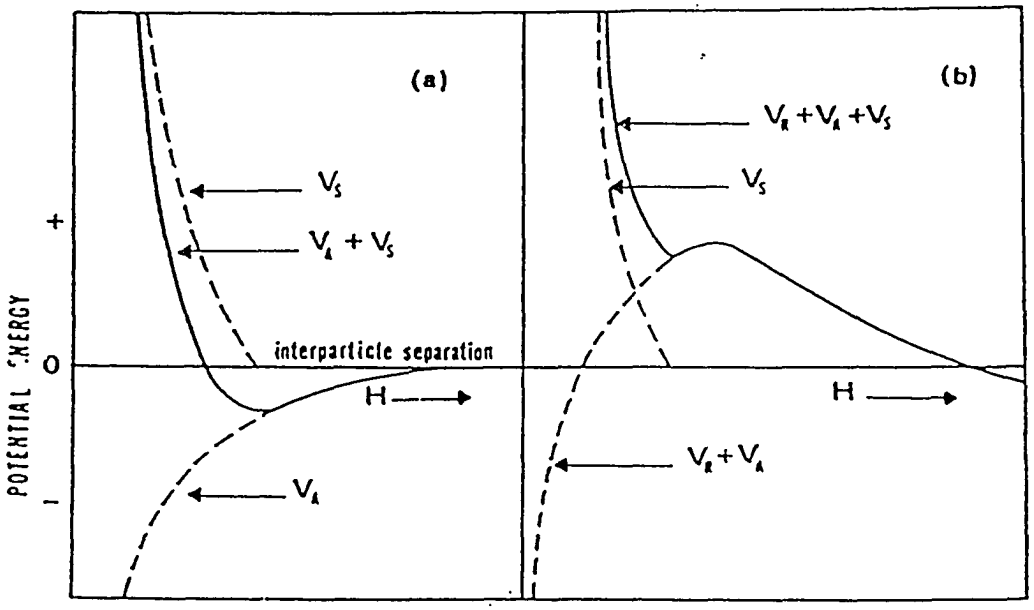

Figure I-6. Potential energy diagrams for a pair of particles with: on the left, a steric barrier (V_S) and dispersion force attraction (V_A); and on the right, with electrostatic repulsion (V_R) added. Reproduced with permission from Ref. (13). Copyright 1980, Butterworths.

1-4 Photon Correlation Spectroscopy

Photon correlation spectroscopy (PCS), which is a dynamic light- scattering technique, was used to measure particle size. PCS is based on measuring the scattered-light fluctuations that occur when particles undergo Brownian motion while being irradiated by laser light. These fluctuations occur on the microsecond (small particles) to millisecond (large particles) time scale. Therefore PCS sizes particles by characterizing the exact time scale of the random intensity fluctuations caused by the changing interference patterns of the diffusing Brownian particles(40).

The time scale of the intensity fluctuations in the light scattered by the diffusing Brownian particles is found by computing the autocorrelation function of the scattered-light intensity. The autocorrelation function is computed by comparing the intensity at any given time to that at a time, τ, later. In this way large slow moving particles change position slowly, causing a slow decay of the autocorrelation function, and vice versa. The laser light scattered from particles undergoing Brownian motion is converted into pulses of photoelectric current and further additively mixed with itself (homodyne) at any given interval to form an autocorrelated power spectrum(41). If the particles in the medium are monodispersed, the autocorrelation function of the scattered-light intensity is a single decaying exponential as expressed in the equations below:

$$G(\tau) = \langle I(t) \cdot I(t+\tau) \rangle \propto \exp(-2\Gamma\tau) \qquad 1\text{-}5$$

$$\Gamma = DK_r^2 \qquad 1\text{-}6$$

$$K_r = (4\pi n/\lambda)\sin(\theta/2) \qquad 1\text{-}7$$

$$D = kT/(3\pi\eta d) \qquad 1\text{-}8$$

where $G(\tau)$ is the autocorrelation function, Γ is inverse of the delay time, n is the refractive index of the fluid medium, λ is the laser wave length in a vacuum, θ is the scattering angle, τ is the delay time, k is Boltzmann's constant, T is the absolute temperature, η is the viscosity of the fluid medium, t is time, I is intensity, K_r is the light scattering factor, and d is the diameter of the particle. If the particles are polydispersed (many sizes), the autocorrelation function is the sum of the exponentials for all component sizes(41).

From each exponential that makes up the autocorrelation function, a diffusion coefficient, D, can be obtained (Equation 1-5 and 1-6). A particle diameter is calculated from each diffusion coefficient via the Stokes-Einstein equation ,1-8, (our instrument, the Coulter N_4, assumes spherical particles)(41). The mathematical analysis for the collective distribution of individual diffusion coefficients, hence particle size, is accomplished through two computer programs: the unimodal (overall distribution, which is analyzed by the cumulant method(41,42) and assumes a log-normal distribution) and the constrained regularization or SDP (CONTIN(41,43), which makes no such assumption).

The schematic diagram of the instrument can be seen in Figure 1-7. It consists of a 4mW helium-neon laser which is focused into the sample cuvette containing the dispersion to be measured. Six fiber optic receptors, a stepper motor, and a photomultiplier detector allow the angle of the scattered-light detection to be varied.

1-5 The Fowkes Acid-Base Mechanism

A mechanism for charging dispersed particles in a non-aqueous medium was proposed and supported qualitatively by Fowkes(6,44). In this mechanism, a polymeric charging agent at or above its critical micelle concentration adsorbs on the surface of a particle. Once it is adsorbed it undergoes an acid-base reaction by either exchange of a proton (Brønsted-Lowry)(45) or electron pair (Lewis acid)(46). It then desorbs into a reverse micelle or associative structure (see Figure 1-8). This micellar or complex polymer structure is necessary for the stabilization of the charged counter-ion. Without the counter-ions the Law of Electroneutrality would be violated and the electric double layer would not exist(47). The stabilization of the charged counter-ion is difficult especially in low dielectric constant media(48). This is why it is important for a critical micelle concentration to be obtained before charging is observed(49).

In the Fowkes acid-base model(6), an acidic charging agent will donate a proton or accept an electron pair from a basic surface site. This will leave the

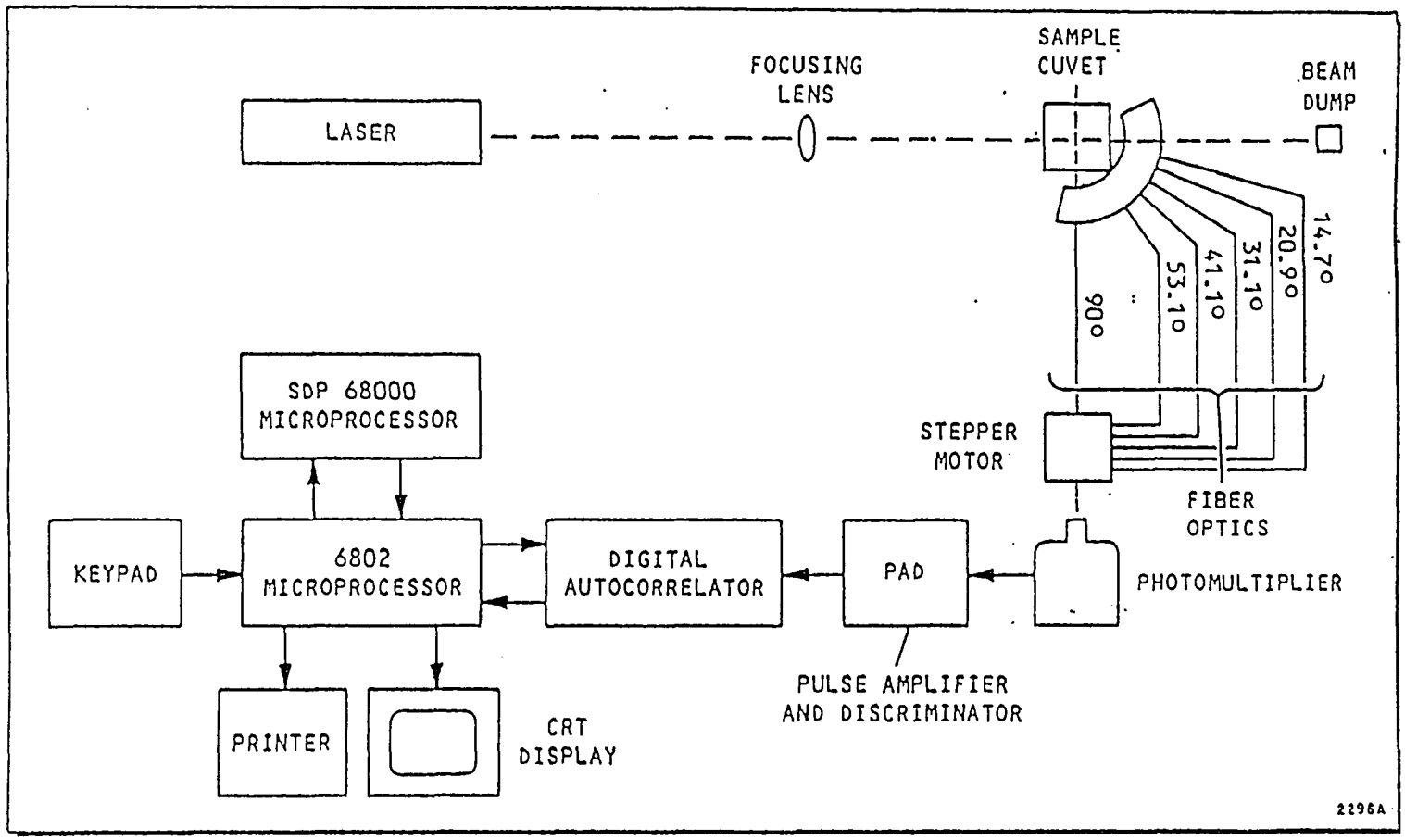

Figure 1-7 Schematic diagram of Coulter N4 MD.

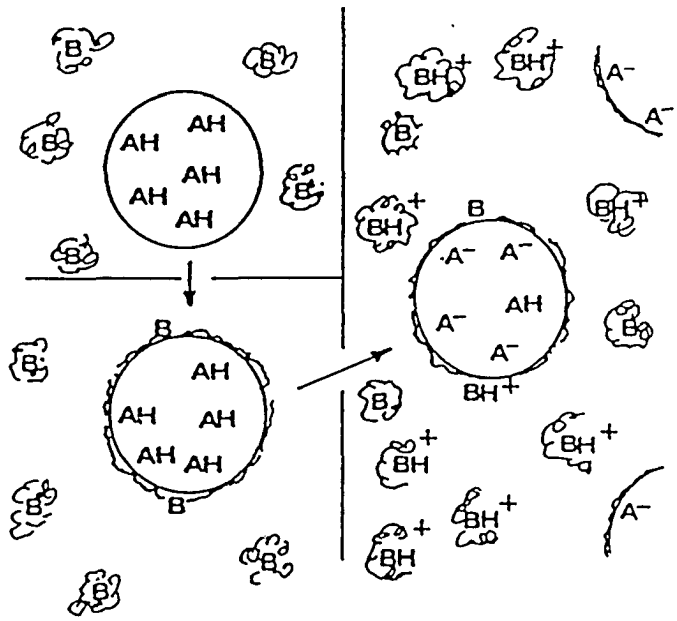

Figure 1-8 Mechanism of electrostatic charging in oil of particles with acidic sites (AH) by a polymeric dispersant with basic sites (B). Reproduced with permission from Ref.(13).Copyright 1982, American Chemical Society.

surface with a net positive charge, hence a positive zeta potential. In addition a negative counter-ion will be produced, which will establish the double layer. The reverse is true for a basic charging agent reacting with an acidic surface site. Since most surfaces are heterogeneous (having both basic and acidic surface sites), a reversal of sign can be observed in some cases when switching from an acidic to a basic charging agent(50) or vise versa. But usually a surface is predominately acidic or basic and the detection of the sign inversion may be impossible because the magnitude of the zeta potential may be very small(51).

1-6 Kitahara's Non-aqueous Charging Mechanism

When plotting the zeta potential as a function of surfactant concentration (in a non-aqueous dispersion) a maximum is obtained as seen below in Figure 1-9(34,50,52,53).

A dissociative, non-aqueous, charging mechanism was proposed by Kitahara(54) to explain the above phenomenon. This mechanism was for an ionic surfactant in a low dielectric constant medium. The surfactant would dissociate forming two oppositely charged ions. Both of these ions could exist in a reverse micelle (especially if they were sodium or potassium ions) making the radii of the solubilized ions quite large. A small amount of one of these ions is preferentially adsorbed to produce a charged surface, as seen by Equation 1-9:

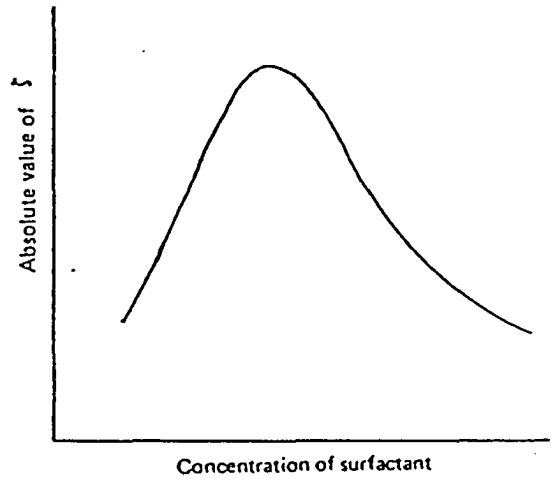

Figure 1-9. Zeta potential versus charging agent or surfactant concentration profile.

$$S + P^{+} \overset{K_e}{=} SP^{+} \qquad 1\text{-}9$$

where S is a surface site, P^+ is a positively charged ion in this example, and SP^+ is the ion-adsorbed surface site. This equilibrium was used to explain the rise seen in figure 1-9, since the charge is increasing with the adsorption of the ions. In addition to the above equilibrium, is the equilibrium due to the migration and adsorption of the oppositely charged counter-ion (N^-) to the ion-adsorbed surface site, as shown below:

$$SP^{+} + N^{-} \overset{K_L}{=} SPN \qquad 1\text{-}10$$

where N^- is the oppositely charged counter-ion and SPN is the neutralized adsorbed surface site. The equilibrium proposed in Equation 1-10 is used to explain the decrease in zeta potential, since the charge is being reduced by the adsorption of counter-ions. It should be noted that the overall mechanism differs from Fowkes' by assuming dissociation in the medium, whereas Fowkes' model assumes dissociation at the surface. By using Equations 1-9 and 1-10, Kitahara(54) derived an equation which expressed zeta potential as a function of concentration of surfactant:

$$\zeta = \frac{4\pi[S]_o}{\epsilon_r \epsilon_o \kappa} \left\{ \frac{1}{1KK_eC^{2.25} + C^{0.75} + (1/KK_L)C^{0.75}} \right\} \qquad 1\text{-}11$$

where C is the concentration of added surfactant, K_e is the equilibrium constant for Equation 1-9, K_L is the equilibrium constant for Equation 1-10, ζ is the zeta potential, $[S]_o$ is the initial concentration of sites, ϵ_r is the dielectric constant of the medium, ϵ_o is the permittivity of free space, κ is a proportionality constant for Debye length as a function of surfactant concentration, and K is a proportionality constant for surfactant concentration as a function of the counter-ion concentration. This model was used to explain the maximum so often found in the zeta potential versus surfactant concentration curve. The equilibrium constants and the charge density obtained from Equation 1-11 are consistent with low dielectric systems(54). Unfortunately, Kitahara did not show how well his equation fits the experimental data. The problem with Kitahara's model is that it does not explain the non-ionic surfactant behavior where dissociation in the medium is not likely to occur(4). One of the major goals of this dissertation is to derive an equation like 1-11 to aid in the prediction of the maximum in the curve of zeta potential versus concentration of non-ionic surfactant or charging agent. This equation will be based on the Fowkes acid-base mechanism.

1-7 Calorimetry

One way to characterize the surface sites is by use of flow calorimetry (55,56,57). A flow calorimeter measures the heat of adsorption of a probe molecule onto the surface of a powder. This determination is accomplished by pumping a

solution of the probe molecule onto a bed of particles (in this project TiO_2 was used) and measuring the heat evolved as a function of time(56,57). A UV detector is downstream of the bed and measures the change in concentration as a function of time(56,57). Thus, flow calorimetry can be used to determine such values as energy/mole of adsorbate or the area occupied per probe molecule.

It has been shown by Fowkes and co-workers(57,58) that the adsorption of polymers onto the surface of pigment particles, as well as the surface charge development, are driven by acid-base interactions. By using a basic probe molecule, such as pyridine, the acidic surface sites can be characterized in terms of enthalpy and number. This enables predictions of surfactant or polymer adsorption as well as the sign and magnitude of the zeta potential. The surfaces of all pigments used in this research were examined by flow calorimetry which will be discussed in more detail in Chapter III.

CHAPTER II

THE STABILITY OF SURFACE MODIFIED RUTILE TITANIUM DIOXIDE PARTICLES IN A LOW DIELECTRIC MEDIUM.

2.1 Introduction

Pigment stability in low dielectric media is important in the printing and paint industries and also has applications in electro-deposition processes (i.e. photocopiers and imagers). The interest in pigment stability of the present work is for applications in the electro-deposition processes, especially where repeated deposition of particles at and discharge from an electrode is required. The pigments of interest are rutile (titanium dioxide) particles. Because the particles are used in the electro-deposition process, they must carry a charge. The charge on the particle is developed by use of a charging agent which has a strongly acidic or basic head group with a hydrocarbon tail. Dispersion stability due to this charging agent is the concern of this chapter.

Since the particles in question are approximately spherical(59) and are observed to move uniformly under a uniform electric field, they can be considered to have the same sign and approximate magnitude of surface charge(21,59,60). Like charges on the particles give rise to electrostatic repulsion. In addition, the particles are attracted to one another by van der Waals forces. These two important aspects

of pigment stability are dealt with under DLVO theory (see Chapter I)(2,3,61). This theory considers the two potentials, repulsive and attractive, which develop from the electrostatic(61,62) and London(61,63) forces that can exist between two particles. The London forces will always be attractive for two particles of the same composition(32) and are dependent on the composition of the medium and dispersed phase. The electrostatic force is dependent on the charge that is developed by either the charging agent or the medium. The charging agent can effect the magnitude of the surface charge, hence the electrostatic force, yet the London forces remain essentially unaffected. Thus, controlling the amount of charging agent is one way of controlling the particle stability. An overall potential energy diagram between two particles is obtained by summing the electrostatic and attractive potentials. A third potential, known as the steric potential, arises from the adsorption of the charging agent's head group onto the particles surface while its tail is in the medium(37,64). If a monolayer of charging agent adsorbs onto the surface of each particle, the film that results can prevent interparticle close approach(63,65). Of course, using a polymeric charging agent can affect both the electrostatic and steric potentials. The sum of these three potentials determines whether two particles will stick to each other (is a process known as flocculation) or remain dispersed(4).

The potentials that can be developed between two particles depend on the charging agent(6,66). The type and concentration of charging agent that is used will not only determine the sign but also the magnitude of the charge that is imparted on

the pigment via acid-base interactions(6,54,66). This charging in turn also depends on the chemical nature of the pigment surface. The purpose of the work in this chapter was to study the effectiveness of two charging agents (one acidic and one basic) on the stability of three rutile titanium dioxide pigments (varying in acidity and basicity) in cyclohexane. Also, the goal was to determine which type of stabilization is most effective in these dispersions.

2-2 Theoretical

This theoretical section deals with the aspect of dispersion stabilization and its quantification.

2-2.1 The Attractive Potential

As stated earlier, long range (greater than 10 Å) attractive forces that arise between colloidal particles of the same material are essentially due to the dispersion or London component of the van der Waals attraction(67). These long range intermolecular forces are a consequence of the instantaneous, but fluctuating, dipole moments that exist between all atoms and molecules(4,32). The London treatment of this phenomenon was derived from second order perturbation theory in quantum mechanics. The London forces can be thought of as a kind of a "quantum mechanical polarization force", where the ensuing interaction is essentially electrostatic(32,67). Therefore an atom or molecule will have an instantaneous

dipole moment which will induce a dipole moment in another nearby atom or molecule(68). The interaction between two induced dipole moments is referred to as a pair potential(4,32,67,68,69). Hamaker theory is based on the summation of all pairwise potentials between two interacting colloidal particles. This summation procedure is known as pairwise additivity(49,32,68). It neglects the effects of nearest neighbors on each pairwise potential(68). Even though this approximation has been shown in some extreme cases to overestimate the effects of the London component by as much as thirty percent, it still gives an upper limit to the attractive potential between two colloidal particles(32). The Hamaker expression for the total attractive ψ^a_{121} potential energy between two spherical colloidal particles in a liquid medium is given below(68,70):

$$\psi^a_{121} = \frac{-A_{121}}{6}\left(\frac{2}{S^2-4} + \frac{2}{S^2} - \ln \frac{S^2-4}{S^2} \right) \qquad 2\text{-}1$$

$$S = (H+2a)/a \qquad 2\text{-}2$$

where a is the particle radius, A_{121} is the Hamaker constant for a particle-medium-particle system (hence the 121 subscript), and H is the interparticle separation. When the interparticle separation is small ($H << a$), Equation 2-1 reduces to:

$$\psi^a_{121} = \left(- \frac{aA_{121}f}{12H} \right) \qquad (68,71) \qquad 2\text{-}3$$

This equation is suitable for small particle separations where the attractive potential dominates(3,39,71). At longer distances (400 Å)its effect is minimal. The shielding factor, f, corrects the Hamaker constant for the "retardation" of the dispersion forces at large interparticle distances. The retardation is due to the fact that the dispersion forces are electromagnetic in nature and require a finite time for their propagation. This "time lag" causes a phase difference between the electronic oscillations (induced dipoles) of interacting molecules(72,73,74). Values of f, which are needed for Equation 2-3, can be obtained from Figure 2-1 (74), for various values of H, and a as a function of λ_1, the characteristic wave length of the most energetic dispersion forces, and can be obtained from sources in the literature (67,69,74,75,76).

The overestimation of the London component using the pairwise summation procedure does not affect the distance dependence of Equation 2-3, but merely alters the magnitude of the Hamaker constant(4,32). Therefore, Equation 2-3 is valid no matter which method is used to calculate the Hamaker constant, be it pairwise summation or one of the continuum theories(4,32). Of all the methods used to calculate the Hamaker constant, the continuum theory of Lifshitz(4,34) is the most successful, but difficult to apply since it is complex and requires frequency dependent dielectric constant data.

Another method developed by Fowkes(77) uses surface energies, as expressed in Equation 2-4:

$$A_{121} = (1.5X10^{-14}\ cm^2)[(\gamma^d_1)^{1/2}-(\gamma^d_2)^{1/2}]^2 \qquad 2\text{-}4$$

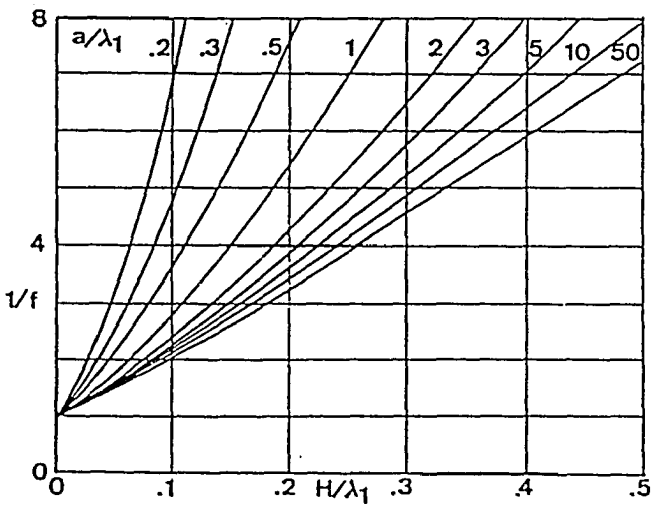

Figure 2-1 Retardation correction factor (f) for dispersion force attractions between spherical particles of radius (a) at separation distance (H), with dispersion force wavelength λ_1. (10)

where γ^d_1 and γ^d_2 are the dispersion force contribution to the surface energies of the particles and medium, respectively. As noted by Fowkes(71) and others(32,34), it appears that the γ^d values are closely related to refractive indices and are a direct measure of the Lifshitz attraction.

2-2.2 Electrostatic Potential

The electrostatic (repulsive) potential also must be taken into account as part of the stability of a dispersion in order to obtain a more realistic picture. As was mentioned in Chapter I, the electrostatic potential is due to the overlap of the electrical double-layers of two approaching particles, it is a consequence of their like surface charge. The electrostatic potential (ψ^e_{121} per pair of particles can be estimated from the Deryagin equation below (78):

$$\psi^e_{121} = 2\pi\epsilon_o\epsilon_r a\psi^2_o \ln[1+\exp(-\kappa H)] \qquad 2\text{-}5$$

where ϵ_o is the permittivity of a vacuum, ϵ_r is the dielectric constant of the medium, ψ_o is the surface potential (which is approximately the zeta potential in low dielectric media), and $1/\kappa$ is the Debye length. The Debye length can be calculated from the Klinkenburg-van der Minne equation below (79):

$$\frac{1}{\kappa} = \left(\frac{\epsilon_o\epsilon_r D}{2\sigma} \right)^{1/2} \qquad 2\text{-}6$$

where D is the diffusion coefficient of the charge-carrying species or counter-ions and

σ is the conductivity due to the counter-ions. The diffusion coefficient can be calculated by the Stokes-Einstein equation corrected for rod-shaped ions, as shown(80):

$$D = \frac{kT}{6\pi r\eta}(f/f_o) \qquad 2\text{-}7$$

where r is the equivalent radius of a sphere, η is the viscosity of the medium, and (f/f_o) is the correction factor for rods.

The electrostatic potential calculated by Equation 2-5 can be added to Equation 2-3 to yield an overall or total potential. The sum of the potentials in the DLVO theory provides a theoretical description of the dispersion stability between two particles. There is another long range force that affects the colloidal stability and hence, the total potential energy described by DLVO theory. This force, or potential that arises from it, is a consequence of the overlap of adsorbed polymer chains (well solvated) extending from the surface of the particle. This potential, as stated earlier, is known as the steric potential.

2-2.3 The Steric Potential

The steric potential arises from the overlap of adsorbed polymer films on the surfaces of two approaching pigments(37,81). The films, in nonaqueous dispersions, are due to the adsorption of the polymer's head group onto a surface site on the pigment while the tail is in the medium. This adsorption can be viewed as an acid-

base interaction or the first step in the Fowkes acid-base mechanism. The present section deals only with the adsorption step of the Fowkes acid-base mechanism (because this gives rise to the steric potential); desorption could lead to charging of the surface (outlined in Chapter I). A charged surface will give rise to an electrostatic potential described in the previous section of this chapter.

Polymers that are designed as steric stabilizers generally are block copolymers which contain two different kinds of repeat units, clustered in long sequences of one kind(82). One of the sequences (head group) will be readily adsorbable to the pigment's surface (insoluble in the medium) while the other sequence (tail group) will be soluble in the medium and non-adsorbable to the surface(82,83). If the steric stabilizer works ideally (assuming monolayer coverage) its head group will adsorb to the surface, while its tail will be in solution normal to the pigment's surface(83). The orientation of the tail is, of course, dependent on the solubility in the medium(84). The solubility is dependent on the temperature, pressure, etc. of the medium, for a change in any of the aforementioned conditions can result in a non-soluble tail, rendering it ineffective at keeping pigments separated(83). A critical flocculation point is reached when a condition is changed such that the tail is in transition between being soluble and insoluble in the medium(84). There can be critical flocculation temperatures, pressures, or concentrations, and conceivably other critical properties(85). It has been demonstrated by Napper and co-workers (86) that the critical flocculation temperature corresponds to the Theta temperature for the

polymer tail. A Theta point is defined as one at which the second virial coefficient of the polymer chain vanishes(87). A zero virial coefficient means that the polymer chain and solvent neither attract nor repel each other; the Theta point is at the transition between solubility and insolubility. As the Theta point is crossed from the solubility side, the polymer tails will become insoluble and will attract each other; flocculation will occur. Therefore polymer solubility promotes dispersion stability in two ways: first, it aids in tail extension normal to the surface; second, it prevents tails from interacting with each other, leading to a repulsive steric barrier(85,86).

From a potential energy standpoint, polymer contact can be repulsive (positive free energy) or attractive (negative free energy) depending of course on the solubility(84), as expressed in the Flory-Krigbaum equation for polymer films on particles in suspension(88):

$$\psi^{s}_{o} = (4/3)\pi kT(\bar{V}_2/\bar{V}_1 V_a)\{\psi(1-H/T))\}(\Delta a-H/2)(3a+2\Delta a+H/2) \qquad 2\text{-}8$$

where, (H is interparticle distance) Δa is the film thickness, T is the absolute temperature, $\bar{V}_1$ is the partial molar volume of the polymer, $\bar{V}_2$ is the partial molar volume of the solvent, V_a is the volume of the film overlap, θ is the Theta temperature, and ψ is defined by Flory(9,88) as the entropy of dilution parameter. The important concepts of this equation are the volume fraction and temperature dependence of the polymer solubility. Dispersion stability depends on polymer volume fraction, since monolayer coverage is essential(82). Unfortunately, this

equation fails to undergo a sign inversion at a critical flocculation polymer concentration or volume fraction (i.e., it will always be repulsive at all volume fractions), which is what is usually observed in most all dispersions(86). Despite this shortcoming, the equation does provide for a critical flocculation temperature and undergoes sign inversion. When T is equal to θ, ψ_o^s, becomes zero. If T is greater than θ, ψ_o^s will be positive and repulsive (good solvent). If T is less than θ, ψ_o^s is negative and attractive (poor solvent).

Equation 2-8 considers contact of the polymer film; it does not however express the concept of chain compression, which always involves a repulsive positive potential energy term. Chain compression is the result of the overlap of polymer films on the surfaces of two approaching particles(85,89). The maximum interparticle distance where chain compression begins to enhance the stability is twice the thickness of the polymer film(85,89,90), whereas the minimum distance is the film thickness(90). The minimum occurs when the approach of two particles force their polymer chains (normal to their respective surfaces) to interpenetrate with each other to the point where the tails touch the opposite surface and are compressed by it. Maximum interpenetration has been shown to be possible in some systems by theoretical calculations(89). Not only does chain compression give rise to a repulsive potential, but indicates that the closest two particles can approach (assuming the molecules are normal to the surface) each other is on the order of the maximum conformational polymer length to twice this value depending on the conditions and extent of chain interpenetration(86,91).

Steric stabilization can be summarized, as a function of polymer concentration, by the Figure 2-2(4,91). At low polymer concentration, the conditions favor bridging flocculation. Bridging flocculation occurs at polymer concentrations lower than that required for monolayer coverage (<50%)(92). At this low surface coverage a polymer molecule can attach to two particles, with little interference. As the concentration is increased to the level where at least a monolayer surface coverage is obtained, a stable dispersion results as long as the chain length is sufficient and the medium is a good solvent for the polymer(4,91). When the polymer concentration is increased, a phenomenon known as depletion flocculation may occur(92,93). Depletion flocculation results when two particles at close interparticle separation coalesce flocculate because the free polymer in solution depletes the medium between the two particles. Essentially this is caused by an osmotic effect(4,92). At larger interparticle separations (i.e., distances where the interparticle separation is greater than one molecular length) energy is required to exclude the polymer chain from between two particles. This thermodynamically unfavorable process is known as depletion stabilization, and occurs if the medium is a good solvent(4,92). As noted by Napper(92) and Hunter(4) the experimental conformation of this phenomenon is still open to some question. Both depletion flocculation and stabilization are a result of free polymer in solution (usually well after monolayer coverage is observed), whereas bridging flocculation and steric stabilization are a result of attached polymer(4,90,92,93).

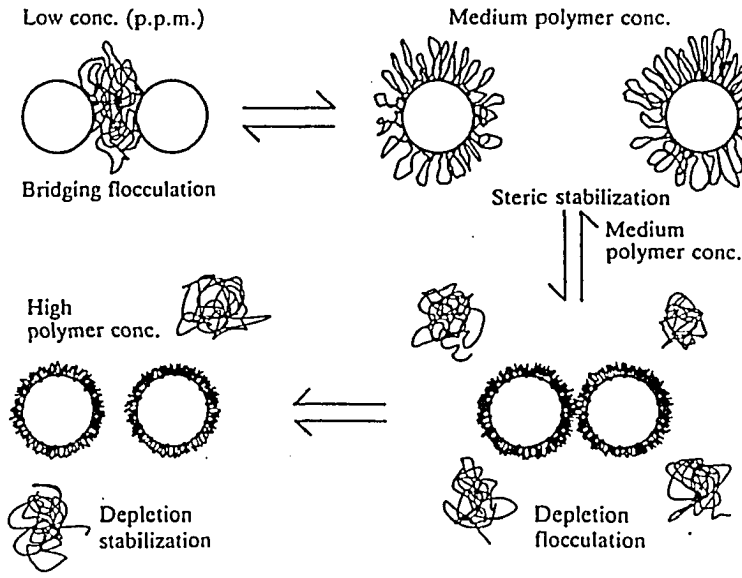

Figure 2-2. Steric stabilization as a function of polymer concentration. Taken from reference 4.

2-2.4 The Stability Ratio

Dispersion stability is an ambiguous term unless it can be quantified. This is usually accomplished through the stability ratio. The stability ratio, W, is defined as the ratio of the rapid flocculation rate constant, k_r (diffusion controlled), over the slow flocculation rate constant, k_s (actual), or the ratio of the slow flocculation half-life, $t^s_{½}$, over the rapid flocculation half-life $t_{½}$ as seen in Equation 2-9 below(3,4,9):

$$W = \frac{k_r}{k_s} = \frac{t^s_{½}}{t^r_{½}} \qquad 2\text{-}9$$

Strictly speaking, the stability ratio is a measure of the number of collisions two particles undergo before a doublet is formed(94). For example, a stability ratio of 50 indicates there are fifty collisions for every doublet formed. The stability ratio can be calculated by using the observed (slow) and calculated (rapid) flocculation rate constants. The rapid flocculation rate constant is the rate constant that would be obtained if the particles were to stick on every collision, driven purely by Brownian motion, hence a diffusion controlled process(4,9,94). Smoluchowski(95) derived an expression for this diffusion controlled rate constant by using a second order kinetic model with Fick's first law of diffusion and the Stokes-Einstein equation to yield:

$$k_r = \frac{8kT}{3\eta} = \frac{1}{t^r_{½}N_o} \qquad 2\text{-}10$$

where η is the viscosity of the fluid medium and N_o is the initial number of particles. Equation 2-10 applies to uniform spherical particles limited to the initial rates of flocculation.

The slow flocculation rate constant is the observed rate constant for the dispersion(9,94); it is based again on the initial stages of flocculation when essentially single pigment particles collide to form doublet flocs. Therefore, the initial stages of flocculation can be viewed as essentially a second order process of doublet formation from single pigment particles as illustrated below:

$$\frac{dN}{dt} = - k_s N^2 \qquad 2\text{-}11$$

$$N = N_o(1-X) \qquad 2\text{-}12$$

$$\frac{dX}{dt} = k_s N_o(1-X)^2 \qquad 2\text{-}13$$

where X is the fraction of doublets, N_o is the initial concentration of singlets, and t is time. Novich and Ring(96) employed a model that related the change in mean hydrodynamic radius with time to that of doublet formation with time:

$$\frac{dR_h}{dt} = R_s(\sqrt{2}-1)\frac{dX}{dt} \qquad 2\text{-}14$$

where R_h is the mean hydrodynamic radius and R_s is the single radius. At the initial stage of flocculation the fraction of doublets is small, so Equation 2-13 can be written as:

$$\left.\frac{dX}{dt}\right|_{t\to o} = k_s N_o \qquad 2\text{-}15$$

Combining Equations 2-14 and 2-15 and using the diameter instead of the radius yields the desired result:

$$k_s = [D_s(\sqrt{2}-1)N_o]^{-1}\left.\frac{dD_h}{dt}\right|_{t\to o} \qquad 2\text{-}16$$

From a plot of particle diameter versus time, an initial slope and intercept can be obtained(96,97). The initial slope of this plot is equal to dD_h/dt and the intercept is equal to D_s(96,97). By using the initial slope, intercept, and initial concentration of particles in Equation 2-16, the slow flocculation rate constant can be calculated, and when used with Equations 2-9 and 2-10, yields the stability ratio.

2-3 Experimental

2-3.1 Materials

The three rutile (titanium dioxide) pigments used in this study were the duPont R100, R901 and Al5 (which is treated R901). All three rutiles differ by the amount of alumina and silica. R100 has the least amount of these (2% for each).

R901 has a higher concentration than R100 (7% and 4%, respectively). The Al5 was prepared by precipitating hydroxylated alumina from a solution of sodium aluminate onto the surface of dispersed R901 by reducing the pH from 11.0 to 8.0. All three pigments were dried in a vacuum oven at 250°C for 8 hours.

The two charging agents used were GAF's RE410, nonyl phenol ethoxylated phosphate ester, and Chevron Chemicals' OLOA 370, a polybutene of about 70 carbon atoms attached to a succinic acid group which is reacted with diethylene triamine to provide the basic anchoring group(98). The RE410 is used as received while the OLOA 370 must be purified since it is supplied as a 50 wt% solution in mineral oil. It was de-oiled by adsorption from toluene onto silica followed by elution with acetone(99,100). The cyclohexane was Aldrich Chemical Company's HPLC grade and was dried over 8-12 mesh Davison 3 A molecular sieves (activated for 8 hours under vacuum at 250°C).

2-3.2 Procedures

All pigment dispersions were made from stock dispersions. An aliquot of 50 ml of stock dispersion was mixed with a 50 ml aliquot of the appropriate solution of charging agent such that a series varying in concentration was prepared for each pigment with each charging agent (a total of six series). Six stock dispersions (two for each pigment) were prepared by sonicating (Branson Sonic Probe) a known weight (between 4 and 6 mg per 100 ml of medium) of a pigment in a liter of

cyclohexane for one half hour. This dispersion was then placed in a sonic bath for a twenty-four hour period, after which 50 ml aliquots were pipetted into 110 ml glass bottles (equipped with teflon-lined caps) containing 50 ml of charging agent solution to make the final dispersion. The charging agent solutions (used in the final dispersions) were prepared from a stock solution of charging agent in dry cyclohexane and diluted to the appropriate concentrations with cyclohexane. These concentrations varied from $1.2x10^{-6}$ to $1.2x10^{-2}$ M for the OLOA 370 series and from $2x10^{-5}$ to 0.4 M for the RE410 series. Each 100 ml final dispersion was probe sonicated for 5 minutes then placed in a sonic bath for 24 hours, after which it was placed on a rolling mill for 5 days (to effect adsorption). Aliquots from the final dispersions could then be taken for adsorption isotherm studies as well as zeta potential and stability studies. In the cases of the zeta potential and stability studies, each final dispersion was probe sonicated for 3 minutes, allowed to come to equilibrium for 5 minutes, then sonicated for 15 seconds before making any measurement. This procedure yielded the minimum mean particle size as evidenced by PCS and SEM. Any further sonication did not lower the mean particle size.

The charging agent concentration in the supernatant was measured by UV-Vis absorption. This measurement was directly possible in the case of RE410 because it has an absorption peak at 276 nm which follows Beer's Law from 0.05 mM to 1.2 mM (0.06 to 1.7 absorbance units). Any of the supernatant concentrations that were above 1.2 mM were diluted with cyclohexane before measuring. The

supernatant concentration in the OLOA 370 case was measured indirectly by the method of Fowkes and Co-workers(66,101,102). Fowkes' method was employed by interacting the basic OLOA 370 with the acidic indicator dye, Bromophenol Magenta E (Eastman-Kodak 6810) in cyclohexane. The indicator dye in cyclohexane is yellow with an absorption at 390 nm. As OLOA 370 is added it turns blue and then magenta with increasing amounts of OLOA 370. Its absorption peak is at 600 nm with an isobestic point at 460 nm. The concentration of OLOA 370 in the supernatant was determined at 600 nm in the Beer's Law region(101,102).

2-3.3 Instrumentation

The zeta potentials were calculated from mobility measurements (those which gave a parabolic flow profile) using the Hückel equation(15,103). Measurements were made using Coulter's DELSA 440 or PEN KEM 3000 micro electrophoretic instrument (described earlier). Experiments were performed in ascending order of charging agent concentration. The electrophoresis cell was conditioned with the appropriate concentration for 2 hours before use except that, with the lowest concentration the time was 24 hours. Both instruments were set in the constant voltage mode, which was set at 300 V/cm. All physical properties required by the instrument were those of the medium and not the pure solvent. These include viscosity, refractive index, and dielectric constant. The viscosities of the media were determined by a Ubbelohde viscometer, placed in a temperature

bath at 25°C. The refractive indices were determined by a Bausch & Lomb Abbe refractometer. The dielectric constants were measured by a WTW (Wiss. Tchn. Werkstätten) Dipolmeter type OMOL.

Conductivity measurements were made using a cylindrical teflon cell with stainless steel ends which served as electrodes and whose positions were adjustable. A 90 V potential was maintained across the cell while the current through the cell was measured by a Keithly model 1420 Electrometer. The conductivity of the dispersion could be calculated from the current by using the cell constant (which was both measured and calculated)(104,105,106). The conductivity due to the counter-ions in the dispersion was obtained by subtracting the dispersion conductivity from the conductivity obtained from the pure solution of charging agent(39,50,105).

The stability studies were accomplished through the use of photon correlation spectroscopy (PCS) with the Coulter N_4MD multi-angle, multi-τ photon correlation spectrometer, which was used at a 90 degree scattering angle and 1000 second run time. Sample times were determined automatically by the auto-ranging option of the N_4MD. Intensities ranged from $5x10^5$ to $1x10^6$ counts/sec. Only data from runs with autocorrelation functions of the shape in Figure 2-3b were judged acceptable(41). If the autocorrelation function deviated greatly from Figure 2-3b and appeared more like Figure 2-3a the data was discarded. Each sample was sonicated for two minutes, equilibrated for 5 minutes, then sonicated for 15 seconds, after which it was immediately placed in the sample chamber prior to commencement of the

Figure 2-3a. Multi-τ

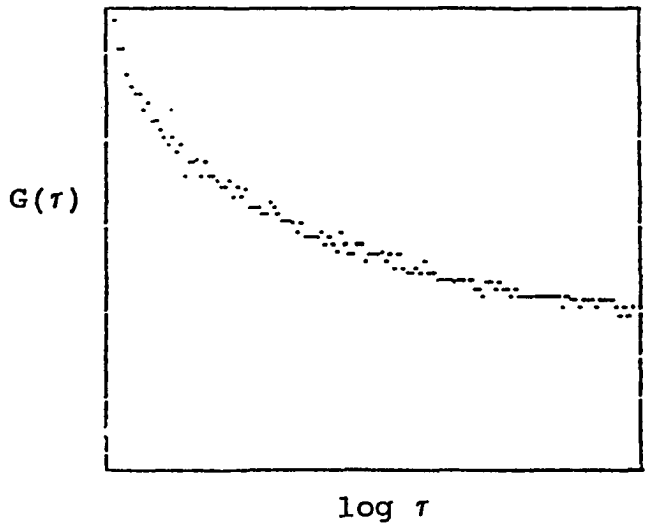

Figure 2-3b. Multi-τ

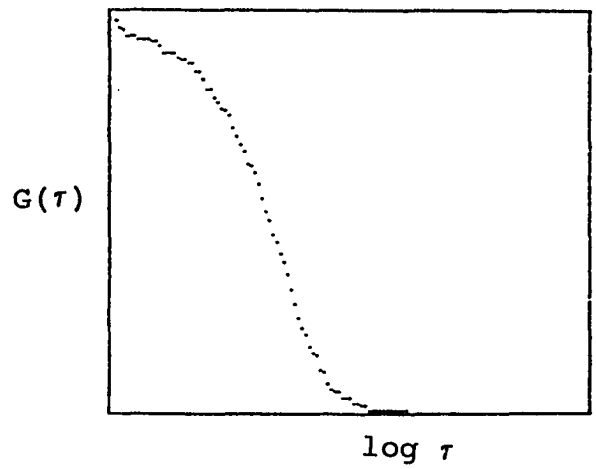

Autocorrelation diagrams. Figure 2-3a is unacceptable while Figure 2-3b is acceptable. Obtained from a Coulter N_4 MD.

measurement. In each case the refractive index of the medium (solvent and charging agent) was measured and used as an instrument parameter. The temperature was kept at 25°C automatically by the instrument heating block.

Surface areas of the dry pigments were determined by nitrogen adsorption with the ASTM monosorb method using a Quantachrom single-point BET instrument. Each sample was first out-gassed (purged with N_2 gas at 100°C) for 24 hours to remove volatile impurities. Sample weights averaged half a gram. Three surface areas were determined for each sample and averaged.

2-3.4 The Structures of the Charging Agents

As was mentioned earlier, OLOA 370 is a 70 carbon polybutene with an amino succinimide head group. The head group can cover a surface area on the order of 44 Å^2(107,108). Previous work (109) has shown that the OLOA 370 can achieve a film thickness of 50 Å. The structure of OLOA 370 can be seen below:

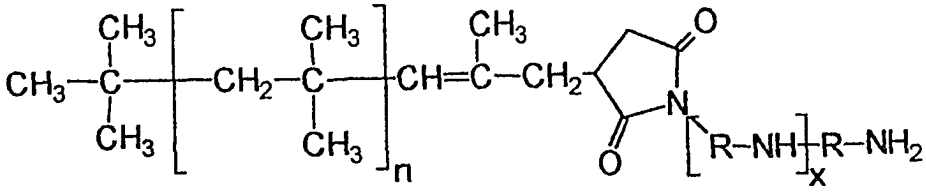

R = C_2H_4

Figure 2-4. The structure of OLOA 370.

The amine head group of OLOA 370 is basic and will accept protons or donate an electron pair to yield a negatively charged surface resulting in a negative zeta potential(110). The hydrocarbon tail is neutral, therefore it does not undergo acid-base interactions and will not affect the charge(110). The tail is soluble in low dielectric media, such as cyclohexane, and will tend to stay in solution while the head group adsorbs to the rutile's surface.

RE410 is a nonyl phenol ethoxylated phosphate ester. Its phosphate head group can cover a surface area on the order of 31 Å^2(108,111). In the proper environment (good solvent) the conformation is such that the molecule is elongated, although still in a random coil, and normal to the surface with a length on the order of 30 Å. This means a film thickness on the order of 30 Å is possible on monolayer coverage if the molecule is normal to the surface. The structure of RE410 is shown below:

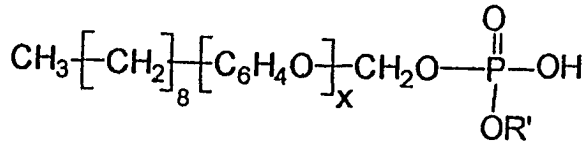

R = -CH_3, -C_2H_5, etc.

Figure 2-5. The structure of RE410.

The phosphate head group is acidic (112) and can donate a proton to or accept an electron pair from the surface, leaving the surface charged positively. The tail is part hydrocarbon chain (end) and part repeating phenyl ether groups (middle). The hydrocarbon end is neutral, as is the tail of OLOA 370, and will not charge the surface(6,110). The phenyl ether middle is basic, electron rich, and could charge the surface negatively(110) or at least interact with acidic sites such as other phosphate head groups or acidic surface sites(108).

2-4 Results And Discussion

2-4.1 Titanium Dioxide ESCA Results

All three rutile titanium dioxide pigments were analyzed by a Perkin-Elmer ESCA instrument courtesy of Perkin-Elmer of Edison New Jersey. The results of the elemental analysis are listed in Table 2-1.

Pigment	Al%	Ti%	O%	C%	Cl%	N%	Na%	Si%	Al/Ti
R100	10.6	16.8	34.6	34.5	0.5	1.1	-	1.3	0.5
	8.6	10.7	55.3	23.5	-	1.1	-	0.7	0.8
R901	11.3	1.0	27.7	55.1	0.4	-	-	4.6	11.3
	16.9	1.3	59.6	14.6	-	-	-	7.6	13.0
A15	24.6	0.7	39.6	29.7	0.9	-	1.6	3.0	35.1
	23.0	0.3	62.7	11.7	-	-	-	2.3	76.7
	20.3	0.4	55.0	21.8	-	-	-	2.5	50.8

Table 2-1. The percentages of the elements on the surface of the three rutile pigments. The last column is the ratio of the percentage of aluminum to titanium.

As can be seen from the table above, the percentage of aluminum increases as the first column is descended, while just the opposite happens for titanium. Therefore the surface with the most aluminum (hence alumina) is Al5, followed by R901 and lastly, R100. This observation is reflected in the last column as the ratio of aluminum to titanium(113,114). Whereas both R901 and R100 have aluminum in the rutile, the R901 has added alumina coated on the surface. R100 has no coating. Al5 was made by increasing the alumina coating of R901. R901 has more silica on the surface than R100 or A15. This silica will make the R901 more acidic; perhaps neutralizing the effects of the alumina and yielding a surface whose acidity is close to R100. It could also yield a surface that is more amphoteric than either R100 or A15. The large percentage of carbon on the surface is from atmospheric organic particulates that tend to plague most samples(114,115).

2-4.2 The Size and Shape of the Pigments

The average particle size for all three pigments is 300 nm, as evidenced by electron microscopy (see Appendix I) and PCS (shown later). The shape is approximately spherical as seen in the SEM pictures in Appendix I.

2-4.3 The Zeta Potential of the Pigments in Low Dielectric Constant Media

The zeta potential was calculated from mobility measurements (listed in Table 2-2) for each of the six dispersion series (i.e,. R100, R901, and Al5 in OLOA 370 and

Mobility $\left(\frac{m^2}{V\text{-}s}\right)$ $(x10^{+10})$

Concentration (M)	R100	R901	A15
RE410			
$1.014x10^{-4}$	0.89 ± 0.18	2.02 ± 0.35	1.86 ± 0.36
$1.014x10^{-3}$	2.07 ± 0.25	3.47 ± 0.40	3.37 ± 0.55
$4.066x10^{-3}$	3.57 ± 0.30	9.17 ± 1.10	3.89 ± 0.39
$6.010x10^{-3}$	4.87 ± 0.44	9.28 ± 0.36	6.22 ± 1.05
$1.016x10^{-3}$	5.30 ± 0.55	5.66 ± 0.71	6.54 ± 1.15
$3.050x10^{-2}$	2.89 ± 0.39	4.76 ± 0.73	5.93 ± 0.82
$6.099x10^{-2}$	2.62 ± 0.28	4.97 ± 0.72	4.97 ± 0.82
$1.016x10^{-1}$	2.94 ± 0.15	4.60 ± 0.30	3.47 ± 0.45
0.2033	2.73 ± 0.51	6.01 ± 0.68	6.35 ± 0.85
OLOA 370			
$6.626x10^{-7}$	4.02 ± 0.63	4.26 ± 0.61	3.62 ± 0.85
$6.626x10^{-6}$	4.98 ± 1.11	5.52 ± 1.21	4.27 ± 0.77
$6.626x10^{-5}$	12.80 ± 1.10	11.60 ± 1.63	8.38 ± 1.42
$6.626x10^{-4}$	7.95 ± 0.81	7.95 ± 0.85	4.69 ± 1.51
$6.626x10^{-3}$	0.86 ± 0.71	3.32 ± 0.65	2.70 ± 0.82

Table 2-2. Mobility measurements for all six dispersion series. Each quantity is an average of ten measurements.

RE410) using the Hückel equation (1-3). The Hückel equation also required viscosity and dielectric constant data (Figures 2-6 and 2-7) for each concentration of charging agent. In addition, all three light scattering instruments needed refractive index data for each concentration of charging agent (Figure 2-8). The dispersions with the highest zeta potential are expected to be the most stable to flocculation, since the zeta potential is a measure of the electrostatic repulsion between particles. If the zeta potential is plotted against charging agent concentration (Figures 2-9 and 2-10), a maximum in zeta potential can be seen for each series. This maximum has been shown to occur in most non-aqueous (52,53,54) as well as many aqueous dispersions(116). It is at this maximum that the electrostatic repulsion is greatest and the dispersions are expected to be the most stable. Therefore at first glance of Figure 2-9 (OLOA 370 series) both R100 and R901 pigments should be more stable than A15. It should be noted that the A15, which has the most basic surface, has the lowest zeta potential in the presence of the basic charging agent OLOA 370. This observation is in accord with the Fowkes acid-base mechanism which predicts that the surface with the greatest number of acidic sites will undergo the most acid-base interactions with a basic charging agent. The more acid-base interactions, the higher the charge that is imparted to the surface, hence a higher zeta potential. Since Al5 has more alumina on its surface than the other pigments, it should have a larger number of basic sites and have less acid-base interactions with OLOA 370. Thus with A15 the predicted lower zeta potential is observed. The converse should

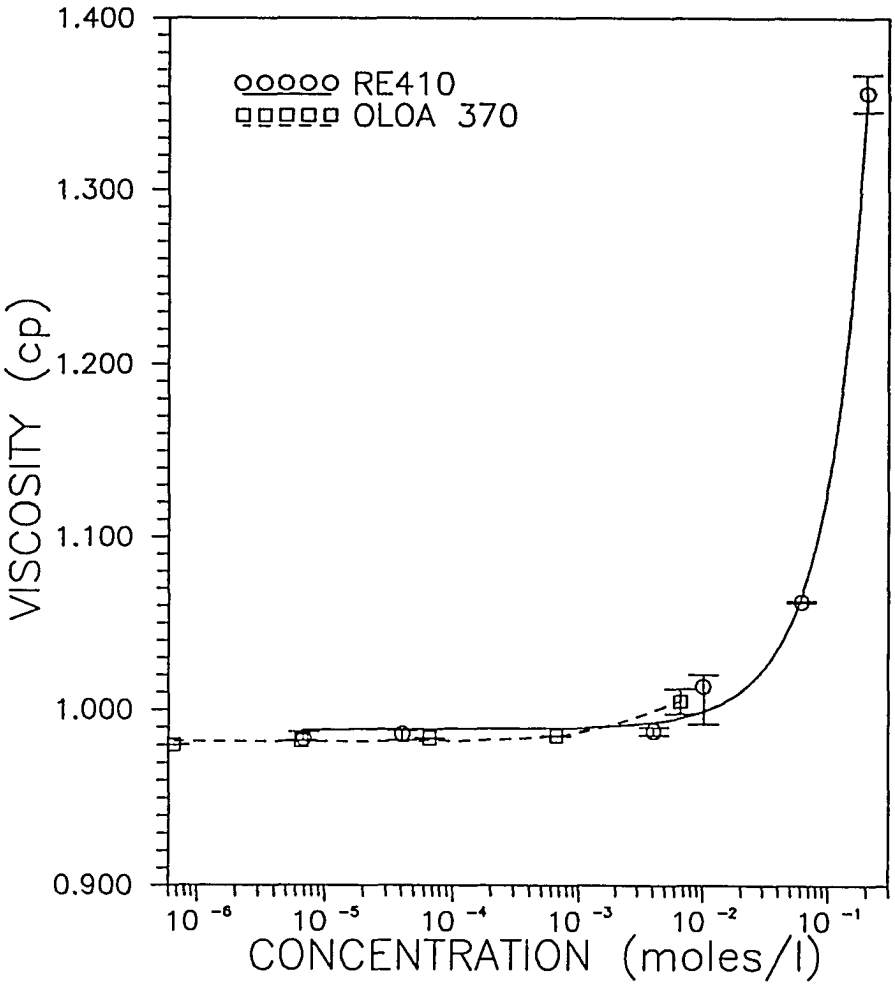

Figure 2–6. The viscosity versus concentration of RE410 and OLOA 370 in cyclohexane. Each point is an average of five measurements.

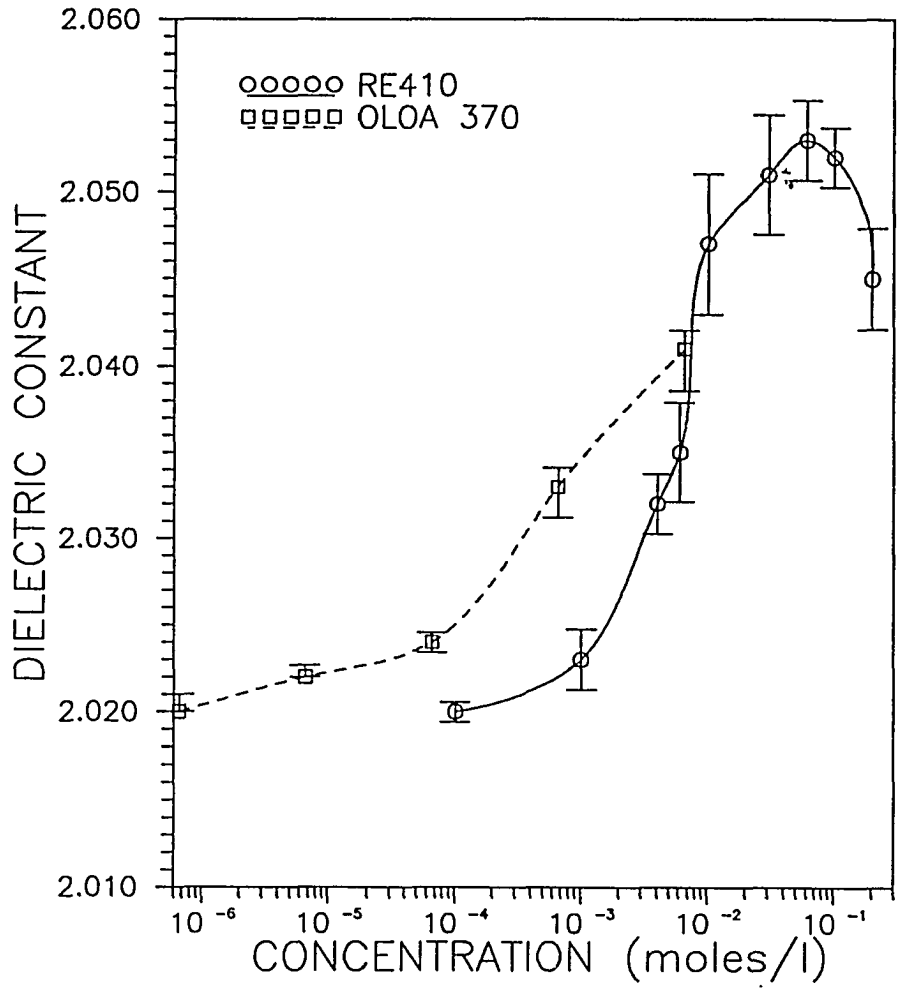

Figure 2–7. The dielectric constant versus concentration of RE410 and OLOA 370 in cyclohexane. Each point is an average of five measurements.

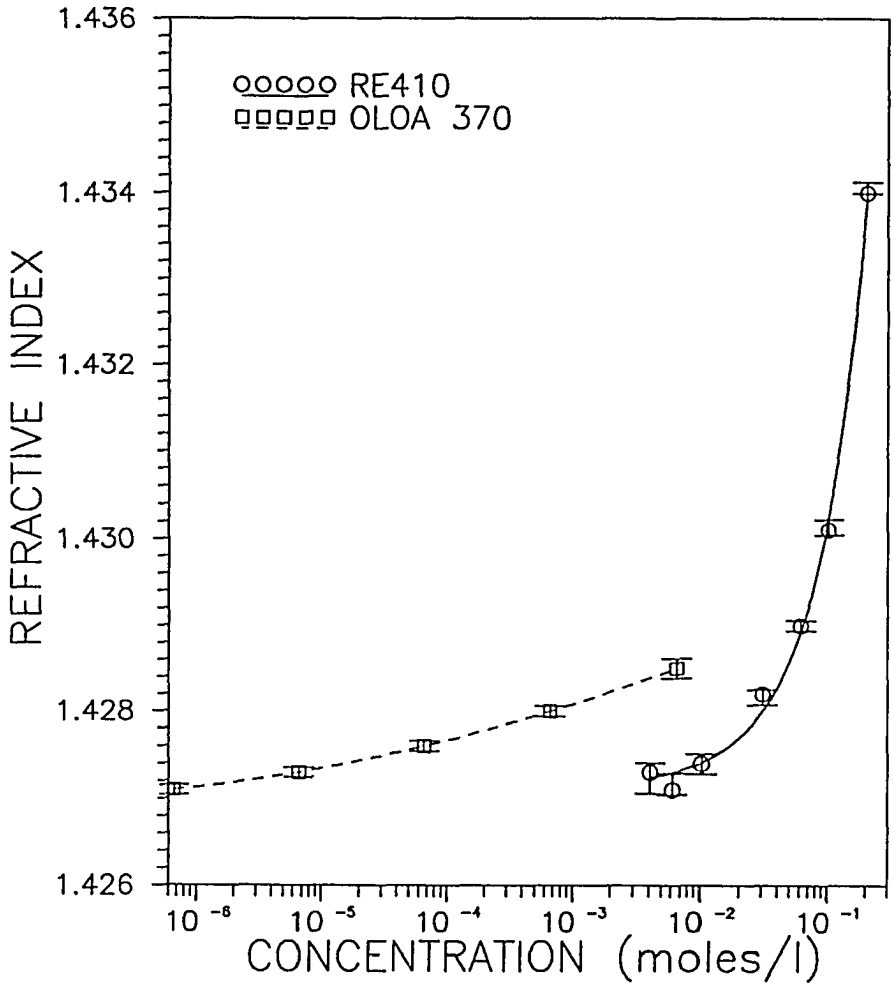

Figure 2–8. The refractive index versus concentration of RE410 and OLOA 370 in cyclohexane. Each point is an average of five measurements.

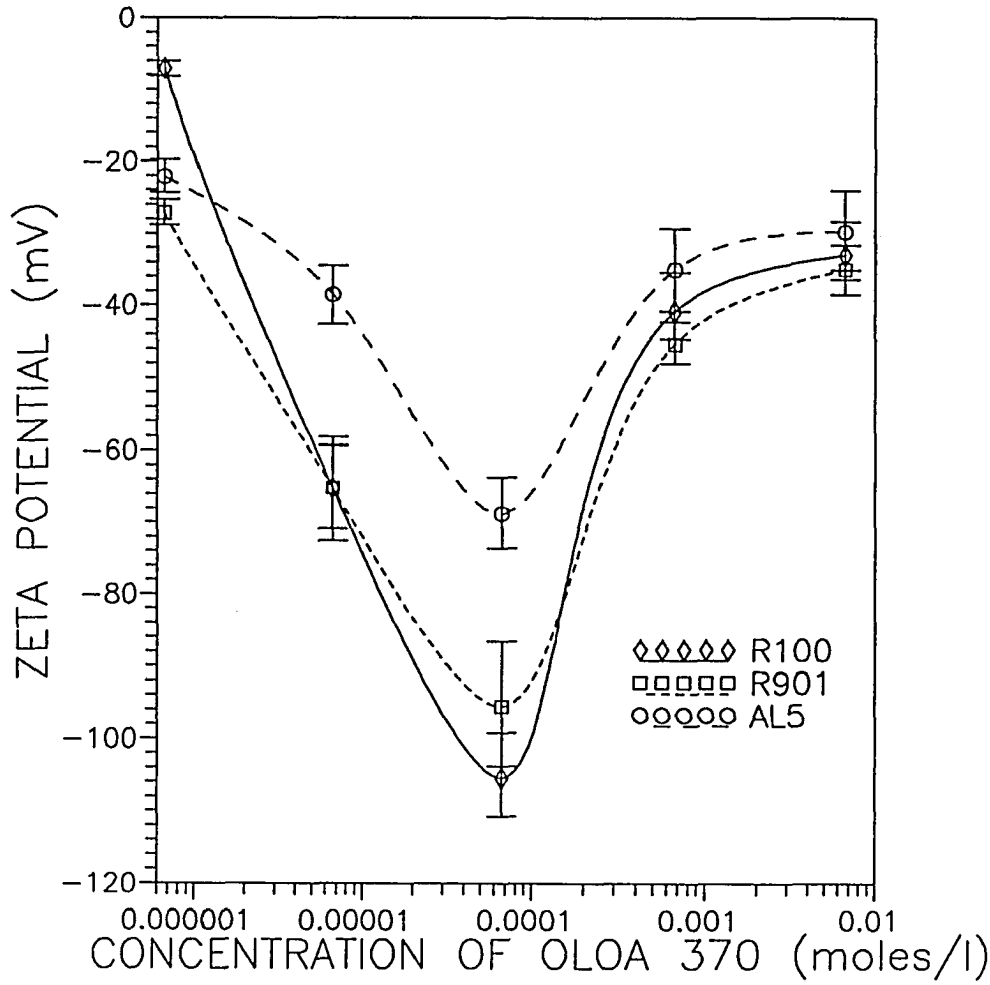

Figure 2–9. The zeta potential versus the concentration of OLOA 370 in cyclohexane for 0.003 wt% of the three pigments. Each point is an average of ten measurements.

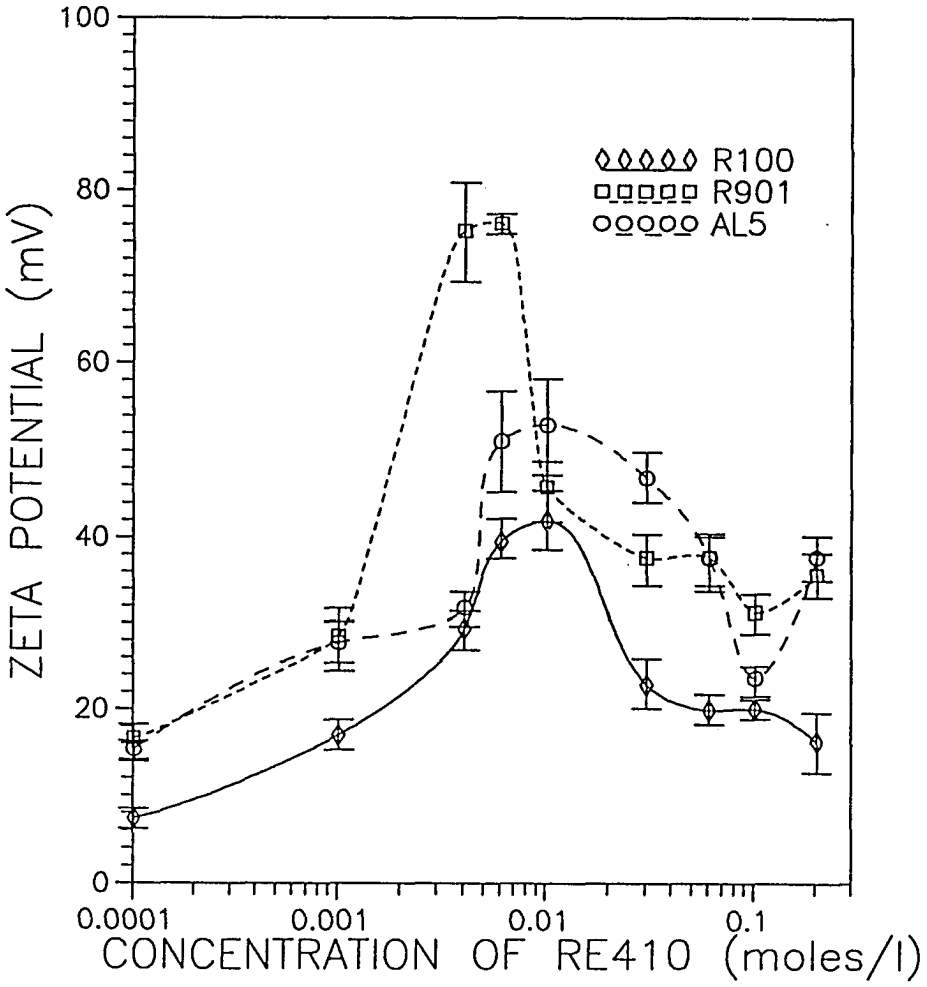

Figures 2–10. The zeta potential versus the concentration of RE410 in cyclohexane for 0.003 wt% of the three rutile pigments. Each point is an averge of ten measurements.

be true for the basic surface sites for the three rutile pigments and the acidic charging agent RE410 (noting that the rutile pigments are heterogeneous and possess both acidic and basic surface sites). In the RE410 series of dispersions, Al5 is expected to have the highest zeta potential. As can be seen in Figure 2-10, no real trend in acidity or basicity is followed. There is no apparent reason for the absence of a trend. The problem becomes complicated when an amphoteric charging agent like RE410 and a heterogeneous surface interact. Several possibilities are likely and will be explored in the following sections.

2-4.4 The Conductivity of The Dispersions

As particles in a dispersion become charged, counter-ions are produced (see Figure 1-3). Therefore the counter-ion concentration can be used as a measure of the surface charge density, which is a measure of the zeta potential. The conductivity of a dispersion can be used as a tool to estimate counter-ion concentrations, since they are directly proportional to each other, as shown by Fowkes(71,109), and by Klinkenberg and van der Minne(117). These workers have shown that the conductivity due to counter-ions only, can be obtained by subtracting the conductivity of the medium (the liquid and additives or the continuous phase) from that of the dispersion. This procedure is valid only at charging agent concentrations beyond that at which minimum conductivity is reached. This subtraction procedure was done for the OLOA 370 and RE410 series (Figures 2-11 and 2-12). As can be seen in Figure 2-11 (OLOA 370 series) both the R901 and R100 conductivity curves coincide, indicating that the counter-ion concentrations are the same. This observation is in agreement with the zeta potential data in Figure 2-9. In addition further agreement can be seen for the Al5 series whose conductivity is less in the intermediate range, the same range in which its zeta potential is less than the R901 and R100 series.

The RE410 dispersion study presents a different story. It appears from Figure 2-12 (RE410 study) that the counter-ion concentration is about the same for each pigment series. This trend is not quite what is observed with the zeta potential data. Figure 2-10 suggests that the peak in the R901 zeta potential curve may be irregular

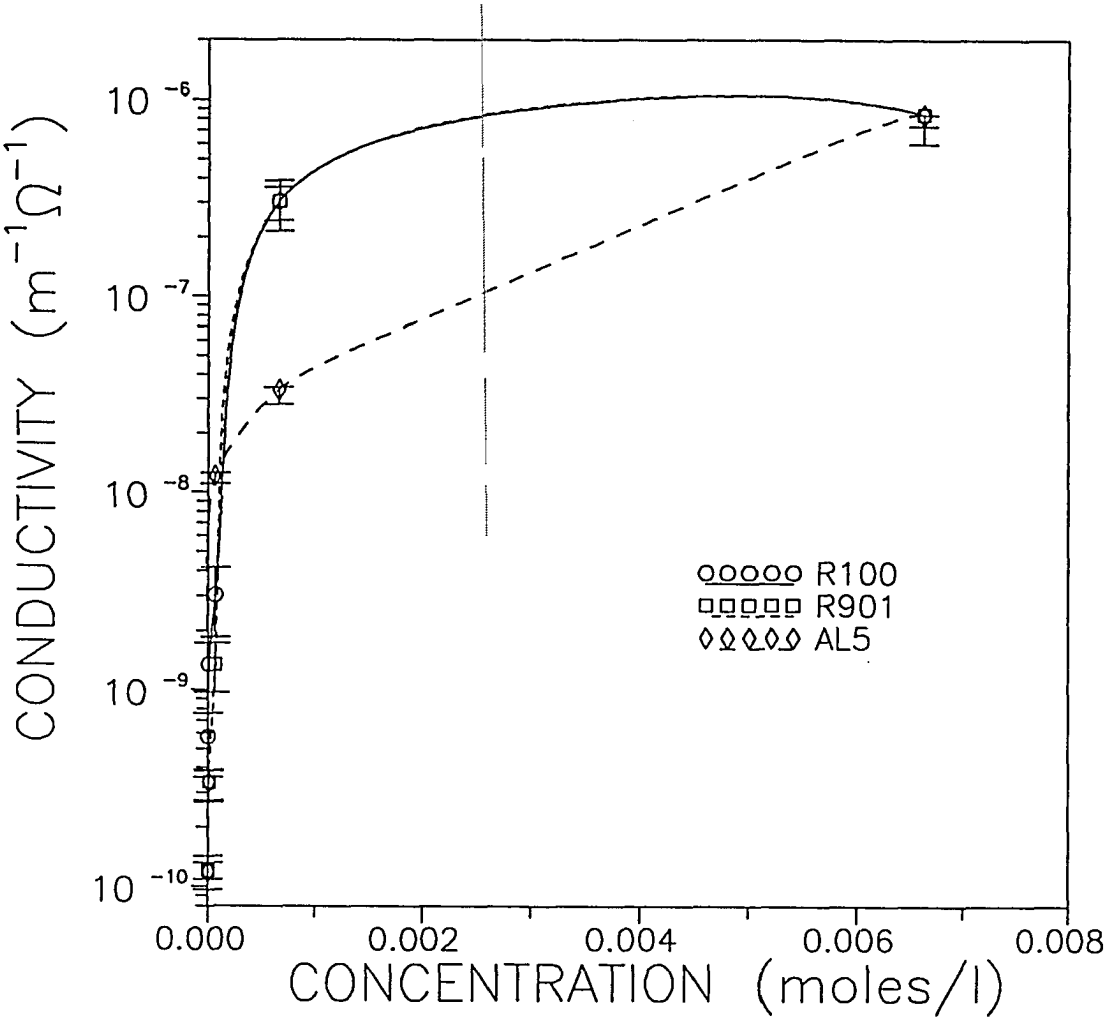

Figure 2–11. The conductivity (due to the counter–ions) versus OLOA 370 concentrations with 0.002 wt% of pigment.

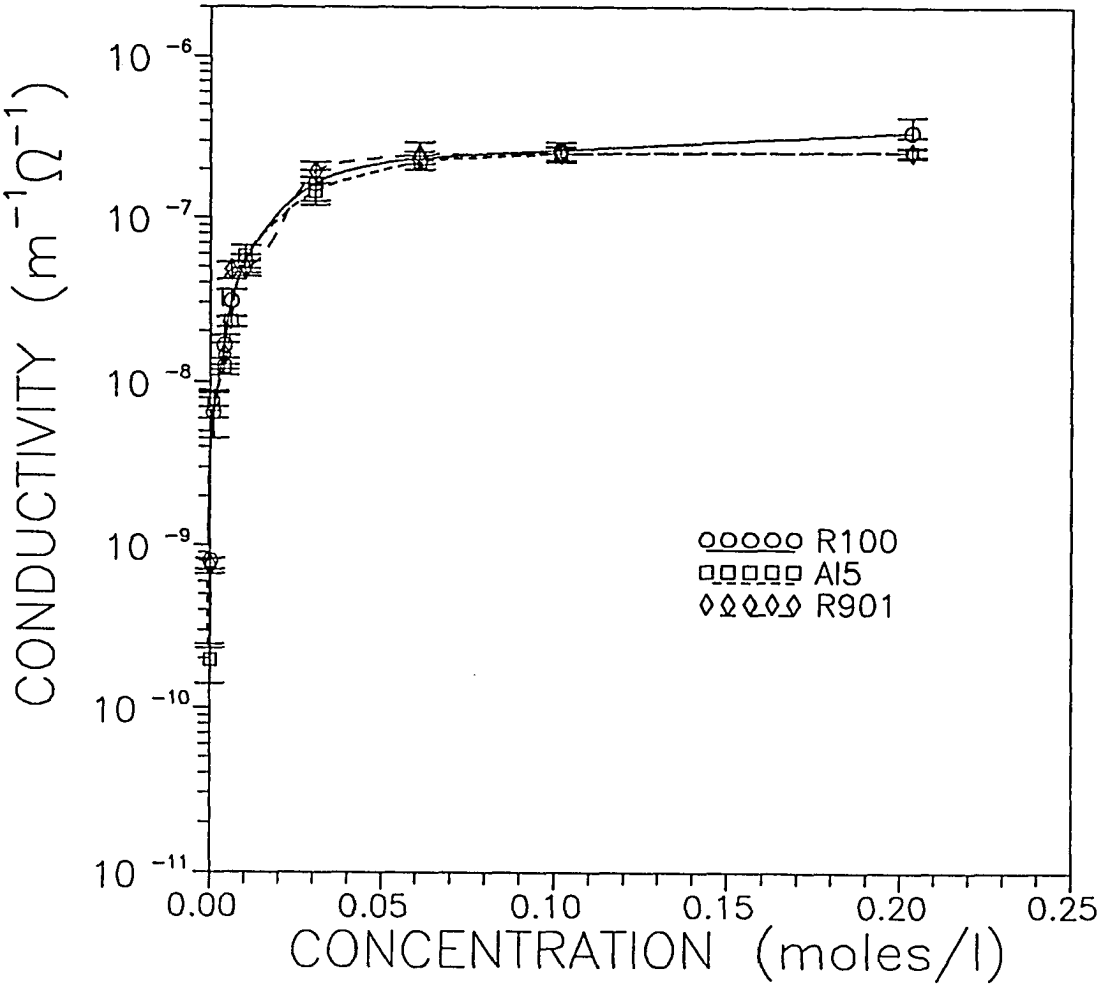

Figure 2–12. The conductivity (due to counter–ions) versus RE410 concentrations with 0.003 wt% of pigment.

and that all three pigments charge equally well. If indeed this is the case, all three pigments would be equally stable from an electrostatic perspective, but at a lower potential than with OLOA 370.

2-4.5 Dispersion Stability

The stability of the six dispersion series was quantified by the stability ratio. As was mentioned in Section 2-2.4, the stability ratio is a ratio of the rapid flocculation rate constant (k_r) over the slow flocculation rate constant (k_s) (Equation 2-9). The rapid flocculation rate constant is calculated from Equation 2-10, but the slow rate constant must be calculated from equation 2-16 using experimental data. The required data consist of the slope and intercept from plots of the apparent particle size (via PCS) versus time data (Figures 2-13 through 2-18). Notice that not all the curves in Figures 2-13 through 2-18 can be compared directly since the rate of floc growth is particle concentration dependent. The initial concentration of particles is accounted for in the calculation of the slow flocculation rate constant (Equation 2-16), thereby "normalizing" the stability ratio(96,97). The stability ratios were calculated (via Equations 2-16, 2-10 and 2-9) from the initial slopes and intercepts of Figures 2-13 through 2-18, to yield Figures 2-19 and 2-20.

For the RE410 series, all three pigments reach their maximum stability ratios at concentrations far lower than that required to obtain their maximum zeta potential. In other words, the electrostatic repulsion contributes very little to the overall stability at the most stable region or even at high concentration. In addition

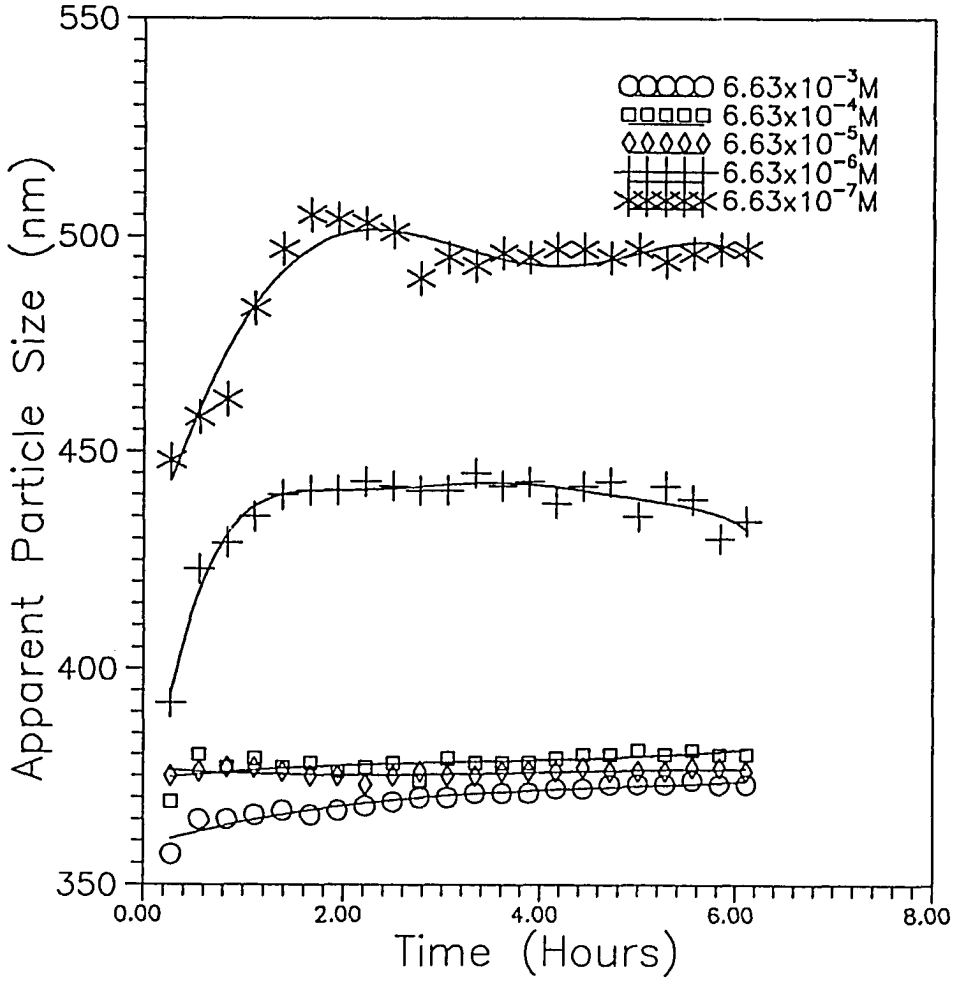

Figure 2–13. The apparent particle size (nm) as a function of time (hours) using R100 rutile titanium dioxide for varying concentrations of OLOA 370 in cyclohexane. Measurements were made on the Coulter N_4MD, a PCS instrument. Error bar sizes are on the order of the character sizes.

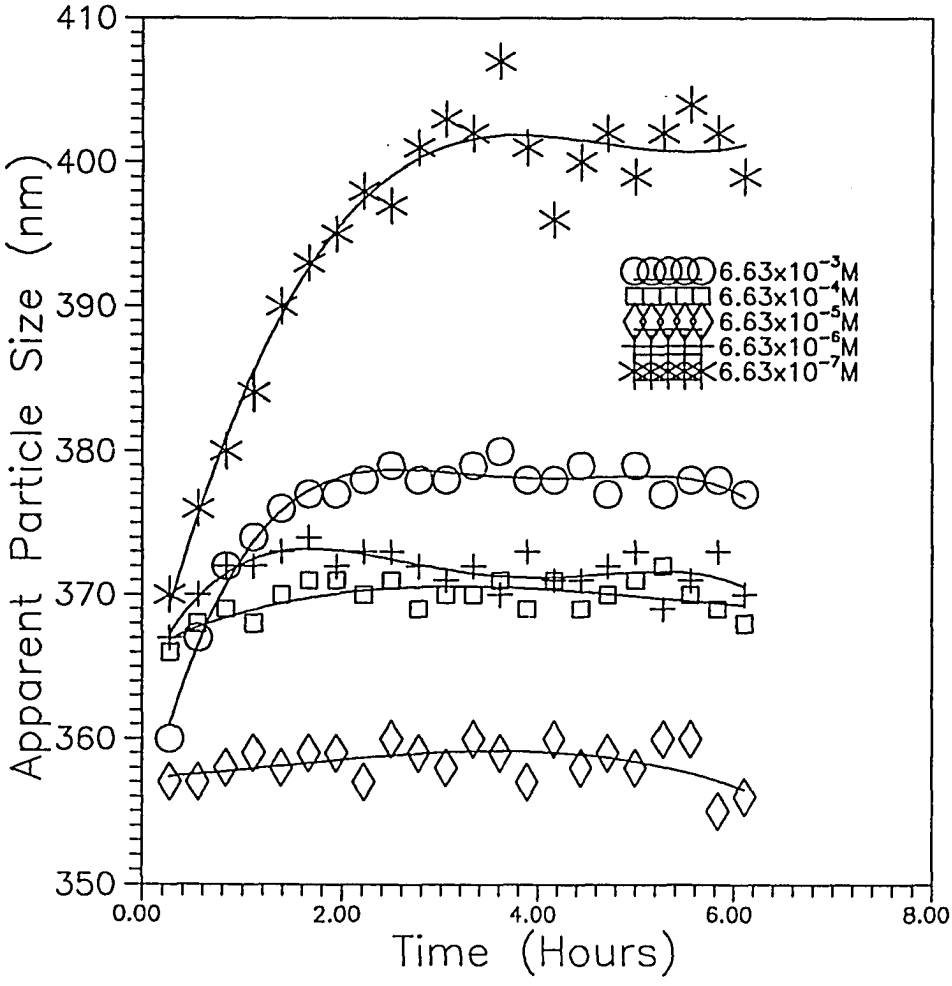

Figure 2–14. The apparent particle size (nm) as a function of time (hours) using R901 rutile titanium dioxide for varying concentrations of OLOA 370 in cyclohexane. Measurements were made on the Coulter N_4MD, a PCS instrument. Error bar sizes are on the order of the character sizes.

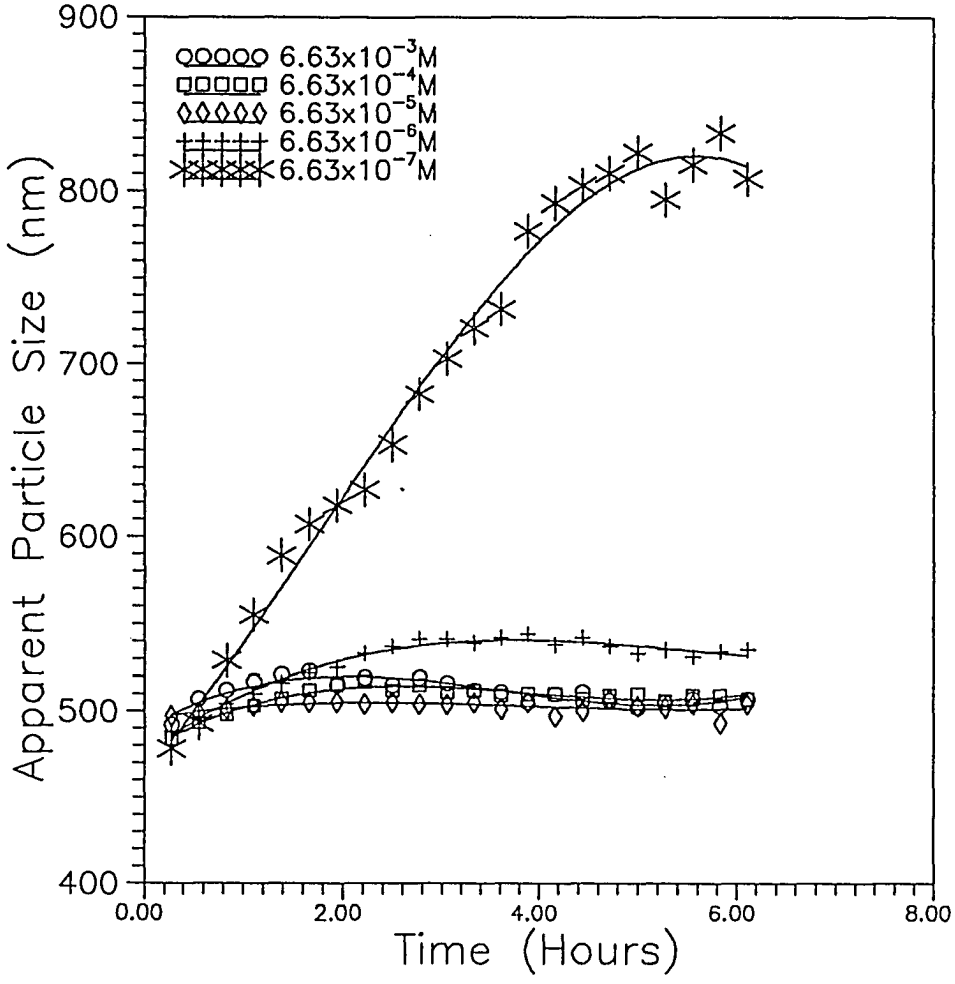

Figure 2–15. The apparent particle size (nm) as a function of time (hours) using Al5 rutile titanium dioxide for varying concentrations of OLOA 370 in cyclohexane. Measurements were made on the Coulter N_4MD, a PCS instrument. Error bars sizes are on the order of the character sizes.

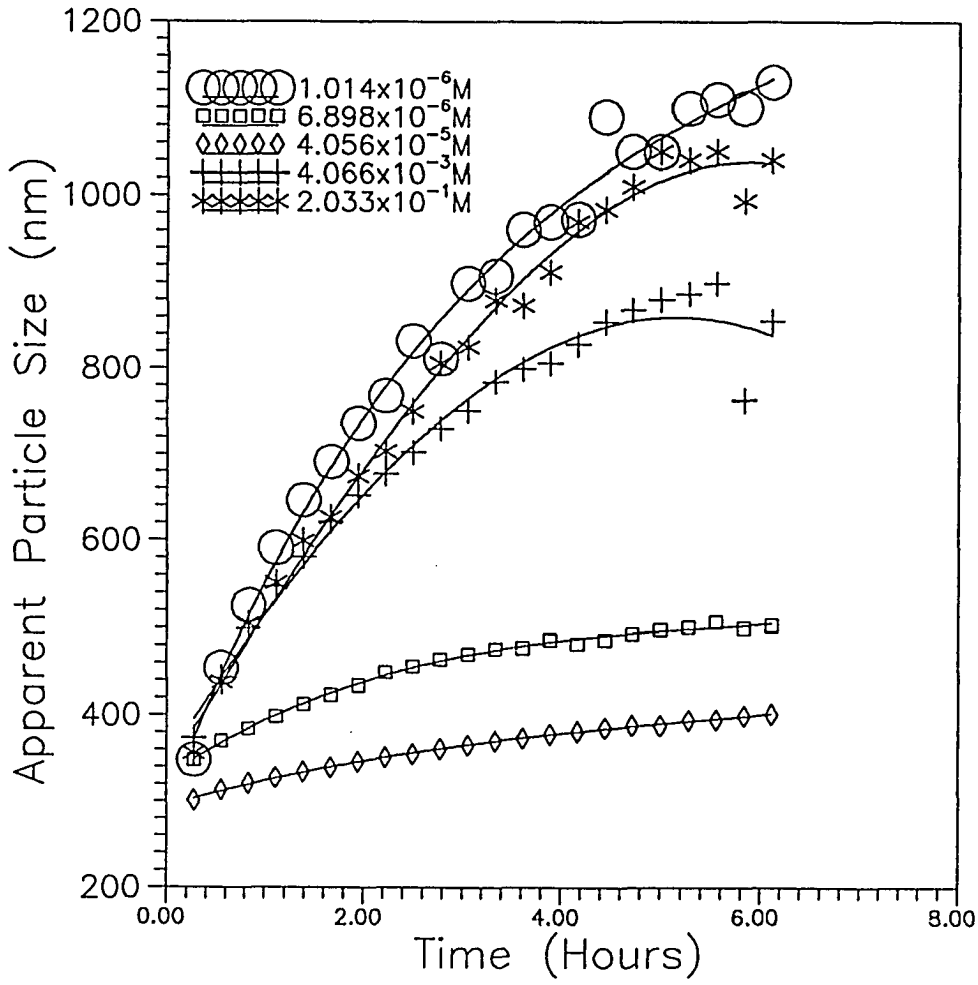

Figure 2–16. The apparent particle size (nm) as a function of time (hours) using R100 rutile titanium dioxide for varying concentrations of RE410 in cyclohexane. Measurements were made on the Coulter N_4MD, a PCS instrument. Error bar sizes are on the order of the character sizes.

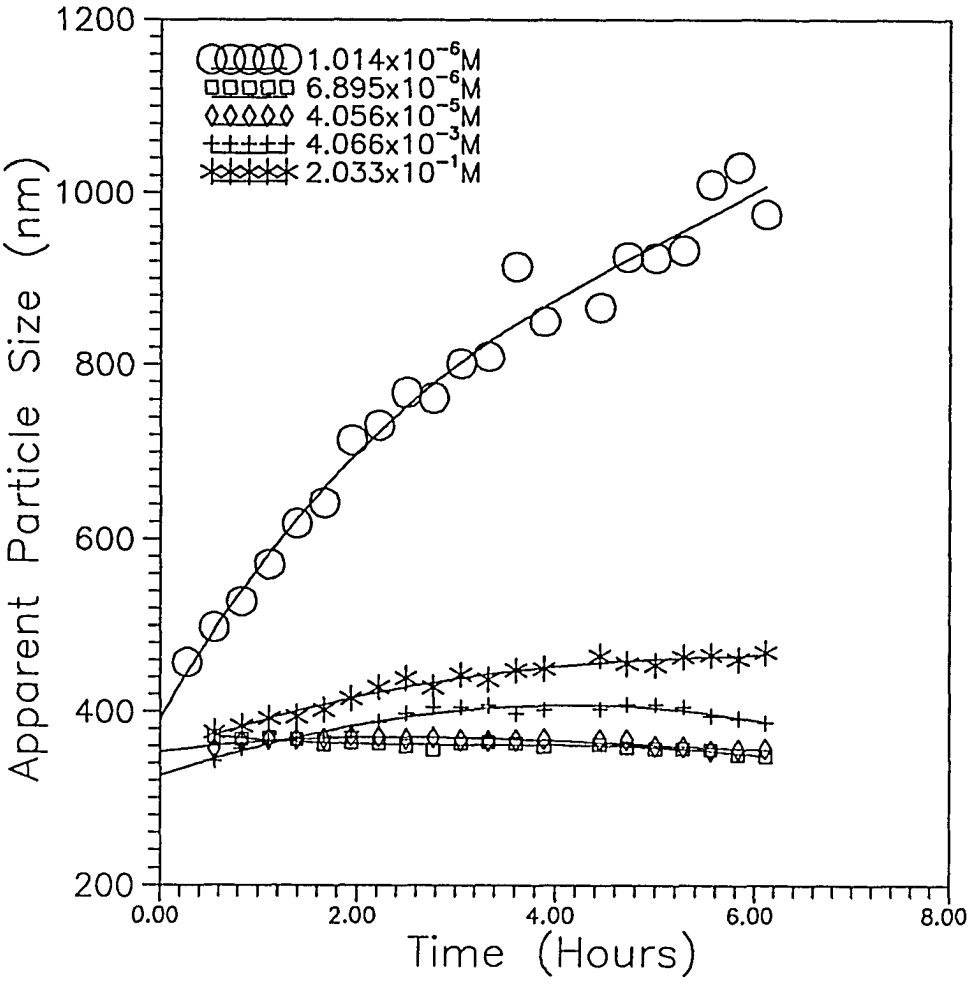

Figure 2--17. The apparent particle size (nm) as a function of time (hours) using R901 rutile titanium dioxide for varying concentrations of RE410 in cyclohexane. Measurements were made on the Coulter N$_4$MD, a PCS instrument. Error bar sizes are on the order of the character sizes.

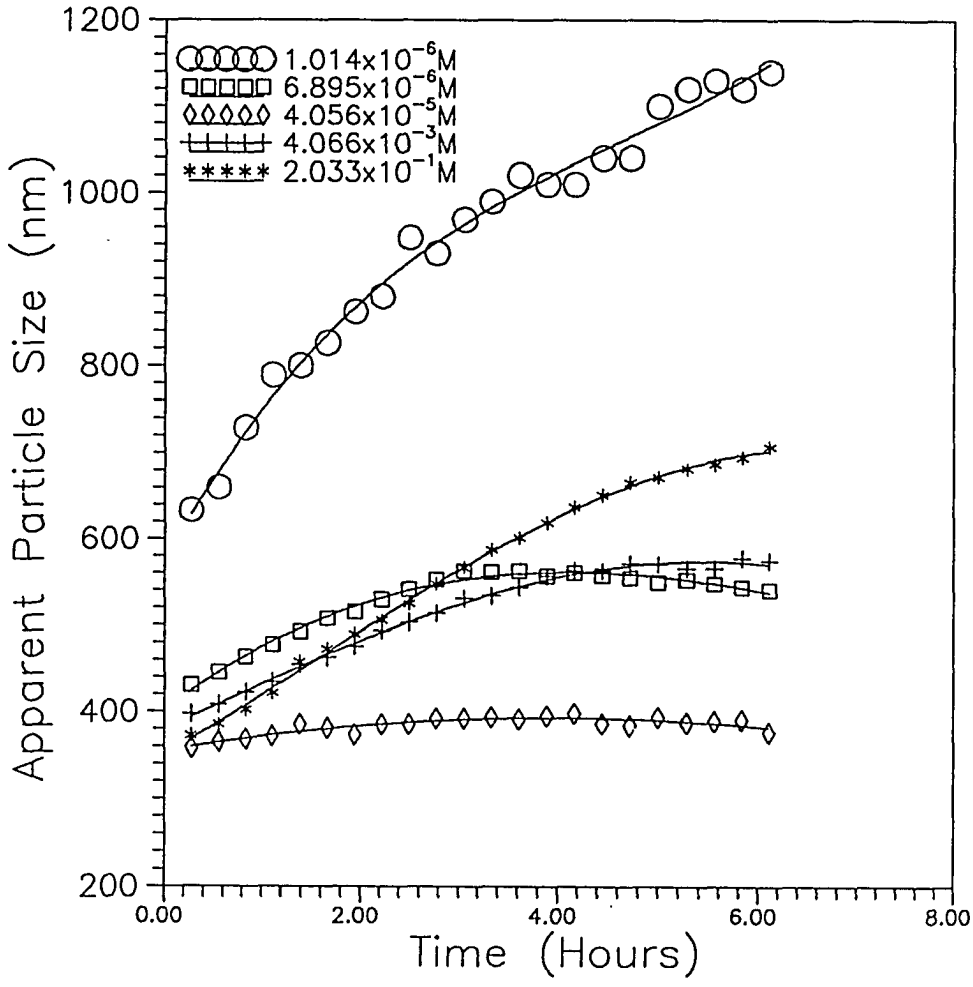

Figure 2–18 The apparent particle size (nm) as a function of time (hours) using Al5 rutile titanium dioxide for varying concentrations of RE410 in cyclohexane. Measurements were made on the Coulter N_4MD, a PCS instrument. Error bar sizes are on the order of the character sizes.

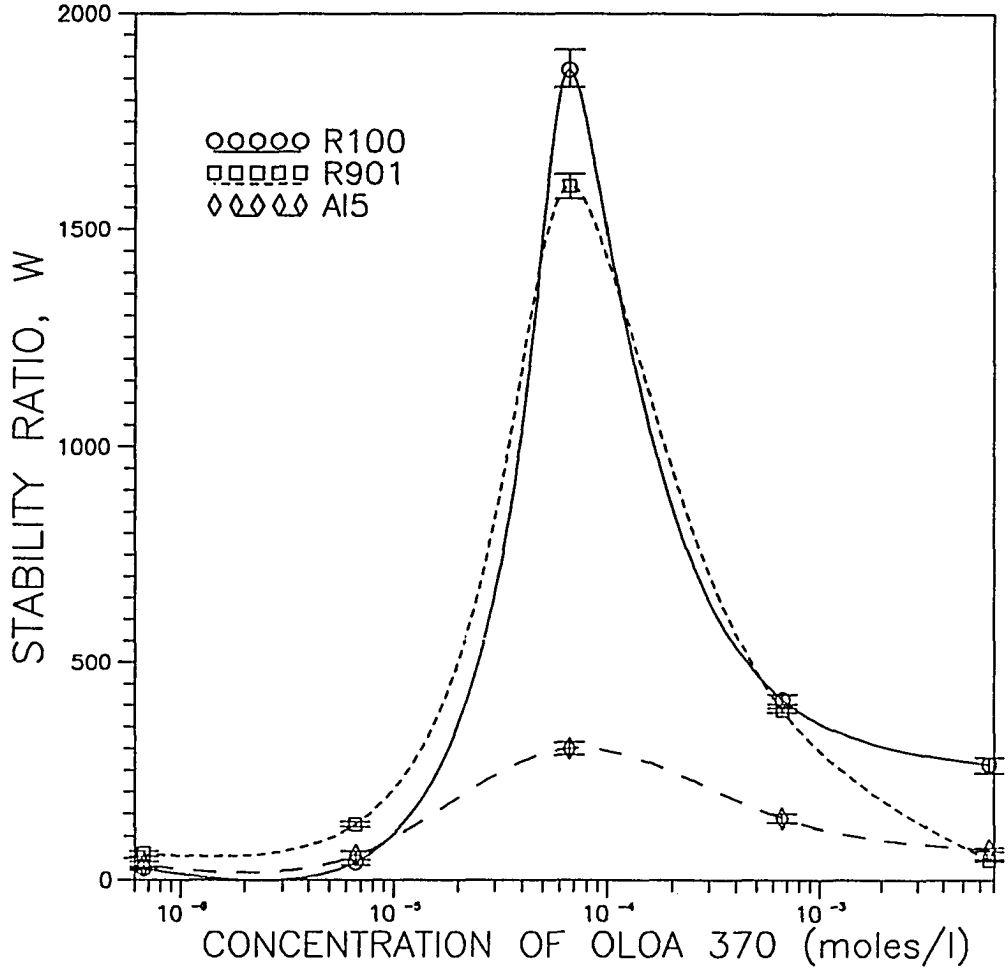

Figure 2–19. The stability ratio for the three rutile pigments R100, R901, and Al5 (0.002wt%) as a function of the OLOA 370 concentration in cyclohexane.

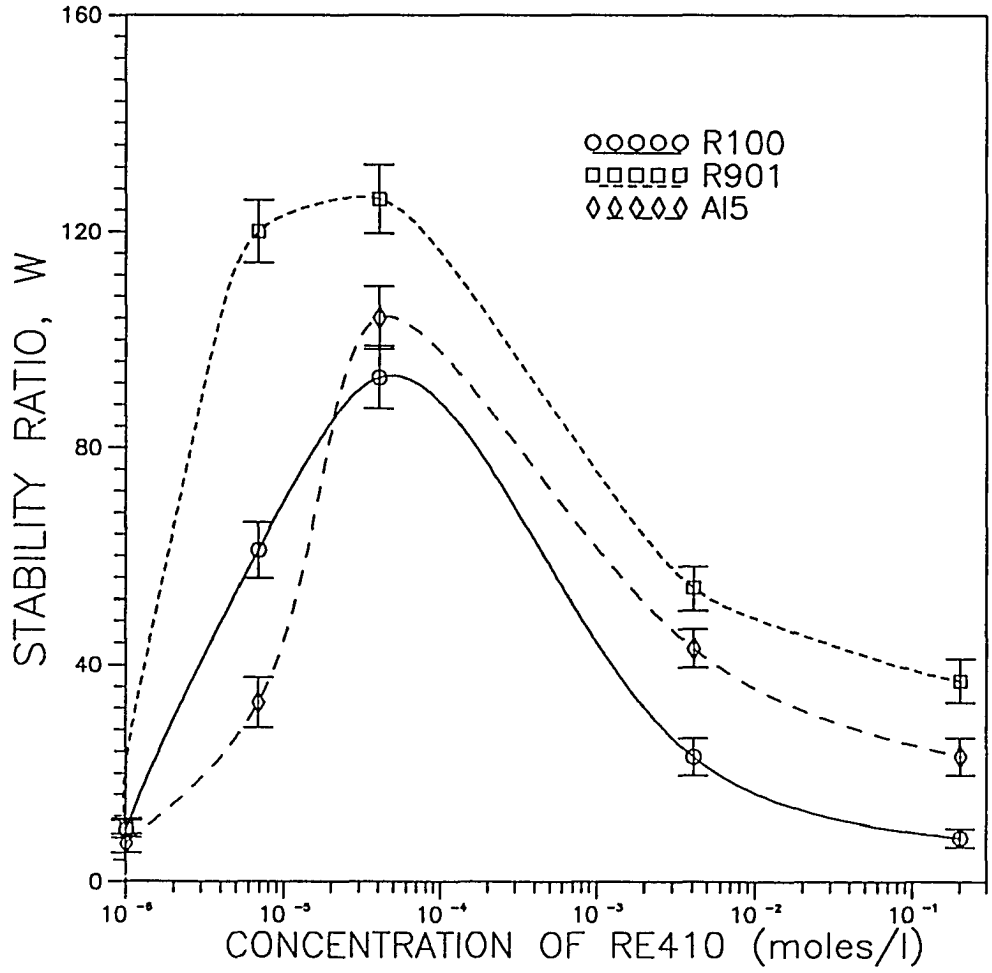

Figure 2–20. The stability ratio for the three rutile pigments R100, R901, and Al5 (0.003wt%) as a function of the RE410 concentration in cyclohexane.

all three RE410 series have much closer maximum stability ratios, and do not follow a trend in order of acidity or basicity of the rutile surface. The absence of a trend indicates that the stability is independent of the metal oxide surface (i.e., no acid-base charging of the metal oxide surface). These observations suggest that the major contribution to the repulsive potential, from RE410 with the three rutile pigments, is due to the steric component.

The OLOA 370 series behaves somewhat differently in that the region of maximum stability coincides with the region of maximum zeta potential (electrostatic potential, Figures 2-9 versus 2-19). There also appear to be significant electrostatic and possibly steric contributions in other concentration regions. The region of maximum stability has a much higher stability ratio than in the RE410 case. It is not apparent how large a role the film barrier plays in the stability. As demonstrated by Fowkes(71) dispersions that have stability ratios of an order of magnitude higher than can be obtained in similar media with OLOA, only when the zeta potential is over 120 mV, indicating that the more important component is the electrostatic potential.

2-4.6 Adsorption Isotherms

Adsorption isotherms can be used to estimate the amount of polymer adsorbed onto the pigment's surface from solution at various polymer concentrations. The amount of polymer and its orientation on the surface, as previously noted, are important factors in determining the effectiveness of the polymer as a steric

stabilizer. By knowing the amount of surface adsorbed polymer, and assuming an orientation, the fraction of monolayer coverage can be calculated. In this way, the adsorption isotherms can be used to assess the charging agent's role as a steric stabilizer. For each pigment and charging agent, the adsorption isotherm was obtained by plotting the moles of adsorbed charging agent per square meter of surface (in moles/m^2, Γ) versus the equilibrium concentration of charging agent in the supernatant (in moles/m^3, C_{eq}). The moles of charging agent on the surface were obtained from the difference of the initial and equilibrium concentrations of charging agent.

In order to convert the amount of charging agent adsorbed to moles per square meter, the surface area had to be measured. The results for the three pigments are listed in Table 2-3 below:

Measurements	R100 (m^2/g)	R901 (m^2/g)	A15 (m^2/g)
1	6.67	29.13	45.04
2	6.65	29.24	47.26
3	6.57	30.12	46.55
Average	6.63	29.53	46.25

Table 2-3. Specific surface areas for the three rutile pigments.

The adsorption isotherms for all dispersion series can be seen in Figures 2-21 through 2-26. Traditionally the Langmuir equation below is applied to the

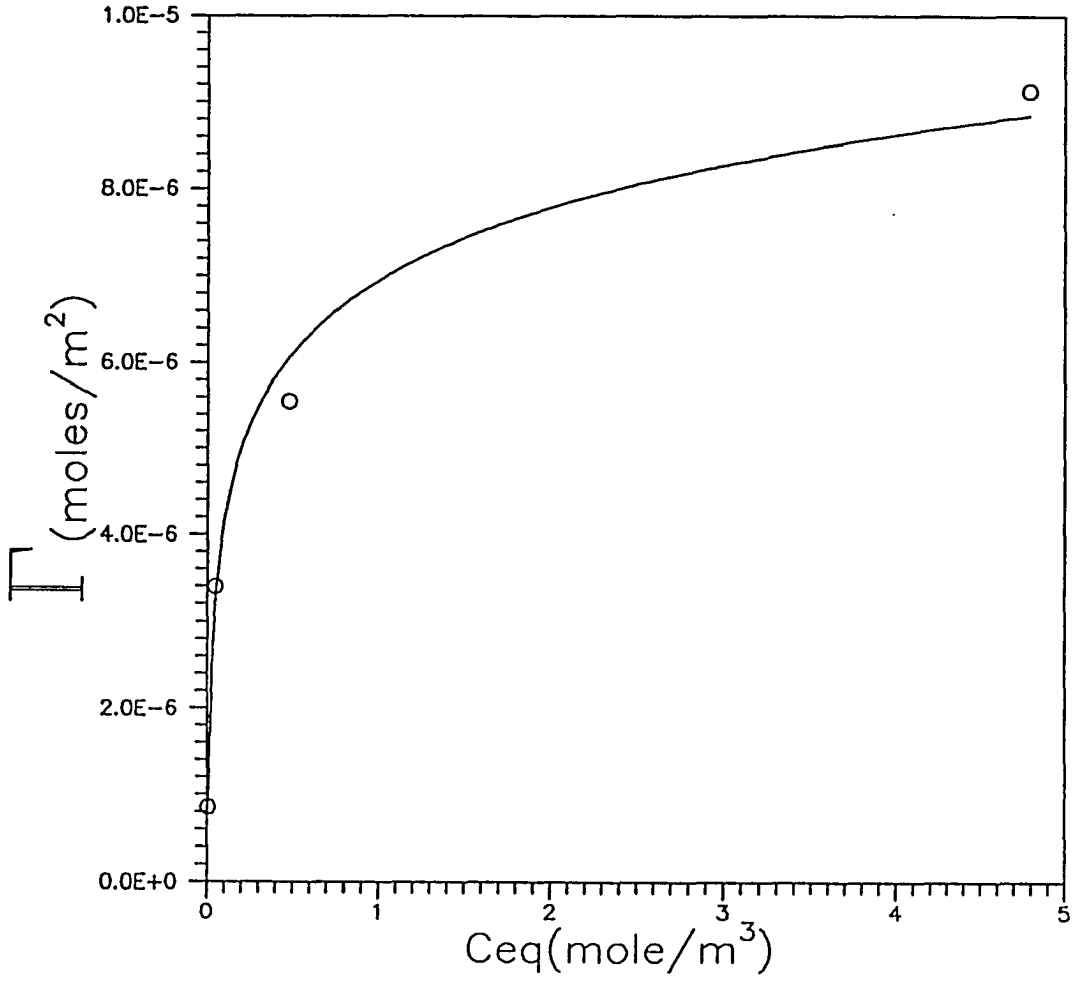

Figure 2-21. Adsorption of OLOA 370 on R100 rutile titanium dioxide 0.002 wt% in cyclohexane.

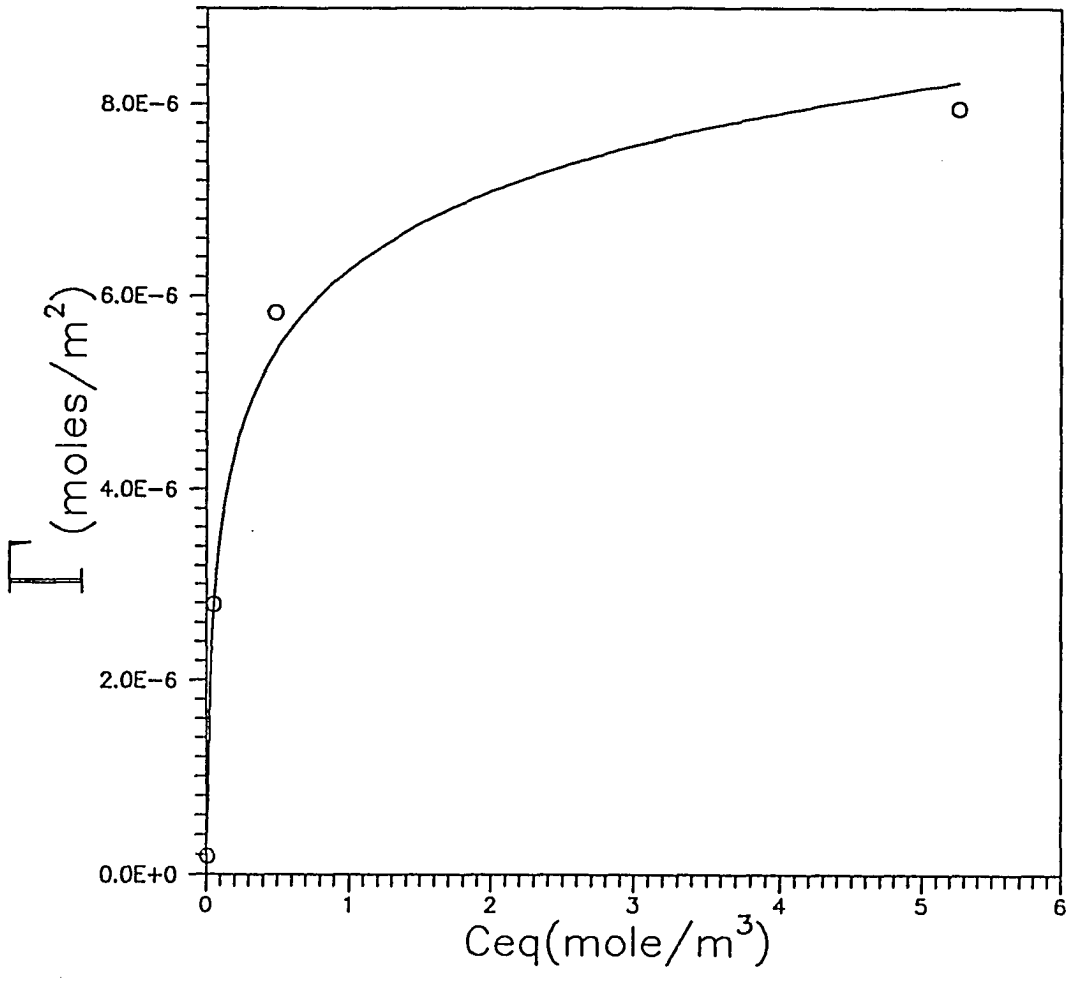

Figure 2-22. Adsorption of OLOA 370 on R901 rutile titanium dioxide 0.002 wt% in cyclohexane.

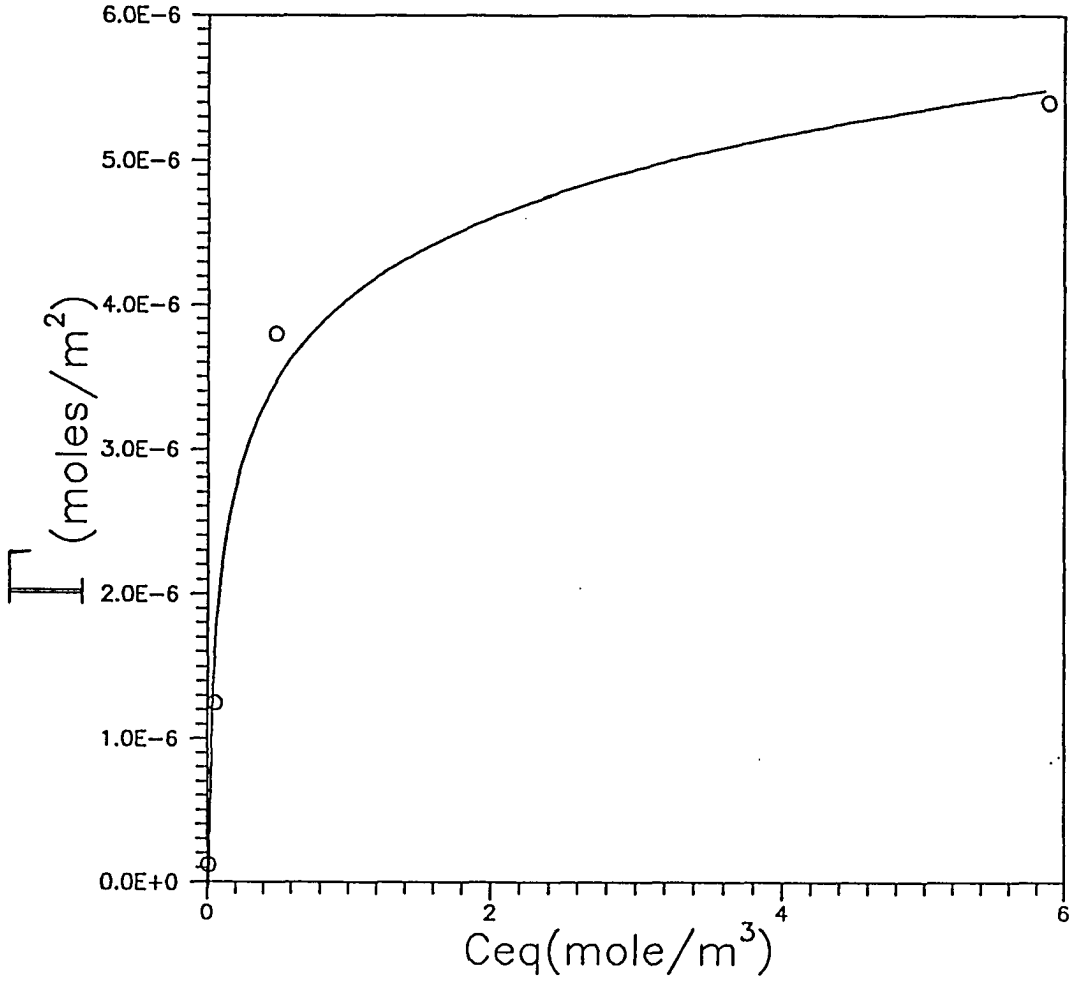

Figure 2-23. Adsorption of OLOA 370 on Al5 (alumina coated R901) rutile titanium dioxide 0.002 wt% in cyclohexane.

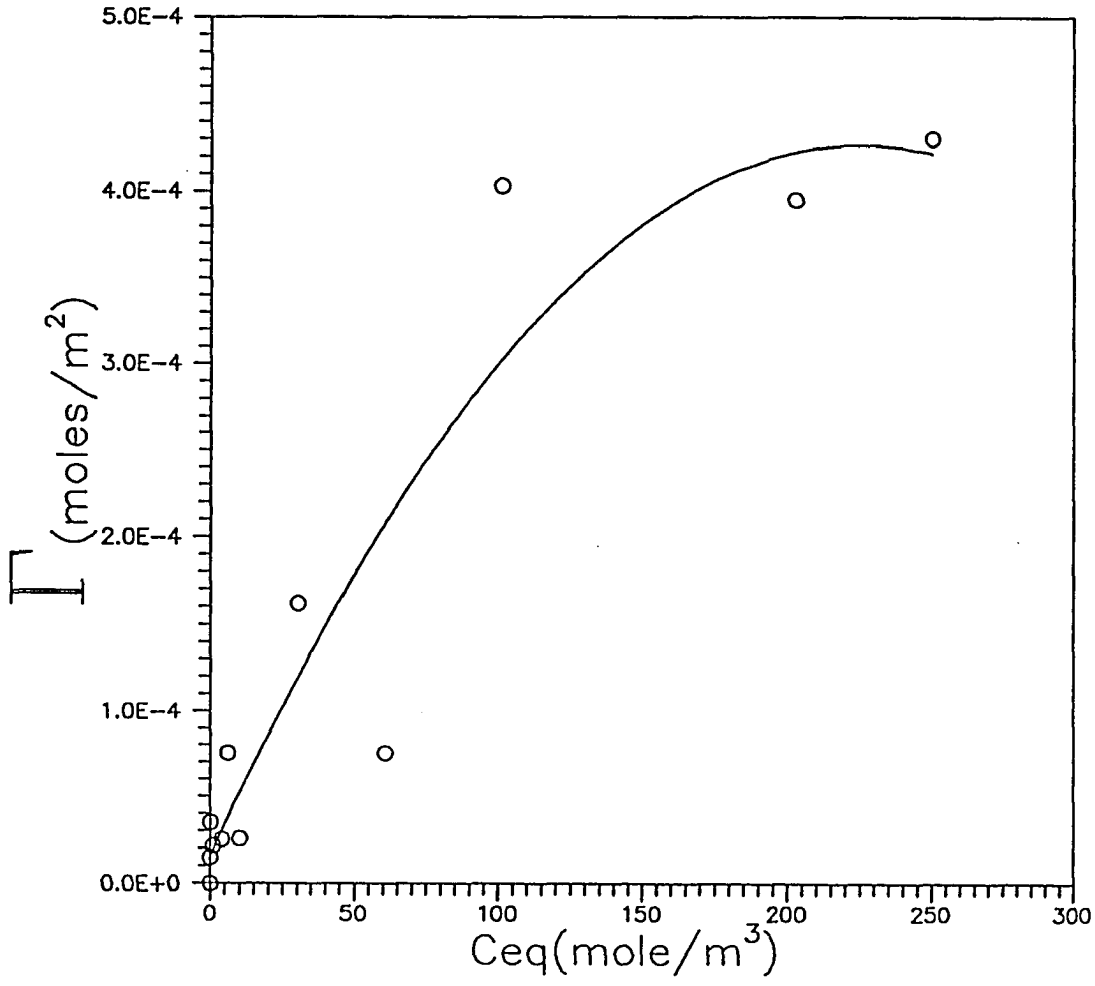

Figure 2-24. Adsorption of RE410 on R100 rutile titanium dioxide 0.003 wt% in cyclohexane.

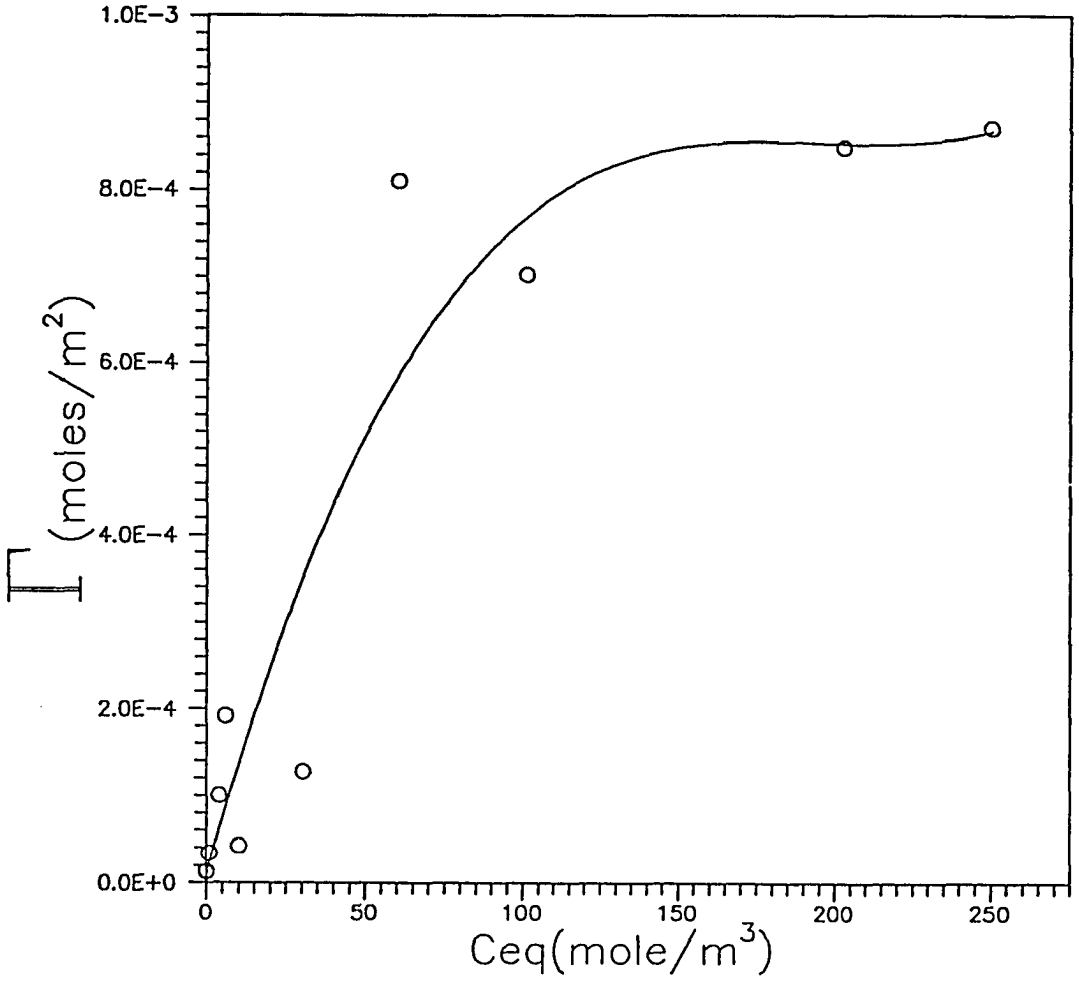

Figure 2-25. Adsorption of RE410 on R901 rutile titanium dioxide 0.003 wt% in cyclohexane.

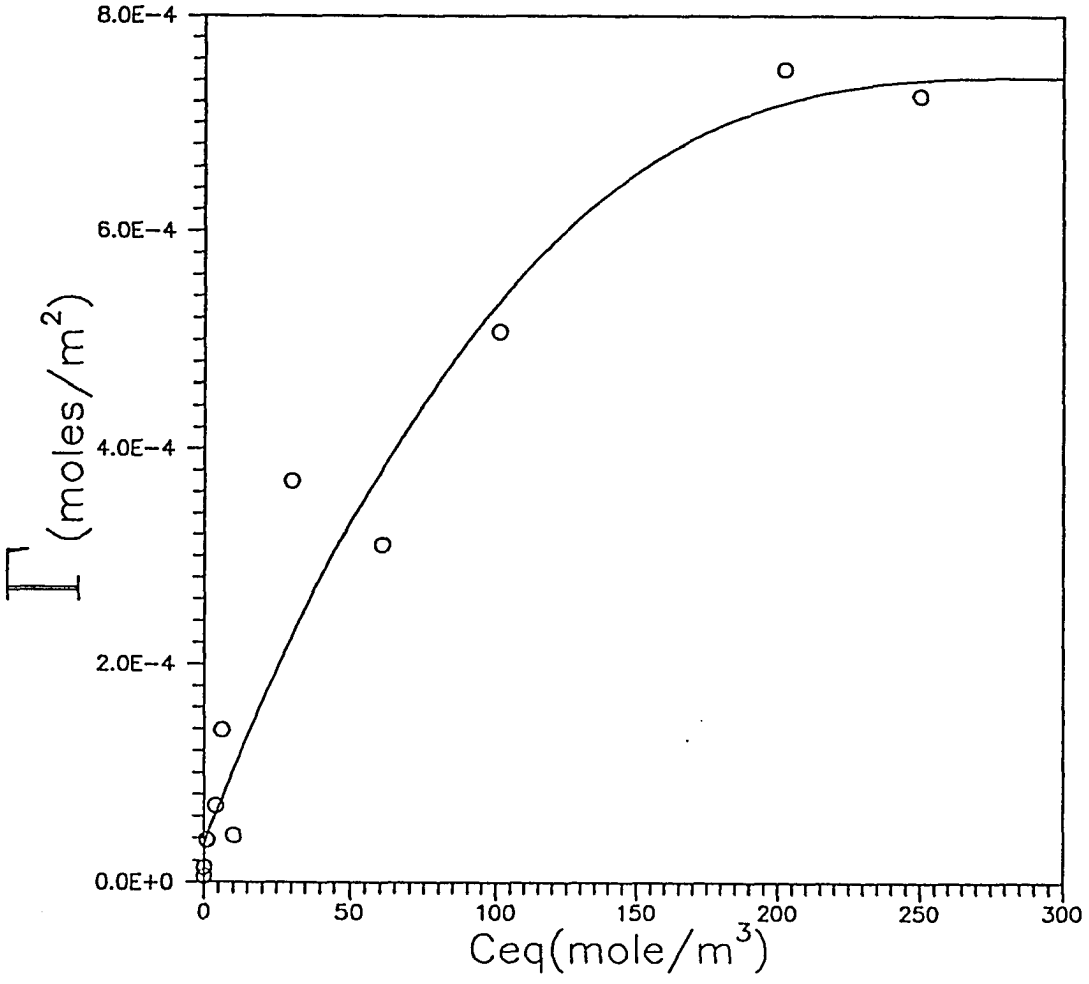

Figure 2--26. Adsorption of RE410 on Al5 (alumina coated R901) rutile titanium dioxide 0.0029 wt% in cyclohexane.

adsorption isotherms.

$$C_{eq}/\Gamma = C_{eq}/\Gamma_m + 1/(K_c\Gamma_m) \qquad 2\text{-}17$$

where Γ is the surface concentration of adsorbed charging agent, C_{eq} is the equilibrium concentration, K_c is the equilibrium constant for the adsorption process, and Γ_m is the surface concentration of the adsorption at monolayer saturation. When applying the Langmuir equation to the OLOA 370 series a straight line fit is obtained, as seen in Figures 2-27 through 2-29. While these plots contain only four points each, it is interesting to see that the value of Γ_m is on the order of what would be obtained at monolayer coverage, where the molecules are normal to the surface. In these cases, "on the order of" means that values of Γ_m, which are between 1.5-2.5 molecules/44Å^2, are approximated as 1 molecule/44Å^2, since an error in the slope or intercept (hence Γ_m) is most likely when only four points are used. These results are consistent with the expected 50 Å film thickness for OLOA 370 in non-polar media(71). In addition the adsorbed monolayer plays a key role in the stability of the dispersions, but not the most significant. At the maximum stability ratio for all three dispersion series containing OLOA 370, monolayer coverage is obtained (Figure 2-30 and Table 2-4). But only pigments R100 and R901 yield substantially higher stability ratios than A15. The dispersions made with Al5 yield significantly lower values at this maximum. The only difference was lower zeta potentials (70 mV as opposed to 100 mV). As shown by Fowkes (71), in low dielectric media, a zeta

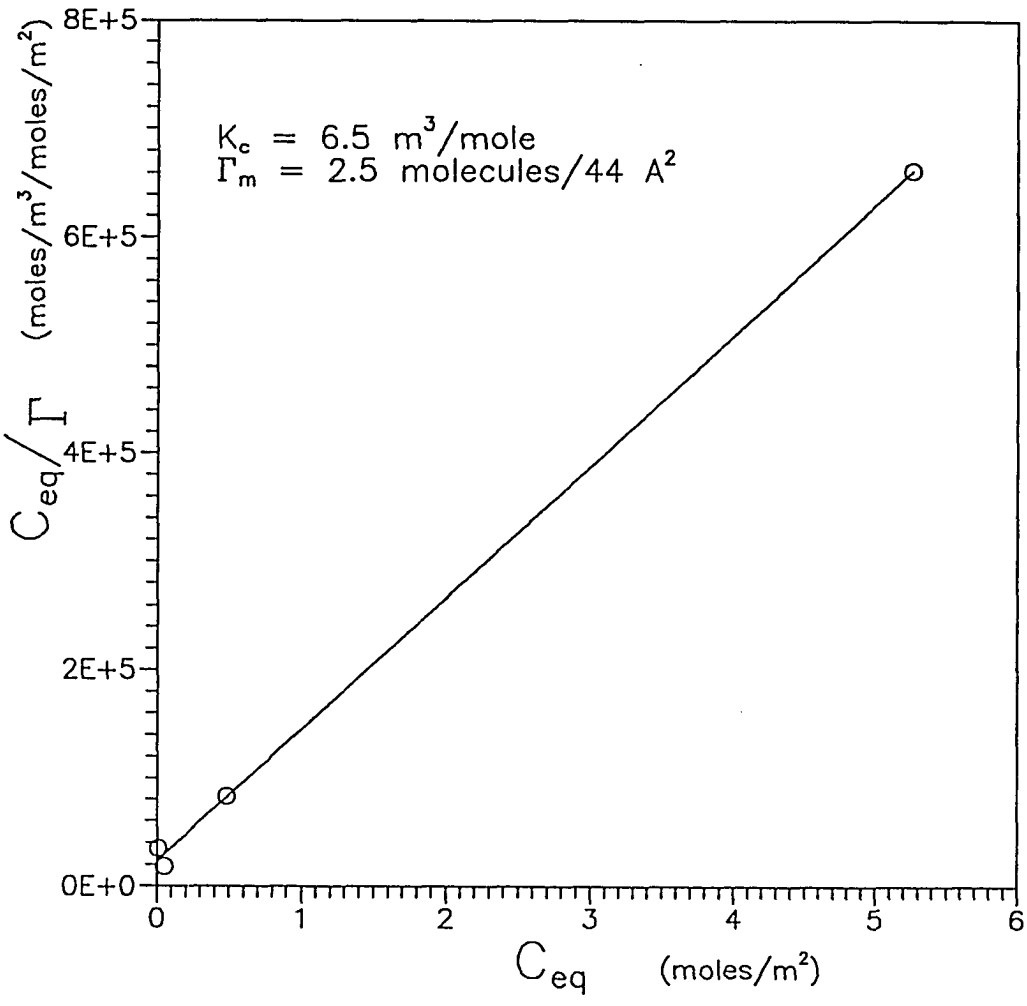

Figure 2–27. The Langmuir plot for R100 with OLOA 370 in cyclohexane.

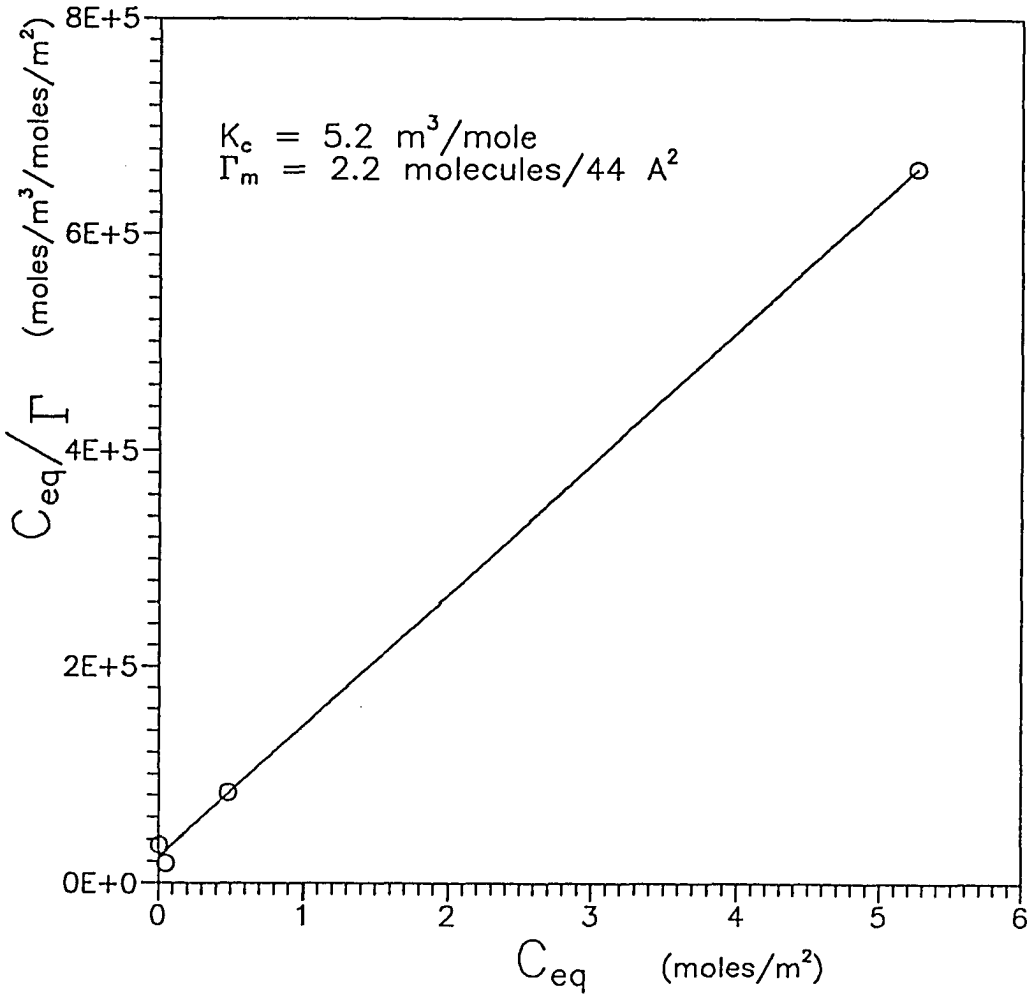

Figure 2–28. The Langmuir plot for R901 with OLOA 370 in cyclohexane.

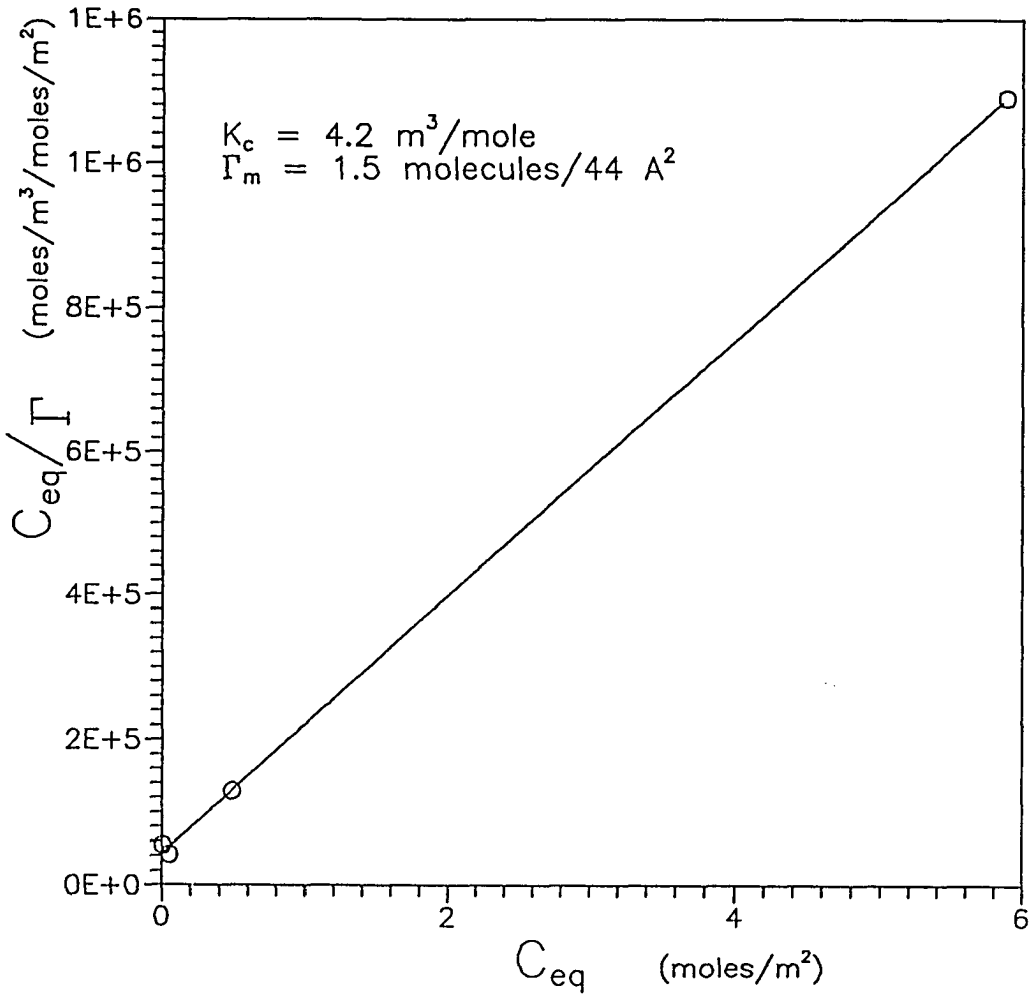

Figure 2–29. The Langmuir plot for AI5 with OLOA 370 in cyclohexane.

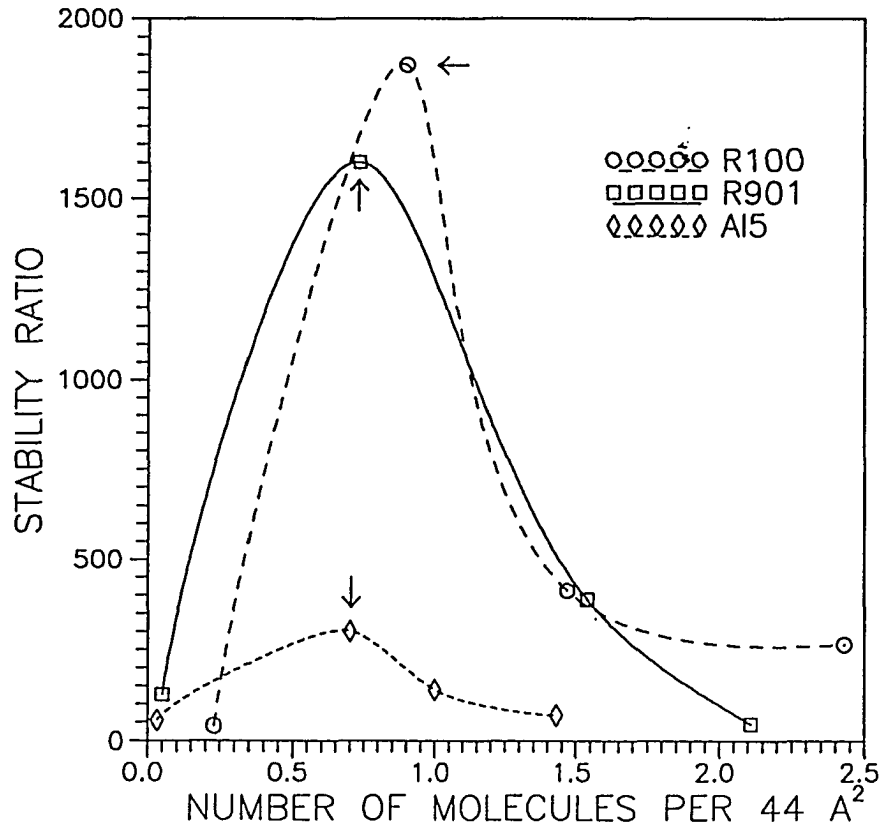

Figure 2–30. The stability ratio versus the number of molecules per 44 A^2 for all three rutiles with OLOA 370 in cyclohexane. The arrows mark the coverage where the largest zeta potential was obtained. The error bars are the same as those in Figure 2–9.

potential of 100 mV or more is needed for pure electrostatic stabilization. The reason is the repulsive potential increases with the square of the zeta potential (Equation 2-5), so that a 30 mV increase becomes significant. Also as the zeta potential lowers at higher concentration so does the stability ratio (50 to 75%) for all three pigment series in OLOA 370, yet monolayer coverage is essentially retained (Figures 2-21 through 2-23), although part of this reason could be a result of depletion flocculation. It appears for the case of the OLOA 370 charging agent that electrostatic stabilization contributes more to the dispersion stability than steric stabilization.

Charging Agent	R100	R901	A15
OLOA (44 A^2)	0.9	0.8	0.7
RE410 (31 A^2)	1.8	2.3	2.4

Table 2-4. The number of molecules adsorbed per head group area for the OLOA 370 (44 Å²) and RE410 (31 Å²) dispersions at the maximum stability ratio. The area represents the coverage obtained if only the head group adsorbs and the tails are perpendicular to the surface.

Unfortunately, in the case of the RE410 dispersion series none of the isotherms fit the Langmuir equation. In addition, twice as many RE410 molecules are adsorbed to the surface at the maximum stability ratio than would be expected if they all were perpendicular to the surface and occupied an area of 31 Å² (Figures 2-31 and Table 2-4). This result can be explained by having one or more layers horizontal to the surface while another top layer remains perpendicular to the

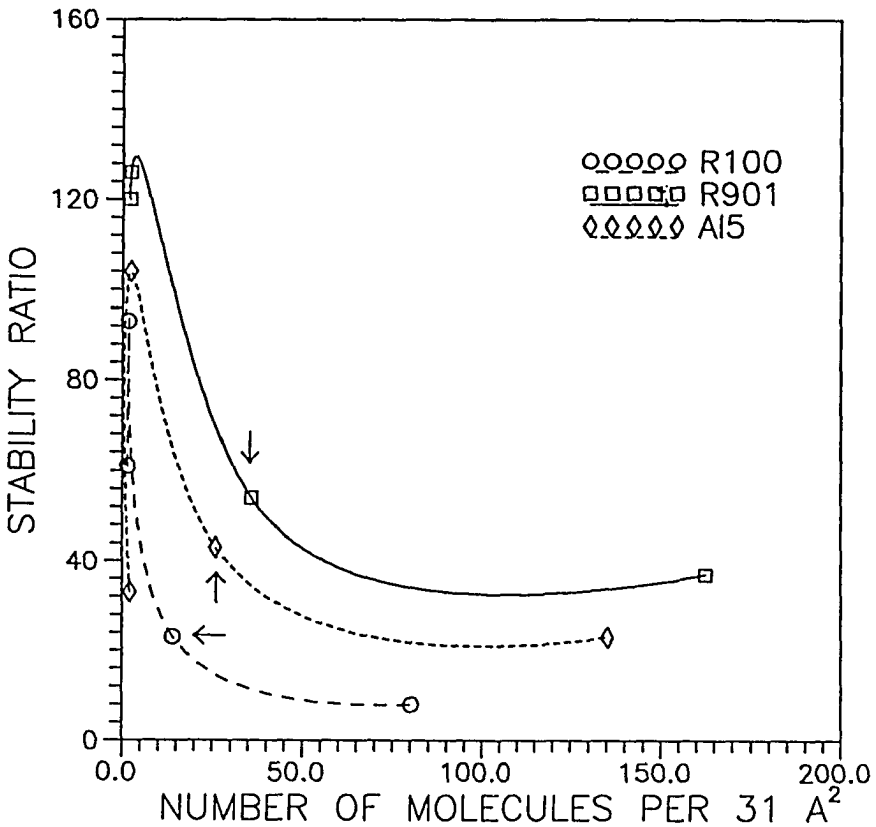

Figure 2–31. The stability ratio versus the number of molecules per 31 A^2 for all three rutiles with RE410 in cyclohexane. The arrows mark the coverage where the largest zeta potential was obtained. The error bars are the same as those in Figure 2–10.

surface. This type of multiple layer adsorption was observed with RE610 which is a similar molecule(111). Any stabilization at this concentration has to be caused by the adsorbed film, since there is no zeta potential. At higher concentrations, where the zeta potential reaches its maximum, the stability ratio decreases and the amount of RE410 (Figure 2-31) on the surface (about 13 to 35 molecules per 31 square Angstroms) increases significantly. This observation suggests that the steric barrier is no longer repulsive and in fact may be attractive (via depletion flocculation). An attractive steric film could out-weigh a repulsive electrostatic potential leading to a net attraction, which could well be the reason for the decrease in the stability ratio while the zeta potential is reaching its maximum value (Figure 2-31). In the case of RE410 the maximum stability is due to the steric potential, while at higher concentrations the steric film appears to be attractive and overrides the contribution from the electrostatic repulsion.

2-5 DLVO Theory Calculations

The above results present a nice qualitative picture of the dispersion stability for the three rutile pigments and two charging agents, but fails to apply a theoretical treatment, such as DLVO theory, based on fundamental colloid principles. Therefore, before concluding this chapter, DLVO theory will be applied to the dispersions used throughout this chapter to validate the previous arguments of electrostatic versus steric stabilization. The theory will be broken down into two

components: the attractive (London forces) potential and the electrostatic potential. The effects of each component will be calculated separately, then summed up to yield a net potential between two particles.

2-5.1 The Attractive Potential

The attractive potential for two identical spherical particles can be calculated as a function of distance using Equation 2-3. As was outlined in Section 2-2.1, the Hamaker constant must be calculated first (Equation 2-4). The same value of the Hamaker constant will be used for all three pigments since the overall London attraction is due to the bulk of the particle(4,32). Any contribution from surfaces or the head group of adsorbed polymers is negligible since it is a small fraction of the total particle. Only within 10Å are surface effects (i.e., Keesom and Debye attraction forces, Born repulsion) significant (4,32,71). Since the interest of this work is to investigate the importance of electrostatic and steric stabilization, which are normally effective at interparticle separations greater than 10 Å(4,34,37), the surface effects are ignored. Any dissolved polymer (such as tail groups) is assumed to have a Hamaker constant the same as that of the liquid medium. This assumption invokes the relationships(31,109):

$$A_{aba} = (A^{1/2}_{aa} - A^{1/2}_{bb})^2 \qquad 2\text{-}18$$

$$A_{ii} = (1.5\text{x}10^{-14}\ \text{cm}^2)\gamma^{1/2}_{ii} \qquad 2\text{-}19$$

where the subscripts, a and b denote the Hamaker constants for two different materials. The subscript i indicates either material. If two materials (a and b) have the same Hamaker constant the overall Hamaker constant is zero, as illustrated by Equation 2-18. The ramifications of zero overall Hamaker constants are that the two materials neither attract or repel each other, but act as one material. In the case of a polymer and liquid medium, this is the condition for solubility. The polymeric charging agents, RE410 and OLOA 370, used in all dispersions throughout this chapter, are soluble in the cyclohexane medium. It is interesting to note that the solubility parameter δ^d is related to the van der Waals attraction (via the cohesive energy (32,77)), and if both the medium and the polymer have the same solubility parameter (a basic requirement for solubility (71)), they should have the same Hamaker constant. By applying the above assumptions, equations 2-18 and 2-19 can be used to calculate the Hamaker constant for the dispersions in this chapter by simply substituting 1 (particle) for the subscript a and 2 for the subscript b. Equations 2-18 and 2-19 can be combined to yield equation 2-4. The Hamaker constant can be calculated using Equation 2-4 and the literature values (77) of the surface energies for cyclohexane (25.5 dyn/cm) and rutile titanium dioxide (143 dyn/cm).

The calculated Hamaker constant, 7.2×10^{-13} ergs (Equation 2-4), can then be used in Equation 2-3 to obtain a plot of the attractive potential, for titanium dioxide in cyclohexane dispersions, as a function of interparticle separation (as seen in

Figure 2-32). A radius of 150 nm was used for all particles. Notice only at a close interparticle approach (300 Å) is the critical flocculation distance obtained, which is the distance between particles when Ψ^a_{121} = -kT (k is the Boltzmann constant and T is the absolute temperature) (71). The quantity -kT is an approximate indication or gauge of the interaction energy between a pair of flocculated particles at a separation, H(32,71). When the energy is less than -kT, the particles tend to flocculate (attraction "wins out" over thermal motion), but if it is more the particles will mostly bounce apart (32,71). Any repulsive potential must overcome the attractive potential (have a net potential greater than -kT) in order to prevent flocculation(4,32,34). This is the topic of the next section.

2-5.2 The Electrostatic Potential

The electrostatic potential that develops between two charged particles is calculated by Equation 2-5, for each dispersion series. Plots can then be made of the electrostatic potential between two identical spherical particles as a function of interparticle separation. The purpose of this plot is to see how the electrostatic potential, for the dispersion series, varies with zeta potential and Debye length (electrical double layer thickness). The Debye length will be calculated from conductivity data (Figures 2-11 and 2-12) by employing Equations 2-6 and 2-7. The diffusion coefficients and correction factors required in Equation 2-7 are listed in Table 2-5.

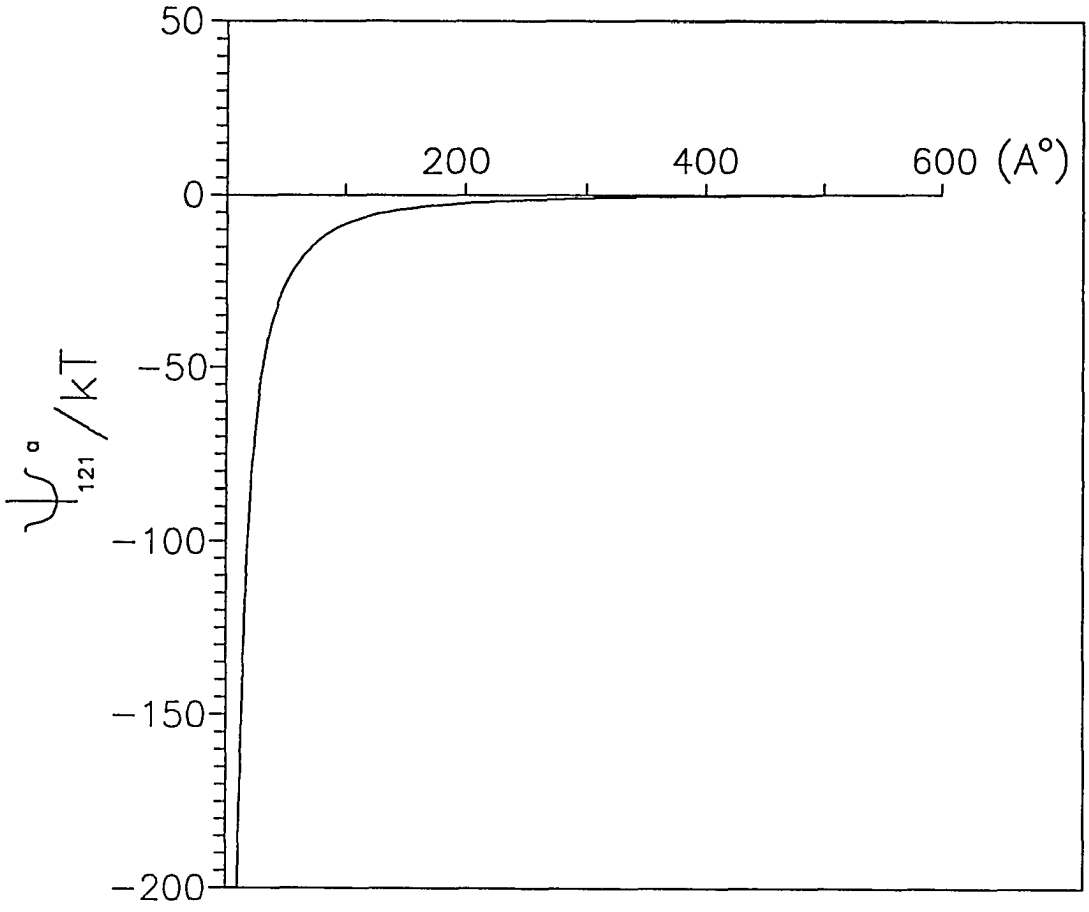

Figure 2–32. The attractive potential between two rutile particles.

	Mole. wt. (g/mole)	Density (g/ml)	(f/f_o)	Diffusion Coef. (M^2/s)
OLOA 370	1200	0.9	1.23	$3.4x10^{-10}$
RE410	625	1.1	1.10	$4.1x10^{-10}$

Table 2-5. The molecular weights, densities, correction factors, and diffusion coefficients for OLOA 370 and RE410.

The Debye lengths for all six series of dispersions were calculated and plotted as a function of charging agent concentration (Figures 2-33 and 2-34). The Debye length decreases rapidly at low charging agent concentration and levels off at higher concentration, indicating that the counter-ion concentration has reached saturation. By contrast, the zeta potential-concentration plots (Figures 2-9 and 2-10) obtain a maximum and then decline to a lower level corresponding to the Debye length leveling off, which indicates charge saturation. These above results are typical(12,54). The mechanism behind this phenomenon will be examined in Chapter III, but the consequences will be illustrated in this section. Using the zeta potential (Figures 2-9 and 2-10) and Debye length data (Figures 2-31 and 2-32) in Equation 2-5, plots of the electrostatic potential versus particle separation can be obtained for all six dispersion series, as shown in Figures 2-35 through 2-40. The potential energy curves that ensue are essentially linear. Usually for dispersions with small Debye lengths (approximately 50-100 Å) the curves have a pronounced curvature, a consequence of the magnitude of the Debye length. In dispersions where the Debye length is large

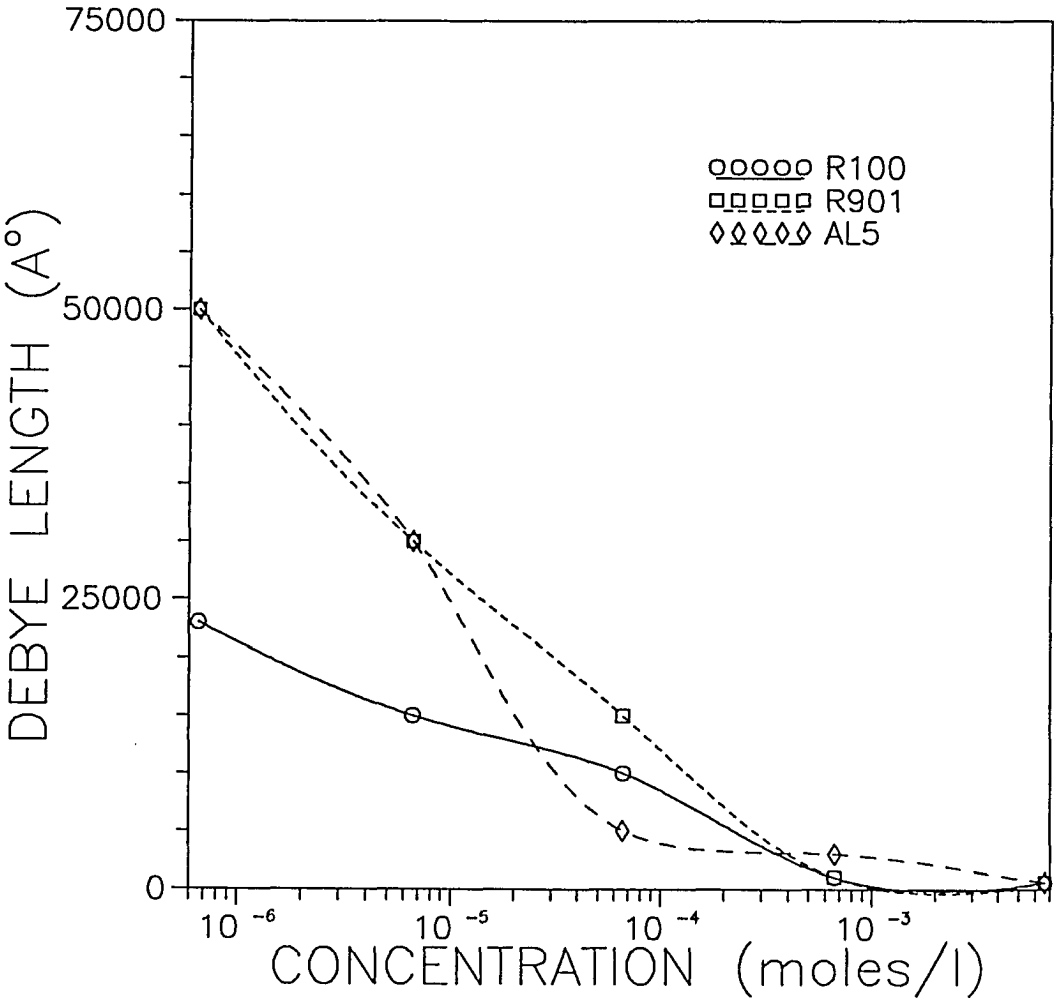

Figure 2–33. Debye length at varying concentrations of OLOA 370 for R100, R901, and Al5 at 0.002 wt%.

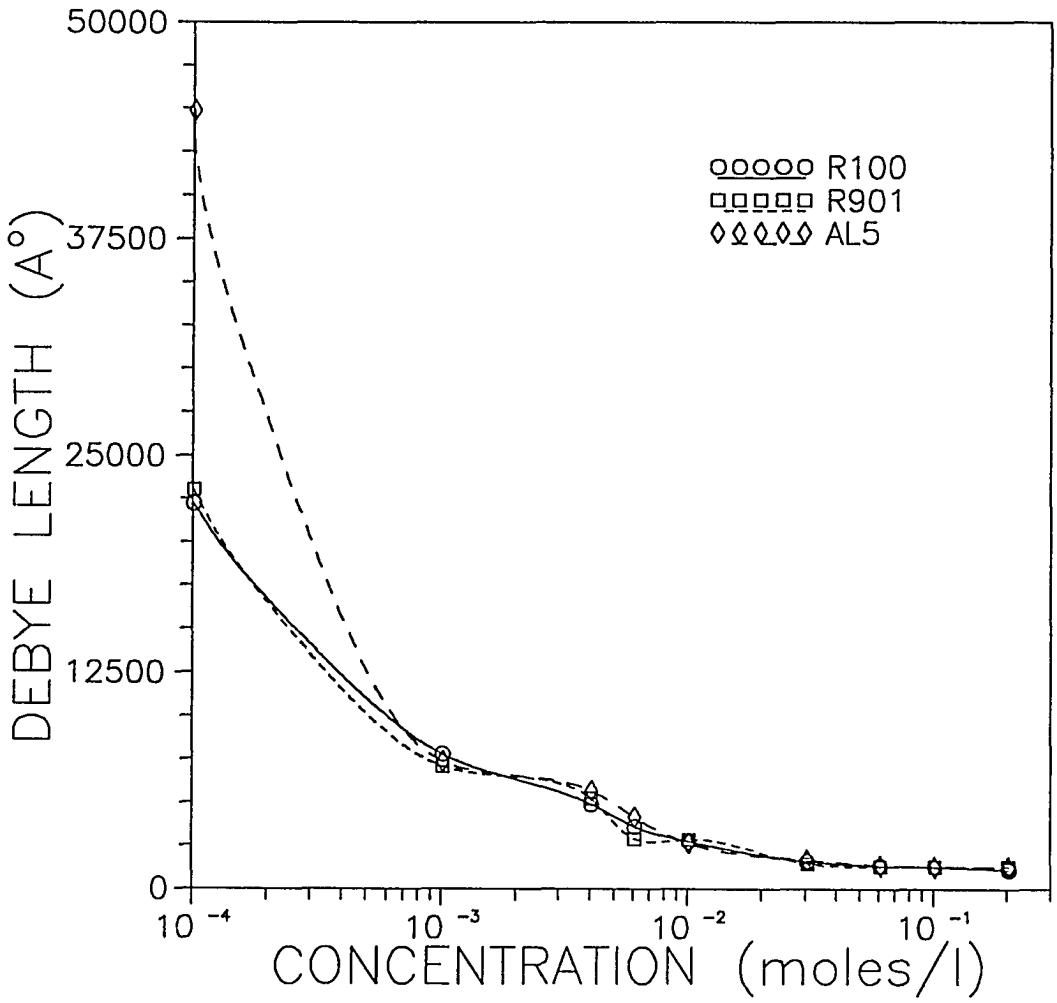

Figure 2-34. Debye length at varying concentrations of RE410 for R100, R901, and Al5 at 0.003 wt%.

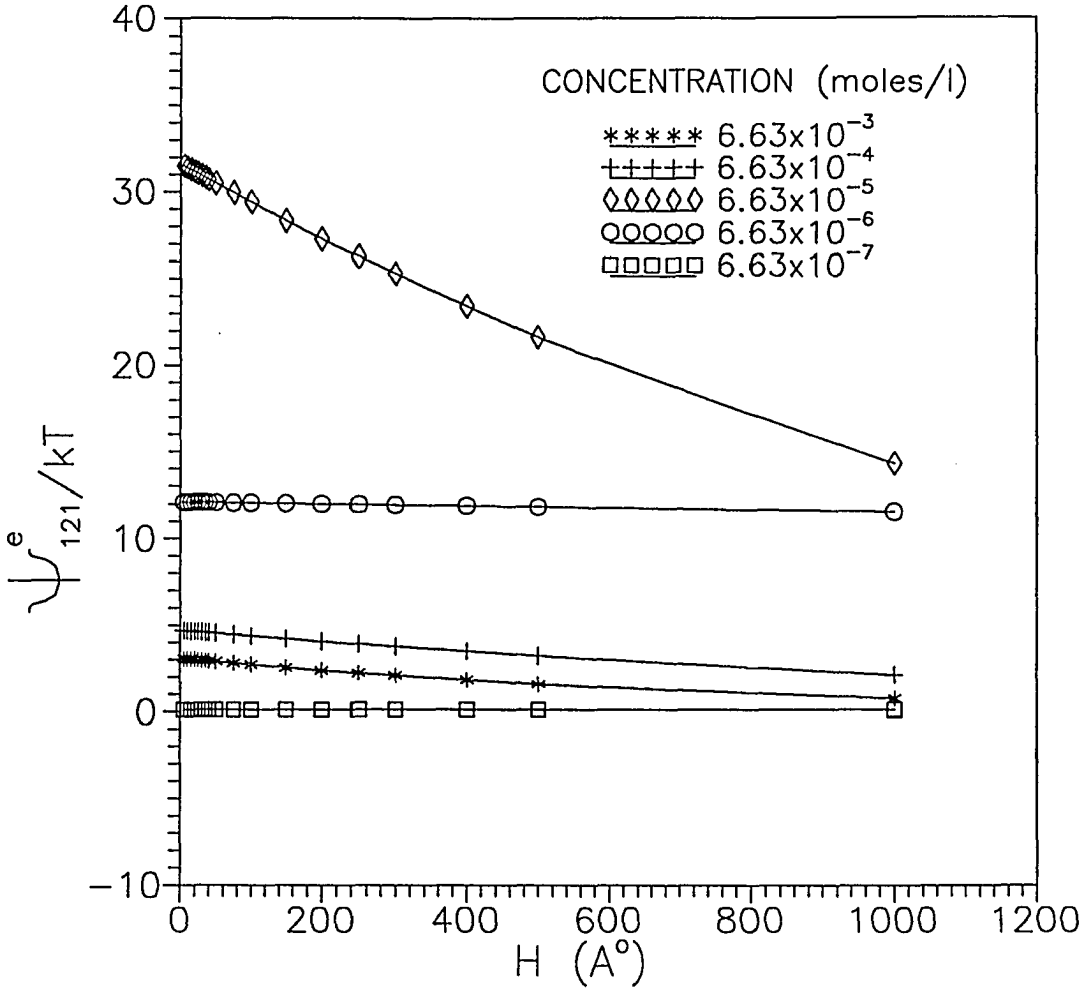

Figure 2–35 The electrostatic potential between two pigments of R100 TiO_2 as a function of the interparticle separation distance H. For a series of OLOA 370 concentrations in cyclohexane.

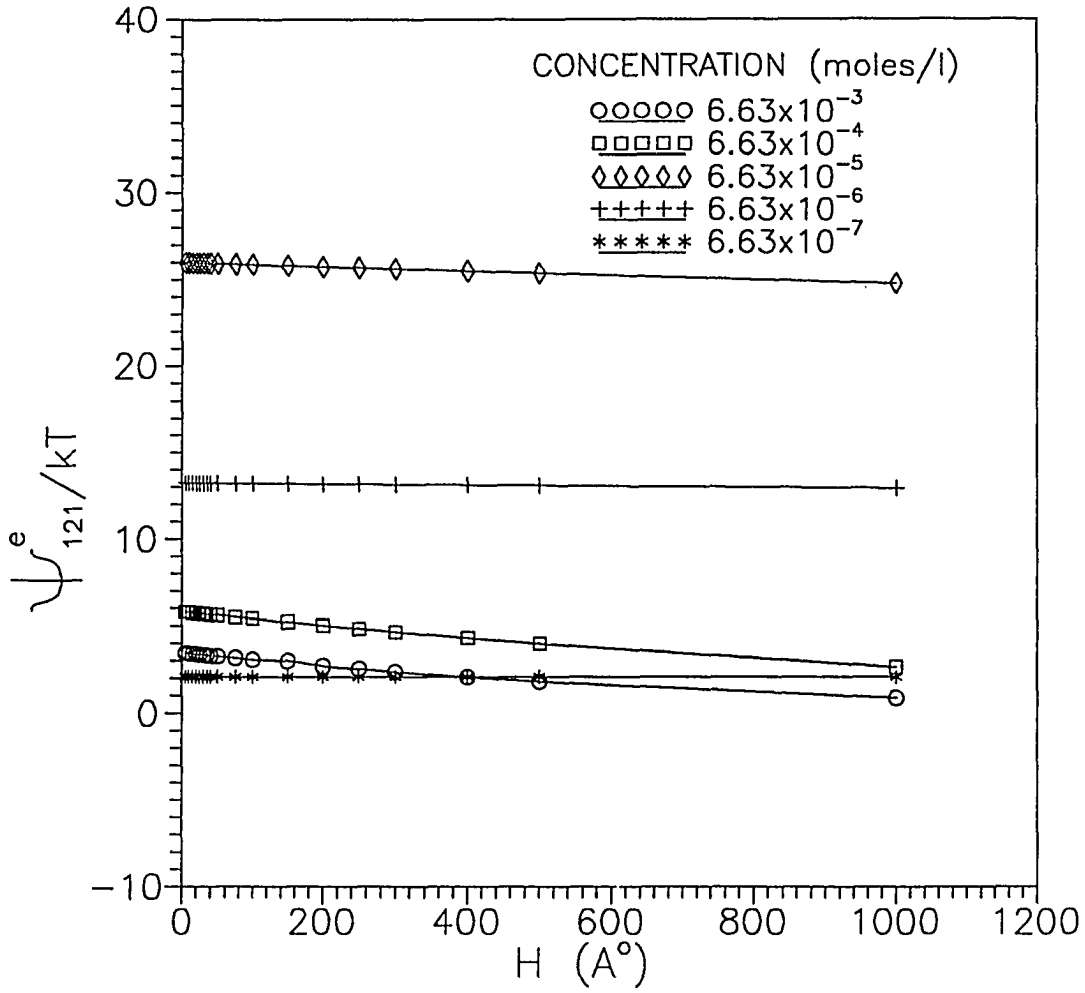

Figure 2–36. The electrostatic potential between two pigments of R901 TiO_2 as a function of the interparticle separation distance H. For a series of OLOA 370 concentrations in cyclohexane.

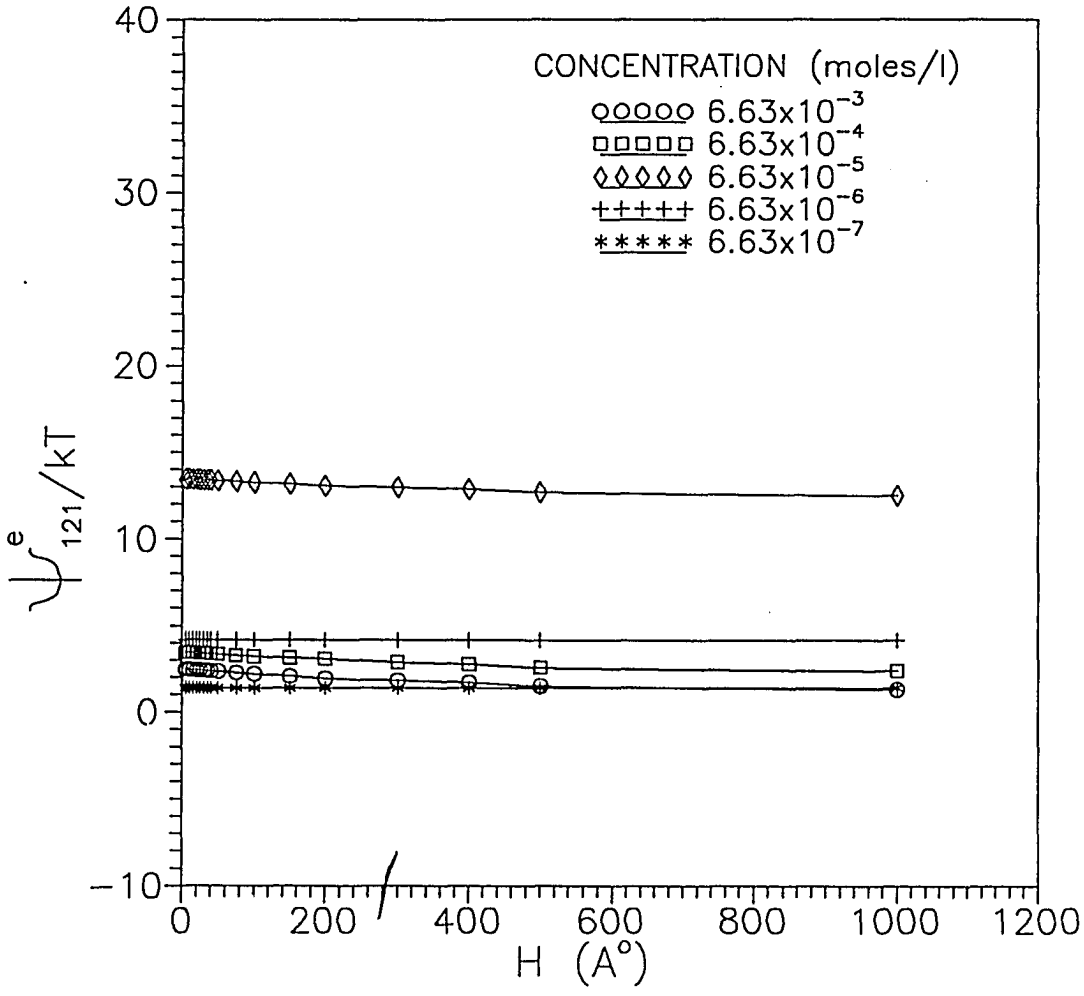

Figure 2–37. The electrostatic potential between two pigments of Al5 TiO_2 as a function of the interparticle separation distance H. For a series of OLOA 370 concentrations in cyclohexane.

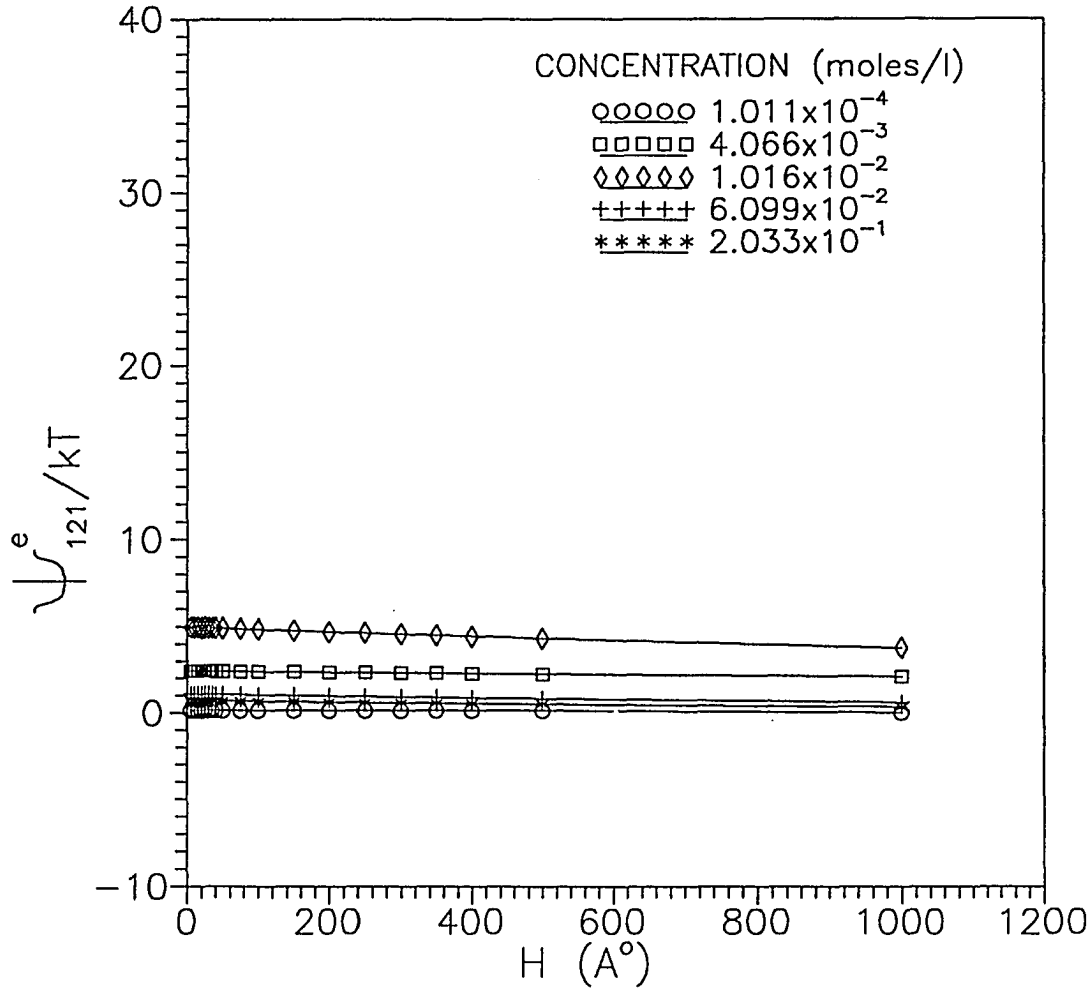

Figure 2–38. The electrostatic potential between two pigments of R100 TiO_2 as a function of the interparticle separation distance H. For a series of RE410 concentrations in cyclohexane.

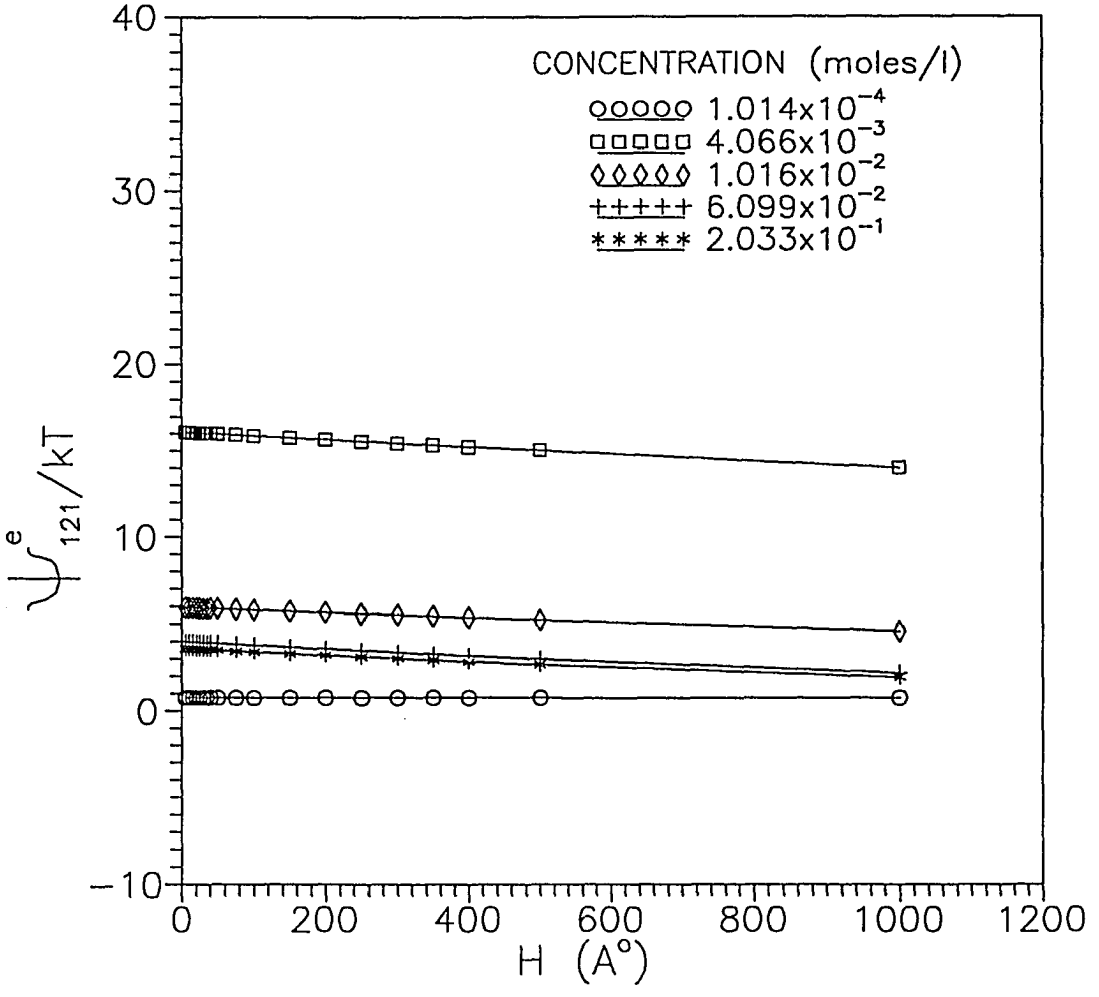

Figure 2–39. The electrostatic potential between two pigments of R901 TiO_2 as a function of the interparticle separation distance H. For a series of RE410 concentrations in cyclohexane.

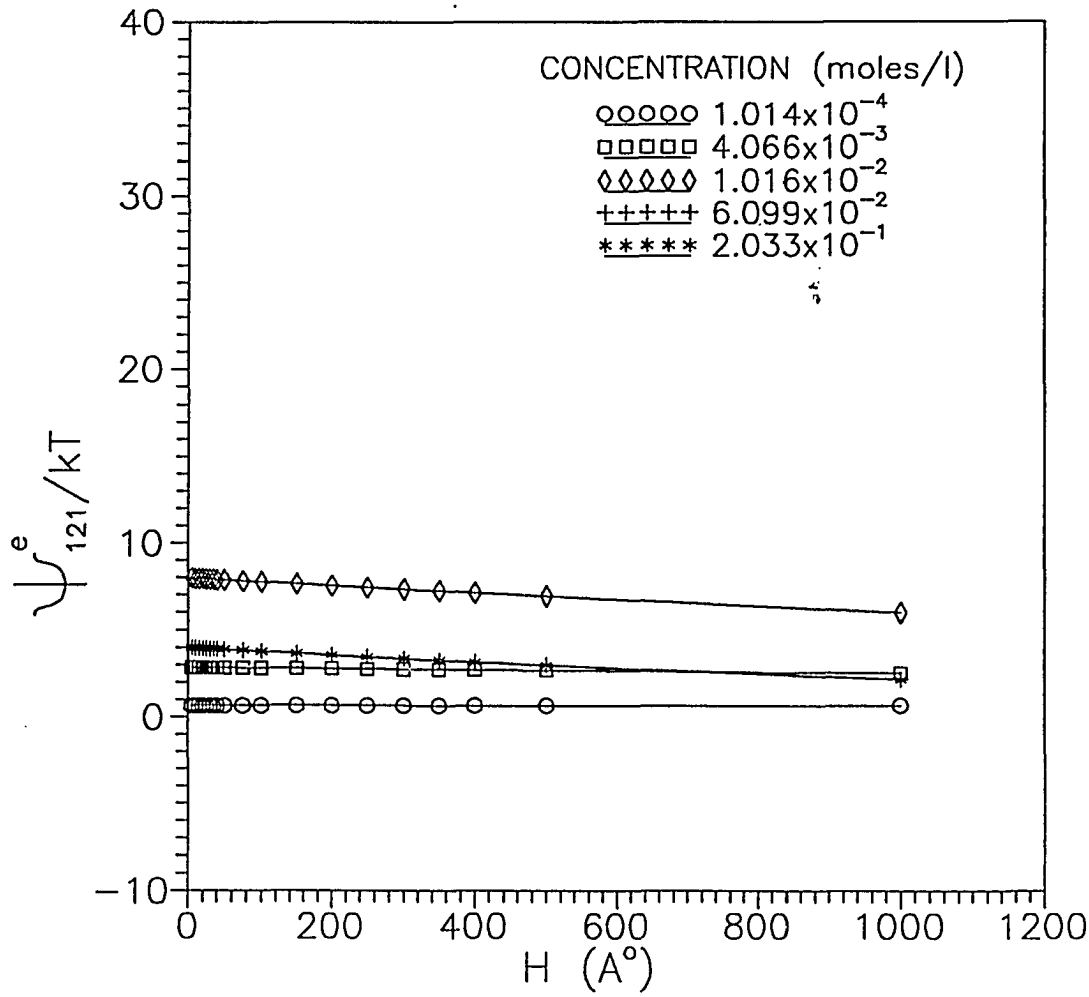

Figure 2—40. The electrostatic potential between two pigments of Al5 TiO_2 as a function of the interparticle separation distance H. For a series of RE410 concentrations in cyclohexane.

(>1000 A), as for these systems, the curvature will be slight. Dispersions in low dielectric constant media tend to be this way since it is difficult to obtain counter-ions which decrease the Debye length. Not surprisingly, the curves that were calculated with the highest zeta potential yield the greates electrostatic potential. If the attractive potential (Figure 2-32) is added to the electrostatic potential (Figures 2-35 through 2-40), the resultant potential curves (Figures 2-41 through 2-46) indicate (positive being repulsive and negative being attractive) which dispersions should be the most stable according to DLVO theory.

Both Fowkes(71) and Vold(118) noted that when only the repulsive potential is operating, an electrostatic potential barrier on the order of 30 kT is needed to maintain a stable dispersion (>6 months). As can be seen in Figures 2-41 through 2-46, at both low and high concentrations of charging agent, the potential is not sufficient to prevent the approach of particles. For some dispersions (A15 with OLOA 370 and R100 with RE410) the highest barrier is less than one-third of the desirable 30 kT barrier required for colloidal stability. Only R901 and R100 in OLOA at the mid-range charging agent concentrations come close (25kT) to the required barrier. The above calculations indicate that most of these dispersions will require the aid of the steric potential if they are to remain stable.

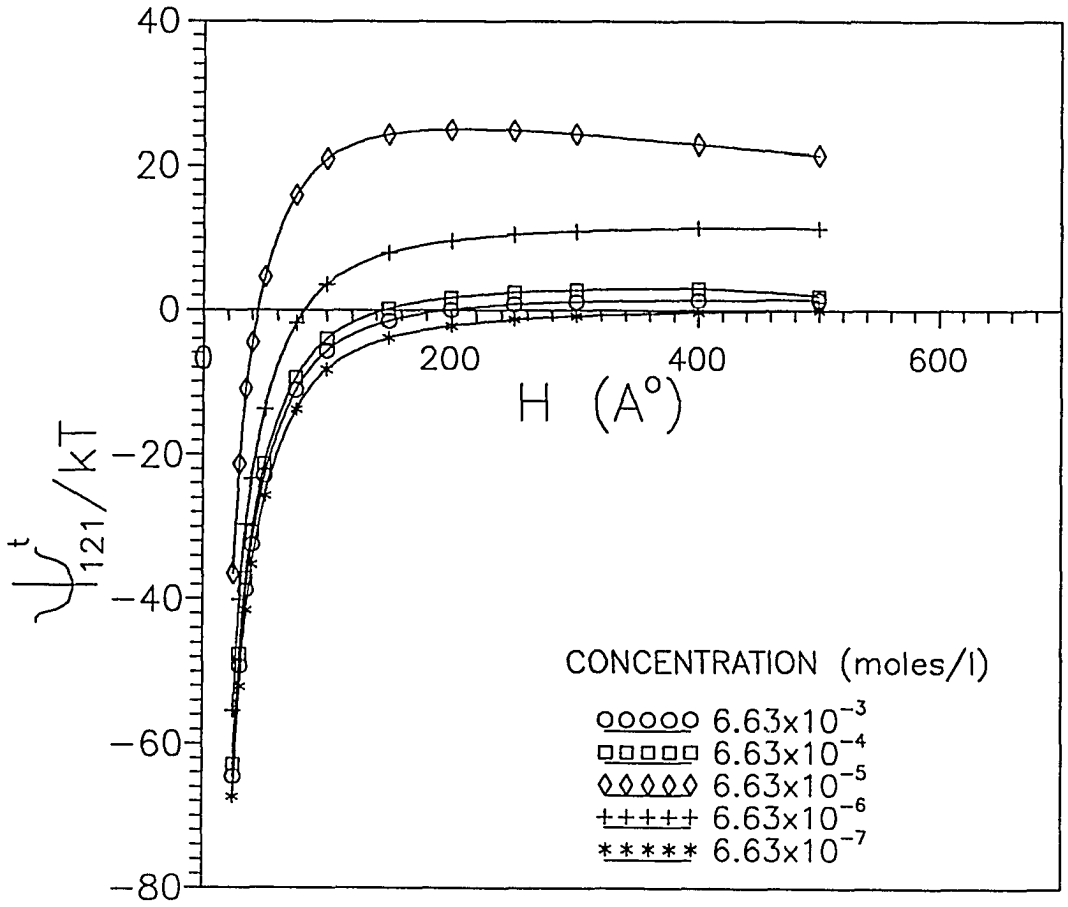

Figure 2–41. The sum of the electrostatic and attractive potentials between two R100 TiO_2 pigments as a function of the interparticle separation distance. For a series of OLOA 370 concentrations in cyclohexane.

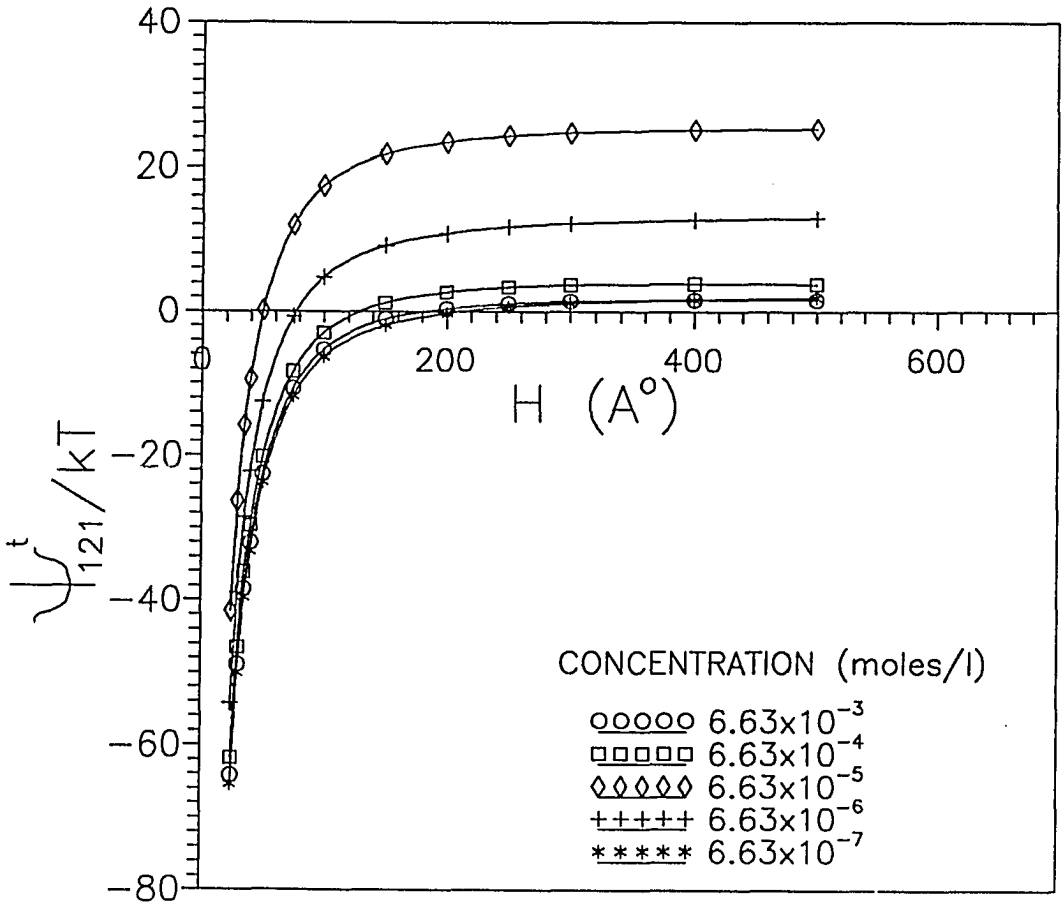

Figure 2–42. The sum of the electrostatic and attractive potentials between two R901 TiO_2 pigments as a function of the interparticle separation distance. For a series of OLOA 370 concentrations in cyclohexane.

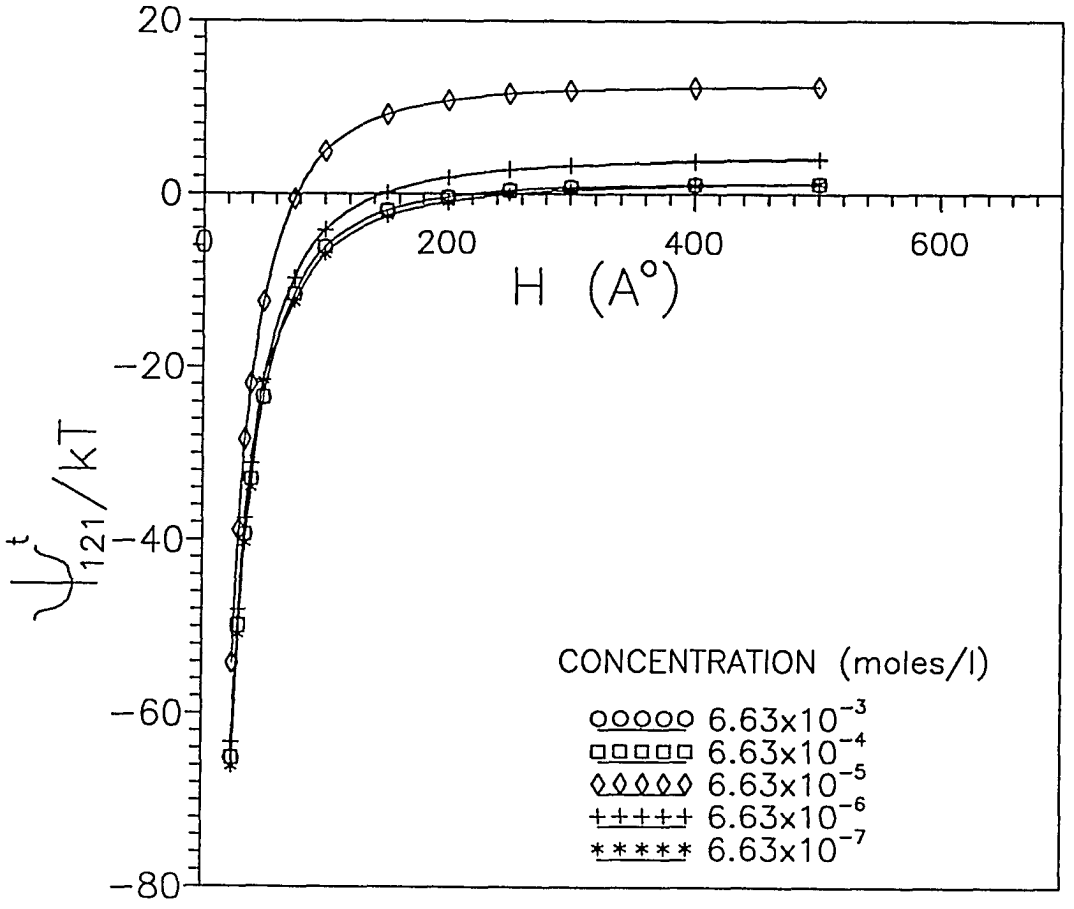

Figure 2–43. The sum of the electrostatic and attractive potentials between two Al5 TiO_2 pigments as a function of the interparticle separation distance. For a series of OLOA 370 concentrations in cyclohexane.

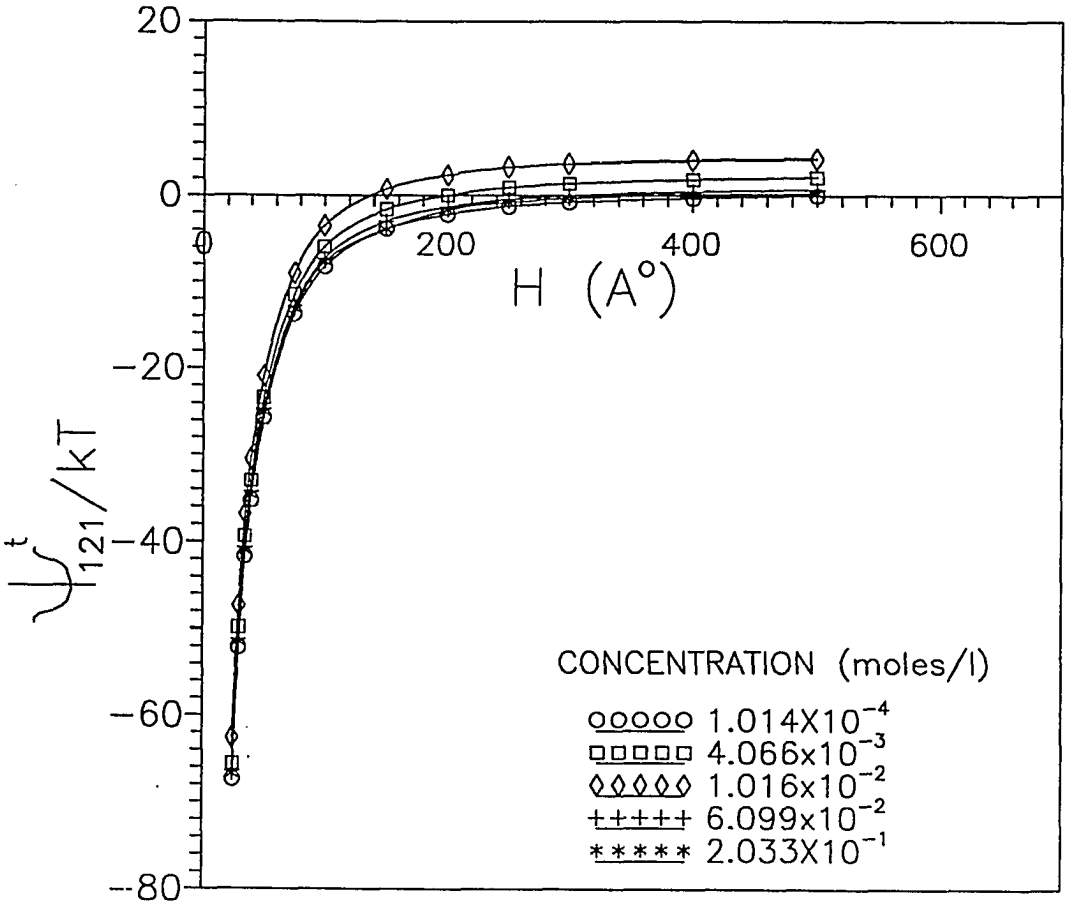

Figure 2–44. The sum of the electrostatic and attractive potentials between two R100 TiO_2 pigments as a function of the interparticle separation distance. For a series of RE410 concentrations in cyclohexane.

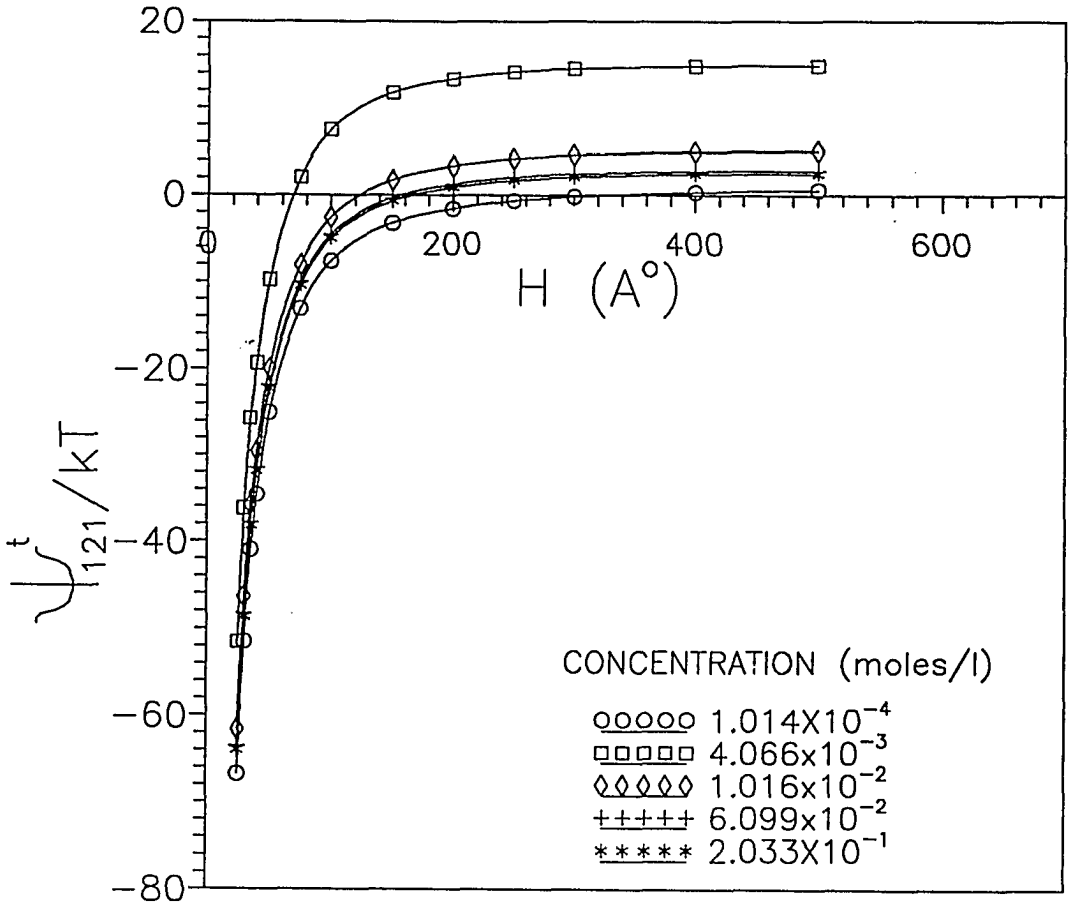

Figure 2–45. The sum of the electrostatic and attractive potentials between two R901 TiO_2 particles as a function of the interparticle separation distance. For a series of RE410 concentrations in cyclohexane.

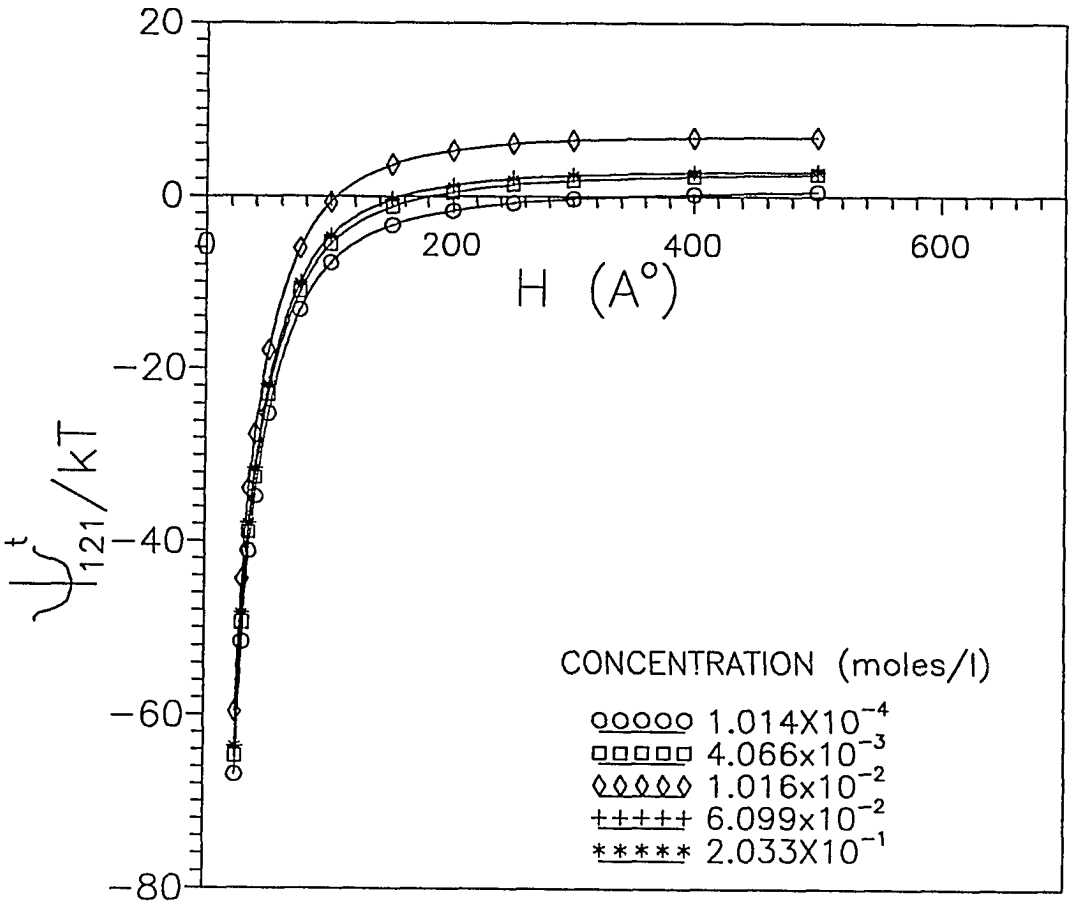

Figure 2–46. The sum of the electrostatic and attractive potentials between two Al5 TiO_2 particles as a function of the interparticle separation distance. For a series of RE410 concentrations in cyclohexane.

2-5.3 The Steric Potential

When molecules of a monolayer of OLOA 370 molecules are normal to the surface of the particle and minimal interpenetration of the tails occurs, a maximum pitment separation of 100 Å is possible. If on the other hand full tail interpenetration occurs, then a maximum of 50 Å is possible. Of course, if the tails are not normal to the surface or if any part of the tail adsorbs to the surface, separations will be smaller than maximum. Since it was shown by Fowkes(71), that the film barriers of OLOA in non-polar organic media are on the order of 50 Å, it is likely that the tails are normal to the surface. If this orientation is true, then a steric potential starting at 50 Å can be added to the potentials in Figures 2-41 through 2-43. The barrier would behave essentially as an infinite wall extending out 50 Å from the abscissa. In such a situation, only the highest potential barriers (i.e., R100 and R901 in OLOA 370) would eliminate the deep primary minimum. A secondary minimum could still be possible. If the wells were eliminated completely, thermodynamically stable dispersions would be obtained under all conditions. Such results would mean that infinite stability ratios would occur, but finite ratios are observed. Therefore some sort of secondary minimum must occur. In addition a 50 Å film barrier is consistent with the stability ratios obtained (the most stable disperisions of R901 and R100 in OLOA both eventually flocculate, but are fairly stable). If the film barrier were increased significantly, again a thermodynamically stable dispersion would be expected. It is concluded that a high degree of chain

interpenetration occurs, and that the electrostatic potential contributes a larger percentage than the steric potential to the overall stabilization of the dispersion.

In the case of RE410 a maximum particle separation on the order of 60 Å is expected if the tails are normal to the surface with minimal tail overlap. If the tail overlap is complete, a distance of 30 Å would be obtained. As shown by Huang(111), studying organic media of low dielectric constant, the first monolayer of RE610 (also a nonyl phenol phosphate ester) tails tend to adsorb onto the surface while additional layers tend to extend into the medium. These findings indicate that less than maximum separations will probably be encountered. Furthermore, an average steric barrier on the order of 120 Å is required to achieve thermodynamic stability at the maximum stability ratio (see Figures 2-44 through 2-46). Again, no infinite stability ratios are observed. In fact, the stability ratios are quite low, even at the most stable concentration, which is not near the concentration for maximum electrostatic potential. What little stabilization there is comes from the steric barrier which is inadequate. The reason for the low stability ratio at larger zeta potentials may be due to depletion flocculation, especially since the medium contains a high concentration of charging agent for that dispersion. In addition, multiple layers of RE410 are on the surface at this concentration. Any charging on the surface must be from polymer-polymer interactions instead of metal oxide-polymer interactions. These results would explain the conductivity results and the failure for a trend in zeta potential-concentration plots. What little stabilization exists can be attributed to the steric film barrier in the case of RE410 dispersions.

2-6 Conclusions

Throughout this chapter it has been demonstrated that when using polymeric charging agents in low dielectric media, both steric and electrostatic stabilization are responsible for dispersion stability. If the zeta potential for these systems is greater than 100 mV, the electrostatic potential between two approaching pigments will be appreciable and a fairly stable barrier to flocculation will result. If the polymeric tail on the charging agent is as long as the critical flocculation distance, then a stable system will result. For these dispersions neither OLOA nor RE410 was sufficiently long to provide stabilization by steric means alone. The RE410 series which achieved it's most stable dispersion from purely steric stabilization did so by forming at least two layers, while the OLOA formed only one at its most stable concentration. The OLOA stabilized the dispersions of R100 and R901 most effectively through electrostatic stabilization and to a smaller extent by steric stabilization. This conclusion is consistent with the Fowkes acid-base theory since both of these surfaces contain much more TiO_2 than alumina on their surfaces (TiO_2 is more acidic than alumina). The Fowkes theory also correctly predicts OLOA 370 will extract a proton from the surface leaving it charged negatively after desorption. The absence of acidic sites is the reason for the low zeta potential for the Al5 pigment using OLOA. This deficiency of acid sites resulted in a much smaller contribution to the electrostatic potential, and was reflected in the low stability ratios.

The RE410 appeared not to charge the rutile pigment's surface but charged adsorbed polymer layers on the surface. This conclusion was formed by the evidence of multiple layers of RE410 found on the pigment's surface before charging took place. The surface charge, or zeta potential, that did develop was insufficient to stabilize the dispersion. In fact, at the concentration at which the zeta potential was greatest the system was less stable than at low concentrations of charging agent where no charging took place. This observation appears to be a result of depletion flocculation which can help overcome the electrostatic contribution. The sign of the zeta potential for all dispersions is in accord with Fowkes acid-base mechanism. The OLOA is basic and will extract protons from the acidic sites on the rutile pigments leaving the surface negatively charged with a positively charged OLOA counter-ion. Since there are more acidic sites on R100 and R901 than there are on Al5, a higher negative zeta potential is expected and obtained. The sign on the phosphate ester (RE410) coated particles is positive, a result which again can be explained by the Fowkes acid-base mechanism. The RE410 has both acidic and basic sites; this duality allows both types of sites to adsorb to the surface. The basic linkages of the modified RE410 surface can interact with the acidic head group of the free RE410 molecule in the medium. When these linkages extract a proton from the RE410 molecule, a positively charged surface results and a negative counter-ion is formed. This mechanism forms the basis for the next chapter.

CHAPTER III

THE EFFECTS OF POLYMERS ON THE ZETA POTENTIAL OF TITANIUM DIOXIDE IN LOW DIELECTRIC MEDIA

3-1 Objectives

The objective is to investigate and model the profile of the zeta potential versus charging agent concentration for dispersions in low dielectric media (Figure 1-9). The model used is based on the Fowkes acid-base mechanism (Figure 1-8) for the charging of colloidal particles in non-aqueous dispersions(13). The dispersion and related data discussed in this chapter are the same as discussed in Chapter II. The only additional data that are included in this chapter are from calorimetric measurements and these procedures are discussed below.

3-2 Materials and Experimental Procedures

The heats of adsorption were determined by using a Microscal flow calorimeter with a Perkin-Elmer LC-75 UV concentration detector down stream of the calorimeter (as seen in Figure 3-1). The technique was discussed in Chapter I. The solvent (cyclohexane HPLC grade) was dried over 8-12 mesh Davison 3-A molecular sieves (activated for 4 h under vacuum at 250 C). The TiO_2 rutile pigments (R100, R901, Al5) were dried at 110 C for 8 h and stored in a desiccator. The pyridine was Aldrich Sure-seal HPLC grade stored under nitrogen which was transferred via syringe to make up all solutions.

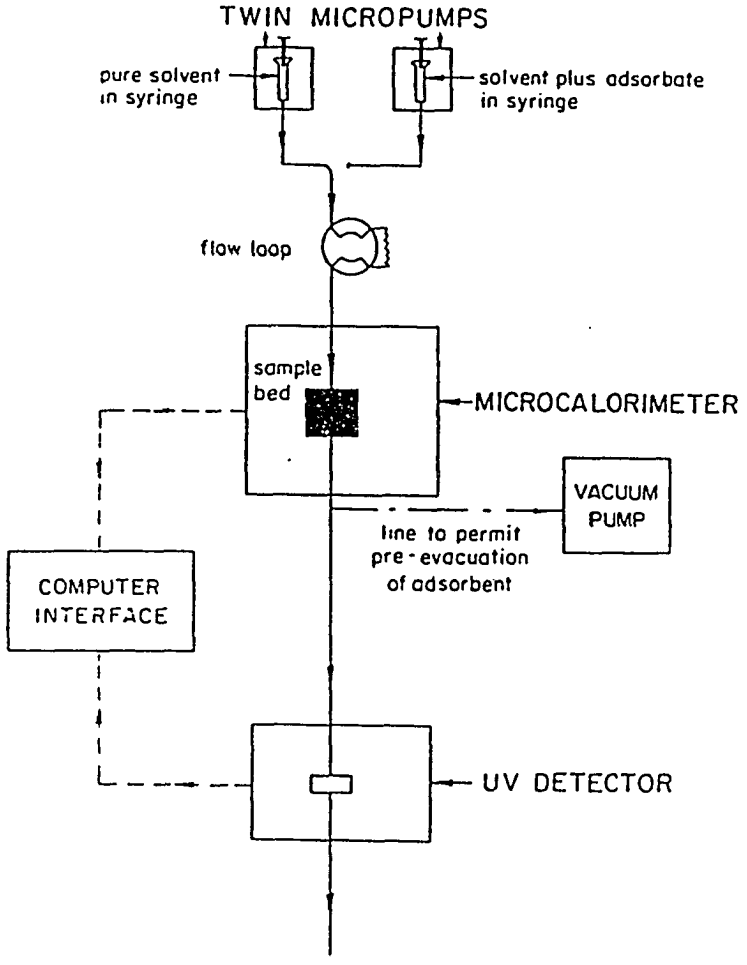

Figure 3-1. Block diagram for the microcalorimetric experimental arrangement.

3-3 The Fowkes Acid-Base Model

The Fowkes' acid-base model will be developed by the author, along the lines of the Kitahara model (Chapter I)(54). This model will then be used to describe the zeta potential versus charging agent concentration profile (Figure 1-9). To begin, the mechanism can be expressed in the equilibrium equation(50,121):

$$p + s \overset{K_1}{=} sp \overset{K_2}{=} s^{+}_{\cdot} + p^{-}_{+} \qquad 3\text{-}1$$

In this expression p is a charging agent (here a polymer molecule) s is a surface site, sp is a polymer molecule adsorbed or reacted onto a surface site (forming an acid-base complex), $s^{+}_{\cdot}$ is a charged surface site (positive if it is basic and negative if is acidic), and p^{-}_{+} is an oppositely charged desorbed polymer molecule, hence the reversal of the sign in the superscript and subscript. The superscript on $s^{+}_{\cdot}$ goes with the superscript on p^{-}_{+} and vice versa for the subscripts. This notation allows for a generalized model to be developed, independent of the sign on the site. From Equation 3-1 two equilibrium equations can be written as below:

$$K_1 = \frac{[sp]}{[p][s]} \qquad 3\text{-}2$$

$$K_2 = \frac{[s^{+}_{\cdot}][p^{-}_{+}]}{[sp]} \qquad 3\text{-}3$$

where the bracketed quantities represent the concentrations of the species as defined above. Combining equation 3-2 with 3-3 yields:

$$K_1K_2 = \frac{[s^+.][p^-_+]}{[s][p]} \qquad 3\text{-}4$$

A material balance equation for the surface sites can be written as follows:

$$[s_0] = [s] + [sp] + [s^+.] \qquad 3\text{-}5$$

where $[s_0]$ is the concentration of initial surface sites (moles of initial sites per square meter). Rearranging equations 3-3 and 3-4 and substituting into Equation 3-5 yields:

$$[s_0] = \frac{[s^+.][p^-_+]}{K_1K_2[p]} + \frac{[s^+.][p^-_+]}{K_2} + [s^+.] \qquad 3\text{-}6$$

which can be put into a linear form:

$$\frac{1}{[p^-_+]}\left\{\frac{[s_0]}{[s^+.]} - 1\right\} = \frac{1}{K_1K_2[p]} + \frac{1}{K_2} \qquad 3\text{-}7$$

Equation 3-7 is not practical to use as it stands; therefore, several relations are developed to enhance its utility.

The number of charged surface sites per particle (mean size) is equal to the total surface charge Q per particle, divided by the electron charge e (where e stands for only the magnitude of the charge). Therefore, the surface concentration of charged surface sites ([s^+]) is proportional to the number of particles, n_o, times the ratio of Q over e. Moreover, Q is proportional to the surface potential, ψ_0, which is approximately equal to the zeta potential, ζ, in non-aqueous dispersions. For a spherical particle at low potential (Debye-Hückel limiting law) Q can be expressed as Equation 3-8 (9, 54).

$$Q \approx 4\pi\epsilon a\psi_0(\kappa a+1) = 4\pi\epsilon a\zeta(\kappa a+1) \qquad 3\text{-}8$$

and

$$\epsilon = \epsilon_o\epsilon_r \qquad 3\text{-}9$$

where a is the particle radius, ϵ_o is the permittivity of free space, ϵ_r is the dielectric constant, and κ^{-1} is the Debye length. The Debye length can be calculated by the Klinkenberg-van der Minne equation (79):

$$\frac{1}{\kappa} = \left\{\frac{\epsilon D}{2\sigma}\right\}^{1/2} \qquad 3\text{-}10$$

where D is the diffusion constant and σ is the conductivity of the charge-carrying species. The diffusion constant can be calculated by the Stokes-Einstein equation corrected for rod-shaped charge-carrying species:

$$D = \frac{kT}{6\pi a\eta}(f/f_o) \qquad 3\text{-}11$$

where k is the Boltzmann constant, T is the absolute temperature, η is the viscosity of the medium, and f/f_o is the correction for rod-shape species.

Equation 3-8 allows the concentration of charged surface sites, $[s^+.]$ in moles/area, to be expressed in terms of the zeta potential.

$$[s^+.] = n_oQ/(eA_oA_{sp}m) = n4\pi\epsilon a\zeta(\kappa a+1)/(eA_oA_{sp}m) = k_s\zeta(\kappa a+1) \qquad 3\text{-}12$$

$$\text{where } k_s = n_o4\pi\epsilon a/(eA_oA_{sp}m) \qquad 3\text{-}13$$

where A_o (Avogadro's number), m (mass) and A_{sp} (the specific surface area) are used to convert to a moles/m^2 concentration basis.

In Fowkes' mechanism a charged surface site is formed by the desorption of a dispersant or polymer molecule from that surface site, leaving a charged surface site and an oppositely charged polymer molecule (a condition that obeys the law of electroneutrality (47)). The moles of charged surface sites are then equal to the moles of counter-ion polymer molecules, even though $[s^+.] \neq [p^-_+]$ because the former is in units of moles/m^2 (a two-dimensional surface) and the latter is in units of moles/m^3 (a three-dimensional dispersion). The concentration of counter-ion polymer molecules ($[p^-_+]$) is also proportional to n_oQ/e which in turn can be expressed in terms of zeta potential.

$$[p^-_+] = n_oQ/(eA_oV_d) = n_o4\pi\epsilon a\zeta(\kappa a+1)/eA_oV_d = k_p\zeta(\kappa a+1) \qquad 3\text{-}14$$

$$\text{where } k_p = n_o4\pi\epsilon a/(eA_oV_d) \qquad 3\text{-}15$$

where V_d is the volume of the dispersion.

If Equations 3-12 and 3-14 are substituted into Equation 3-7 an experimentally accessible equation is obtained.

$$\frac{1}{\zeta(\kappa a+1)k_p}\left\{\frac{[s_0]}{\zeta(\kappa a+1)k_s}-1\right\}=\frac{1}{K_1K_2}\frac{1}{C_{eq}}+\frac{1}{K_2} \qquad 3\text{-}16$$

where C_{eq} is the equilibrium concentration of polymer in solution and is approximately equal to [p] (non-charged polymer in solution).

It has been indicated in the last chapter as well as shown in other work (119,120), that there is typically one basic and/or one acidic site per thirty to forty square Angstroms for the rutile surfaces (i.e., titanium dioxide, alumina, silica, and adsorbed polymers). For a spherical particle of 300 nm in diameter there is a minimum of approximately half million sites. At a 50mV surface potential (in a low dielectric medium of about 2) there are about ten electron charges per particle. Therefore, the ratio of initial sites to charged sites far exceeds unity.

$$[s_0]/\zeta(\kappa a+1)k_s=[s_0]/[s^+.]>>1 \qquad 3\text{-}17$$

This condition means that Equation 3-16 can be written as follows:

$$\frac{1}{\zeta^2(\kappa a+1)^2}=\frac{k_pk_s}{K_1K_2[s_0]}\frac{1}{C_{eq}}+\frac{k_pk_s}{K_2[s_0]} \qquad 3\text{-}18$$

The above equation is the linear form of the desired result. A plot of $1/\zeta^2(\kappa a+1)^2$ versus $1/C_{eq}$ should yield a straight line if the Fowkes acid-base mechanism is applicable. In addition, K_1 and $K_2[s_0]$ can be obtained from the intercept and slope as seen below:

$$K_1 = \frac{\text{intercept}}{\text{slope}} \qquad 3\text{-}19$$

$$GK_2 = \frac{k_p k_s}{(\text{intercept})n_o} \qquad 3\text{-}20$$

where n_o is the number of particles and G is the moles of initial sites per square meter per particle. Once K_1 and GK_2 (equilibrium product) are determined they can be used in the rearranged version of Equation 3-18 to predict the zeta potential as a function of equilibrium concentration (Equation 3-21).

$$\zeta = \left\{\frac{C_{eq}[s_0]K_2}{k_p k_s\{(1/K_1)+C_{eq}\}}\right\}^{1/2}\left\{\frac{1}{(\kappa a+1)}\right\} \qquad 3\text{-}21$$

The above equation will be analyzed in the discussion to help give some insight into the acid-base interpretation.

3-4 Results and Discussion

The Fowkes intepretation can now be tested quantitatively by using Equation 3-18. In order to carry out this objective the equilibrium concentration (C_{eq}), the zeta potential (ζ), and the Debye length ($1/\kappa$) must be obtained for each dispersion. These results have already been obtained previously in Chapter II, since C_{eq} can be taken from the adsorption isotherms (Figures 2-21 through 2-26) and ζ and $1/\kappa$, taken from Figures 2-9, 2-10, 2-33, and 2-34. The Debye lengths and zeta potential versus equilibrium concentration are plotted in Figures 3-2 through 3-5 for all three pigments for each charging agent. Not surprisingly, they are very similar to Figures 2-9, 2-10, 2-33, and 2-34 since C_{eq} is approximately equal the total concentration of charging agent (especially at high concentration). If these results from Figures 3-2 through 3-5 are used in Equation 3-18 and plotted as $1/[\zeta(\kappa a+1)]^2$ versus $1/C_{eq}$ a crude linear fit is obtained for all six dispersion series (i.e., R100, A15, R901 with OLOA 370 or RE410), as seen in Figures 3-6 through 3-11. These linear plots support the Fowkes acid-base mechanism even though the measurements of conductivity, zeta potential, and concentration have a high degree of uncertainty.

The equilibrium constants extracted from the slope and intercept of these plots are listed in Table 3-1. The constants k_p and k_s which were used in the calculation of the equilibrium product constants (GK_2) are listed in Appendix II.

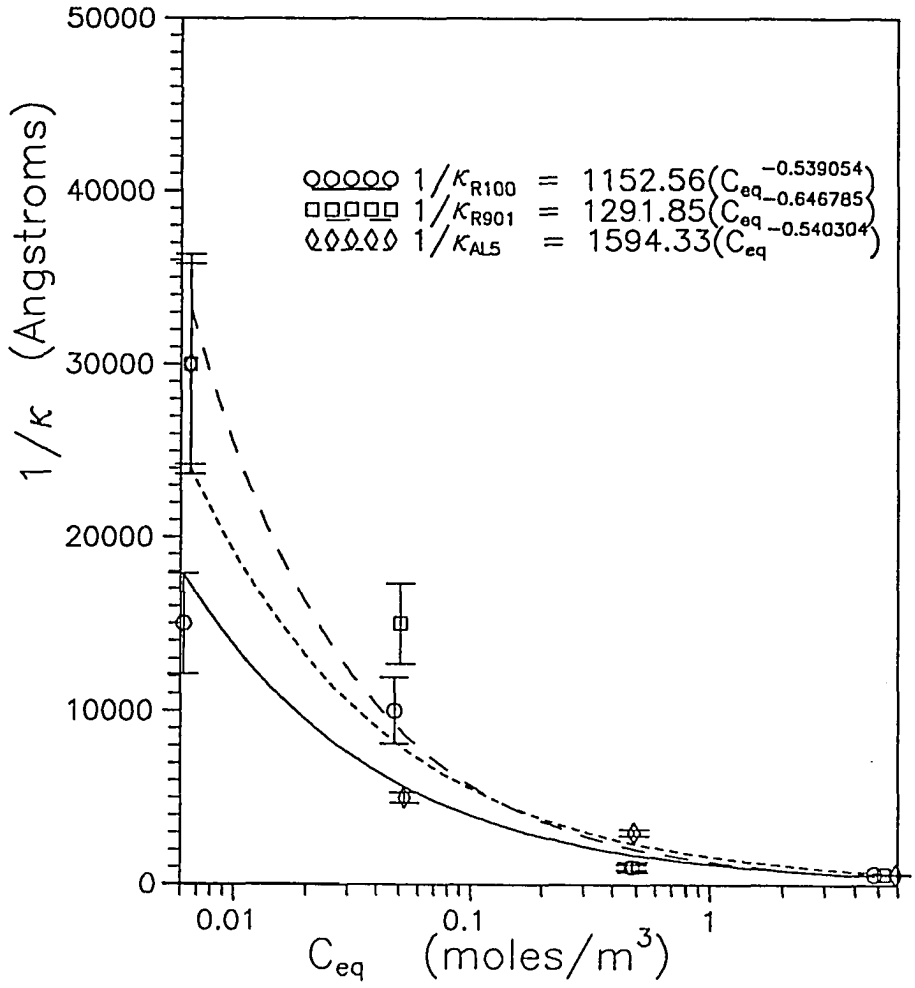

Figure 3–2. The Debye length, in Angstroms, for the three different rutile pigments as a function of the equilibrium concentration of OLOA 370 in cyclohexane.

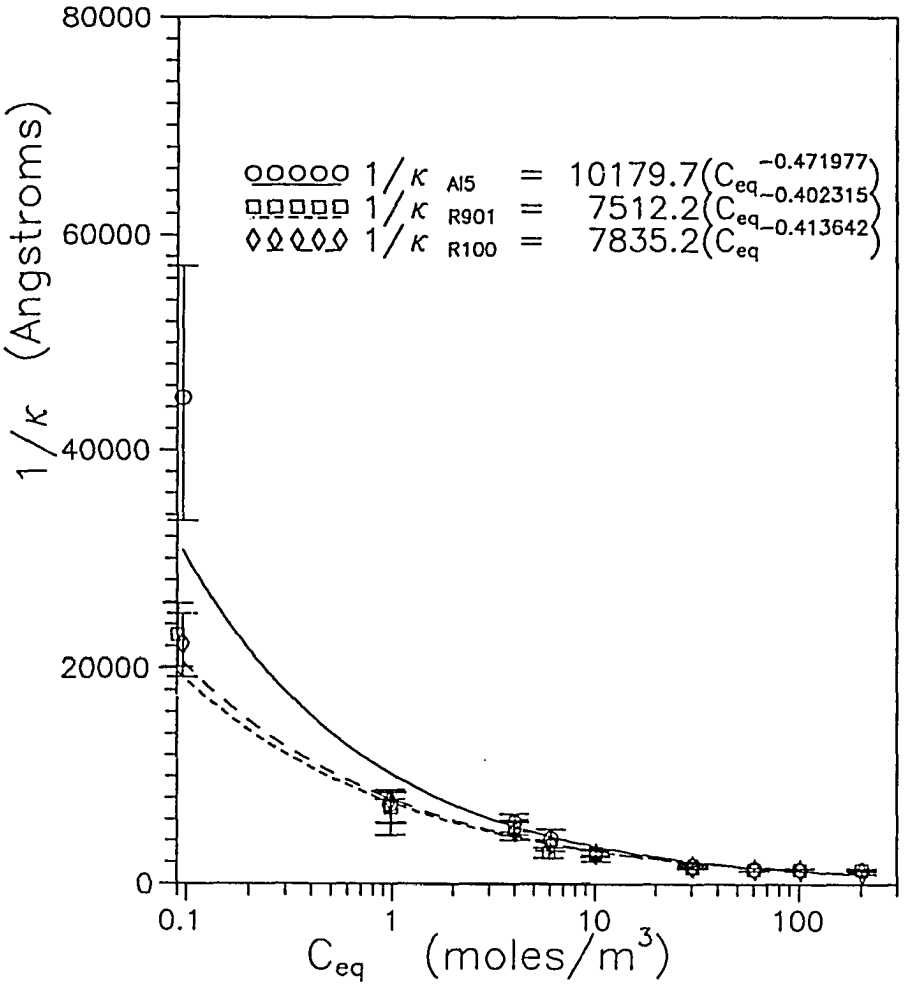

Figure 3–3. The Debye length, in Angstroms, for the dispersion of the three rutile pigments (R100, R901, AI5) as a function of the equilibrium concentration RE410 in cyclohexane.

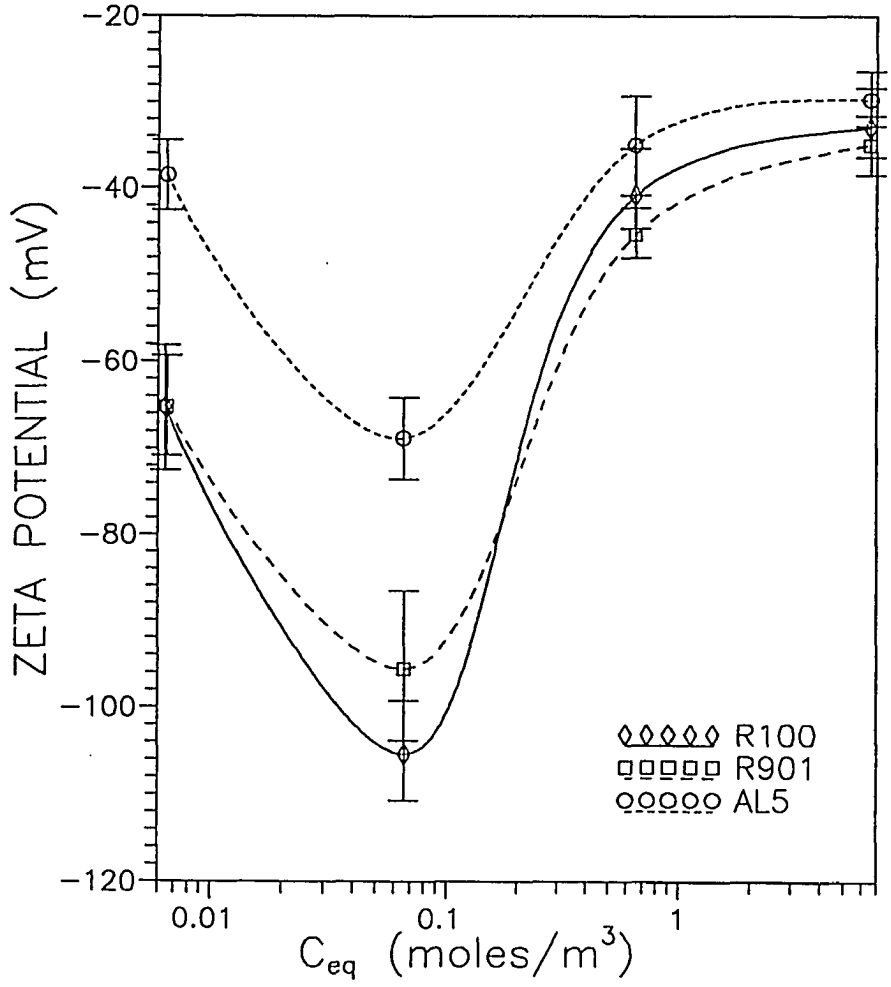

Figure 3–4. The zeta potential versus equilibrium concentration of OLOA 370 in cyclohexane for 0.003 wt% of the three pigments.

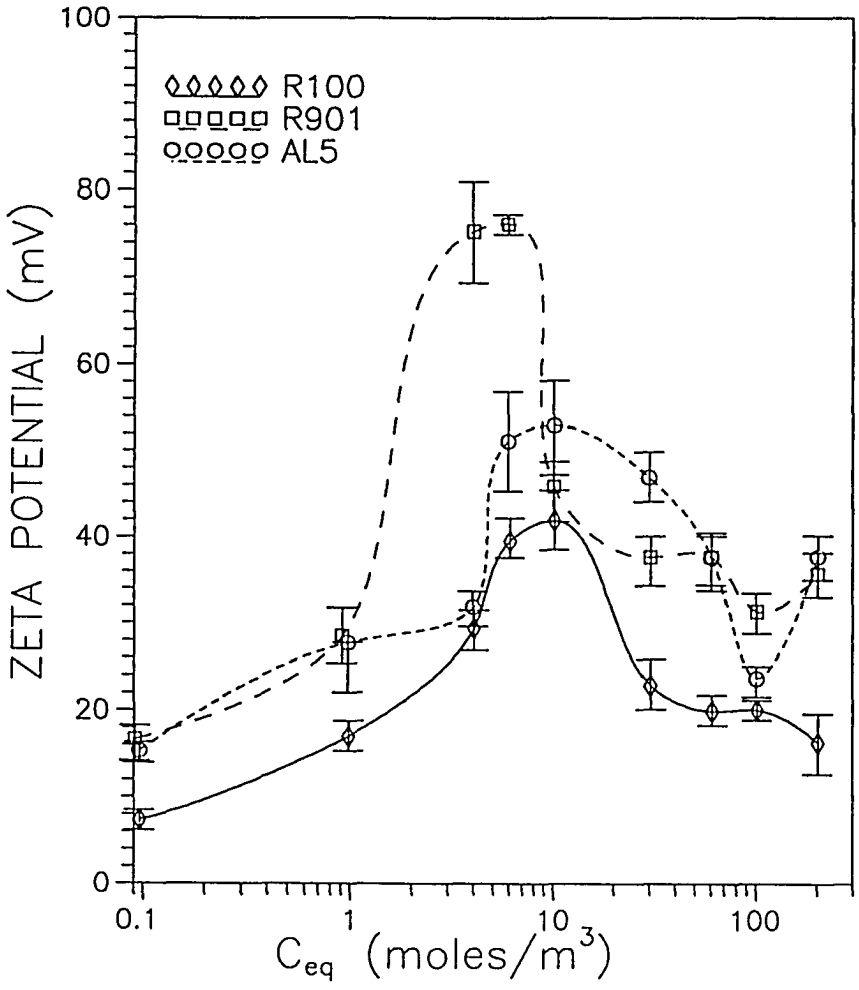

Figure 3–5. The zeta potential versus equilibrium concentration of RE410 in cyclohexane for 0.003 wt% of the three rutile pigments.

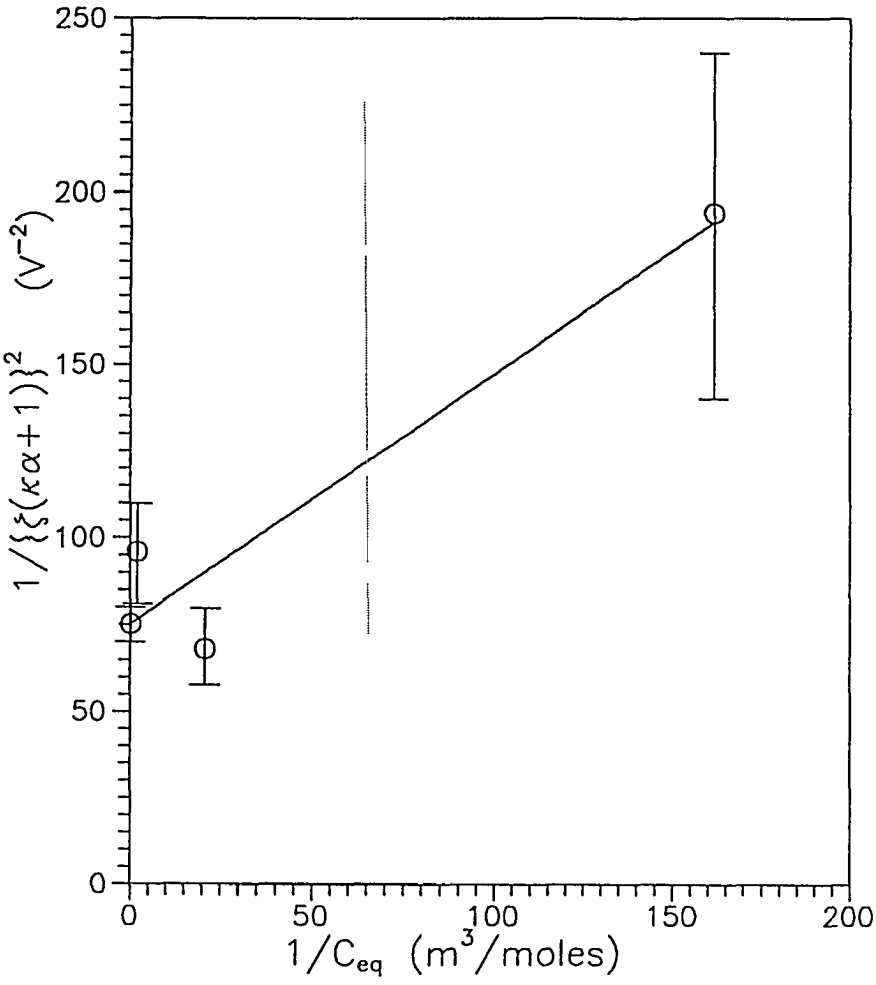

Figure 3-6. The linear plot for the equation (3-18) derived from the Fowkes acid-base model using 0.002 wt% R100 with OLOA 370 (C_{eq}) in cyclohexane.

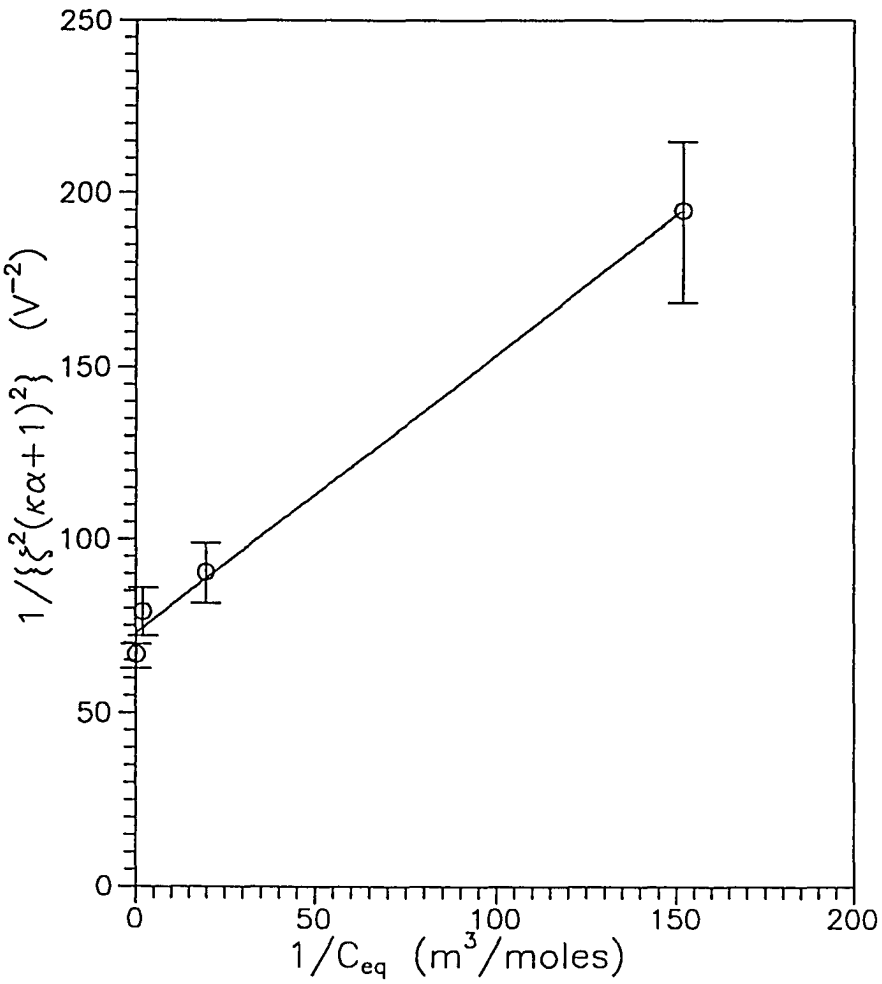

Figure 3–7. The linear plot for the equation derived from the Fowkes acid–base model using 0.002 wt% R901 with OLOA 370 (C_{eq}) . in cyclohexane.

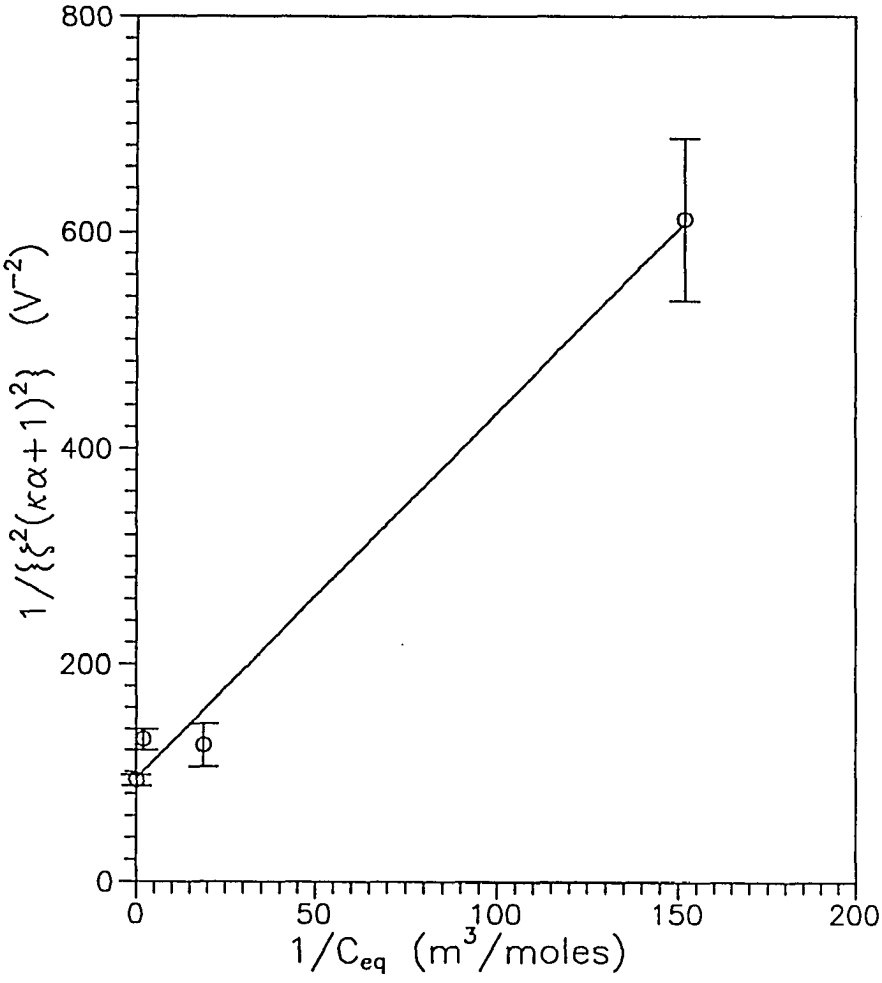

Figure 3–8. The linear plot for the equation (3–18) derived from the Fowkes acid–base model using 0.002 wt% Al5 with OLOA 370 (C_{eq}) in cyclohexane.

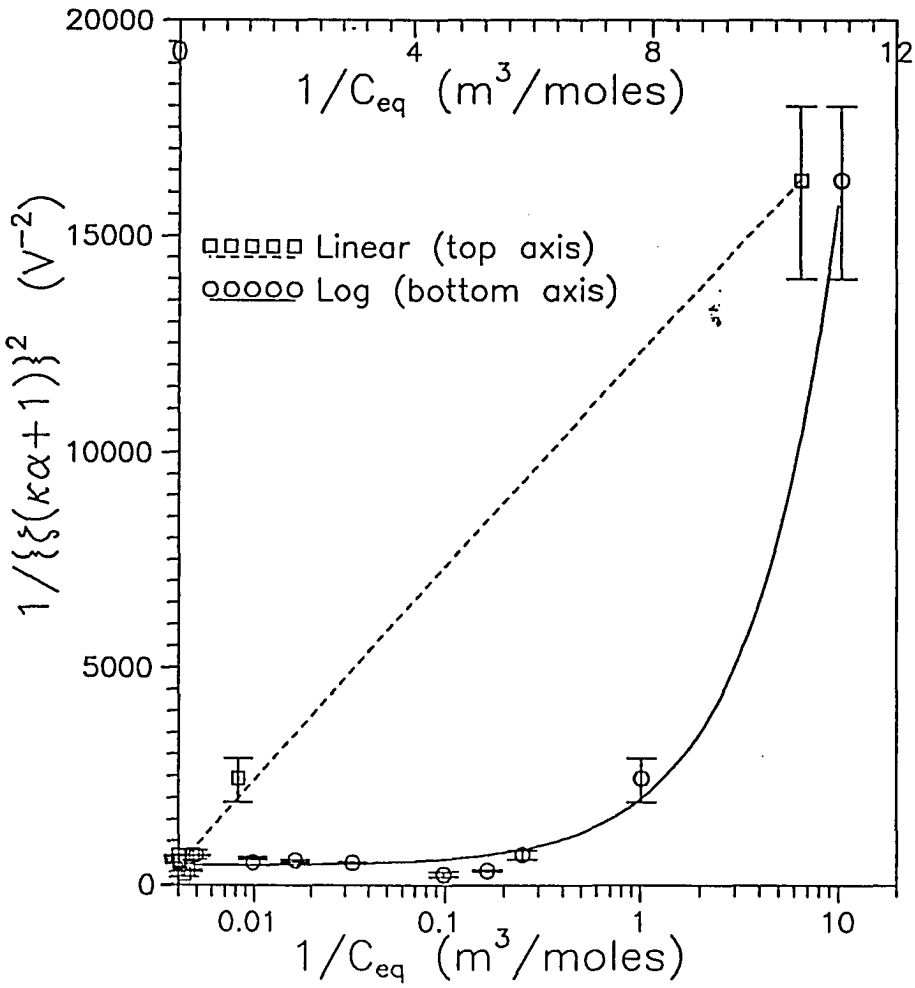

Figure 3–9. The plots for the equation (3–18) derived from the Fowkes acid–base model using 0.003 wt% R100 with RE410 . in cyclohexane.

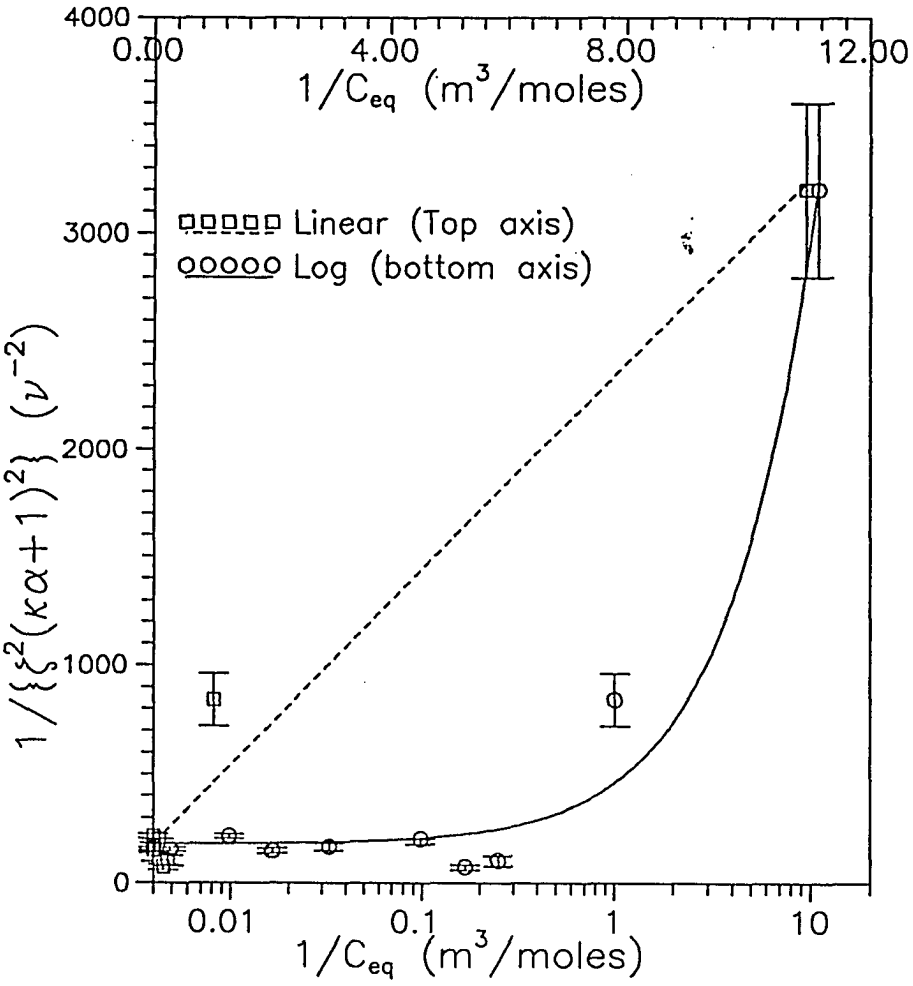

Figure 3–10. The plots for the equation (3–18) derived from the Fowkes acid–base model using 0.003 wt% R901 with RE410 (C_{eq}) in cyclohexane.

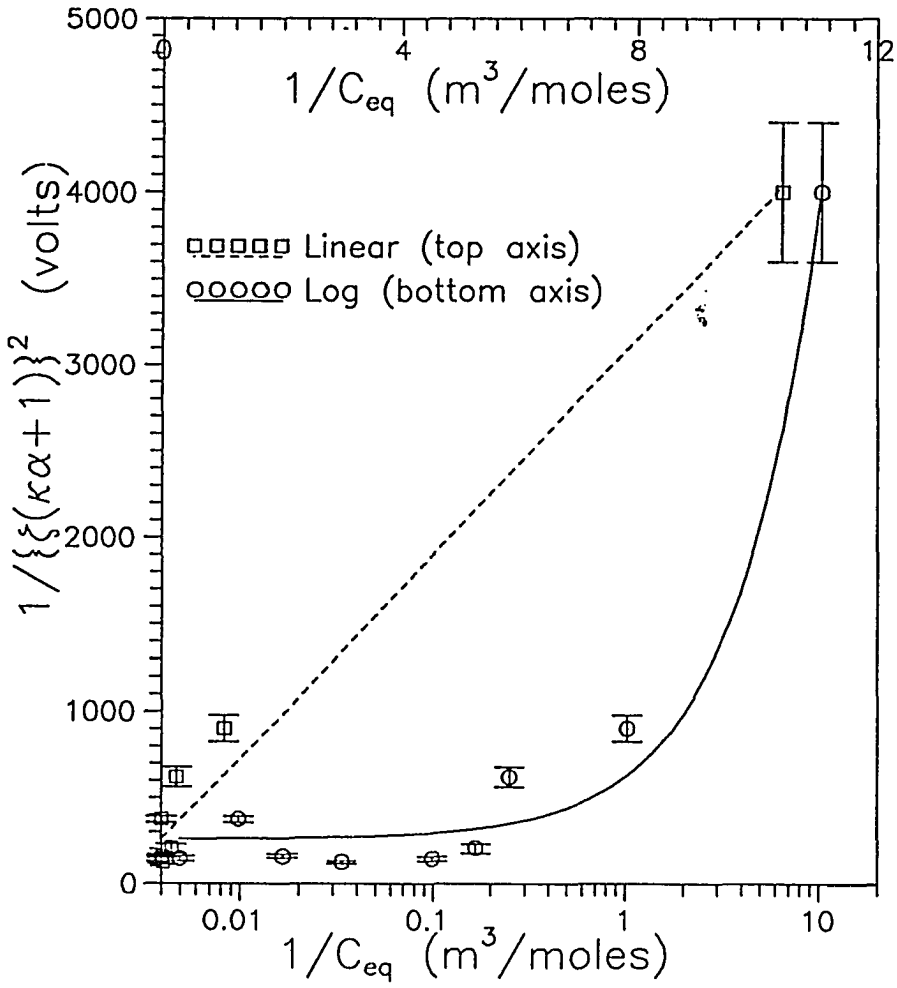

Figure 3–11. The plots for the equation (3–18) derived from the Fowkes acid–base model using 0.003 wt% Al5 with RE410 (C_{eq}) in cyclohexane.

	RE410		OLOA 370	
	K_1(m^3/moles)	GK_2 (moles^2) (m^5 particle)	K_1(m^3/moles)	GK_2 (moles^2) (m^5 particle)
R100	0.3	$7.4x10^{-31}$ ($9.8x10^{-30}$)	104	$4.2x10^{-29}$
R901	0.7	$2.9x10^{-30}$ ($1.6x10^{-29}$)	90	$1.0x10^{-29}$
A15	0.6	$2.8x10^{-30}$ ($2.3x10^{-29}$)	28	$5.4x10^{-30}$

Table 3-1. The equilibrium constant K_1 and the product of the equilibrium constant, K_2, and G (moles per square meter per particle) for all three pigments using both charging agents. These were extracted from the slopes and intercepts of the graphs in Figures 3-6 through 3-11. The constants in brackets were obtained by assuming that charging has its origin at an adsorbed polymer layer and not at the metal oxide layer. In this case it is assumed that the new surface has a surface area of a sphere. See Appendix I for constants k_s and k_p.

The value of K_1 should be an indication of the surface acidity or basicity since it corresponds to the adsorption step in the Fowkes acid-base mechanism. As was stated in Chapter II, the three rutile pigments should vary in acidity or basicity, since varying amounts of alumina were used in their preparation. The expected order of basicity is: A15 > R901 > R100. Therefore a trend in K_1 should appear in the above table from the most acidic surface (R100) to the most basic (Al5). It is interesting to note that not only does the equilibrium constant K_1 decrease significantly with increase of basicity for the OLOA 370 case, but the values of K_1 for R100 and R901 are close, reflecting the fact that their surfaces are similar and

different from Al5 (as evidenced by Table 2-1). For acidic RE410 a trend in K_1 is not observed. The absence of a trend is consistent with the adsorption isotherm results. These results suggest that multiple layer build-up of RE410 occurs on the surface of all three types of pigments, well in advance of surface charge development by the free RE410. The new modified polymer surfaces of all three pigments should yield nearly identical surfaces.

By contrast, the OLOA 370 for all three pigments forms a monolayer as it charges the surface, indicating the charging of the metal oxide surface instead of a polymer coated surface. In other words, the metal oxide surfaces are charged by OLOA 370, whereas it is suggested for the RE410 case that the free RE410 charges at the new polymer-medium interface. Therefore the values of K_1 for the three pigments should not differ greatly where RE410 is used as the charging agent. This concept is reflected in Table 3.1, since no real trend is seen with the expected order of basicity nor are the differences in the values of K_1 large. In summary, the values obtained for the K_1 equilibrium constant are consistent with the adsorption isotherm work in Chapter II lending credence to the Fowkes acid-base mechanism.

The equilibrium constant K_2 is more difficult to analyze because it cannot be separated from the quantity G, which is the number of moles of initial sites per square meter per particle, if G is not known from a separate experiment. In the case of RE410, G should be the same for all three pigments, since this agent appears to be charging at the polymer layer, indicating that all three types of pigments would

effectively have the same surface. Therefore the quantity GK_2 should be approximately constant over all three cases. The quantities in brackets in Table 3-1 (assuming all polymer coated pigments have smooth spherical surfaces) appear to reflect this constancy, since no discernible trend can be observed in relation to the native surfaces (Table 2-3). For the OLOA 370 case the trend should be for the most acidic pigment to have the largest K_2 value. The true magnitude of K_2 is somewhat uncertain since G depends on the initial concentration of sites, which is difficult to determine or define. The value of G is difficult to define because a polymer molecule could adsorb to an area that may contain more than one site, denying access to these sites by other polymer molecules. If a probe molecule, such as pyridine, is used to estimate the initial number of sites, a much larger number may be obtained, than if a larger polymer molecule is used. This overestimation is because pyridine is smaller and will access more sites. Therefore, no attempt is made to evaluate G.

Another check of the equilibrium constants obtained by the above analysis is through the use of the heats of adsorption. The heat of adsorption (using a basic probe molecule) should follow the same trend as the equilibrium constant, K_1, obtained from the OLOA 370 case. That is, increasing $-\Delta H$ means increasing bond strength and shift of $:S+P \rightleftharpoons SP$ toward adsorption. Since the oxide surface is different for each pigment, a different heat of adsorption as well as K_1 is expected. The results of the heats of adsorption (two consecutive cycles) measurements, using pyridine as a probe molecule, are listed in Table 3-2:

	kcal/mole (1st ads.)	kcal/mole (2nd ads.)
R100	11.5	9.9
R901	9.7	8.3
A15	5.8	4.2

Table 3-2. *The heats of adsorption for the three pigments R100, R901, and Al5. Pyridine (20 mM) was used as a probe molecule and cyclohexane was the solvent.*

On this concept, pyridine will react with the acidic sites on the pigment surface and will occupy a surface area of 25Å^2, (i.e., about half the area that the amine head group of OLOA 370 will occupy).

As can be seen in Table 3-2, the heat of adsorption for R100 is the largest, followed by R901 and then Al5 following the order of decreasing acidity or increasing alumina. Following the expected trend is the decreasing equilibrium constant K_1, derived from the Fowkes acid-base model (Equation 3-21).

Equation 3-21 should predict the experimental zeta potential for a given C_{eq} and corresponding $1/\kappa$. By using the power series fit in Figures 3-2 and 3-3, the Debye lengths were calculated for the various C_{eq}. The same C_{eq} and $1/\kappa$ values along with the equilibrium constants in Table 3-1 and the constants in Appendix II were used in Equation 3-21 to yield Figures 3-12 through 3-17, which are the fit of the experimental data for each pigment and charging agent. While the fit is not perfect it does indicate that Fowkes acid-base mechanism can at least describe the system semi-quantitatively.

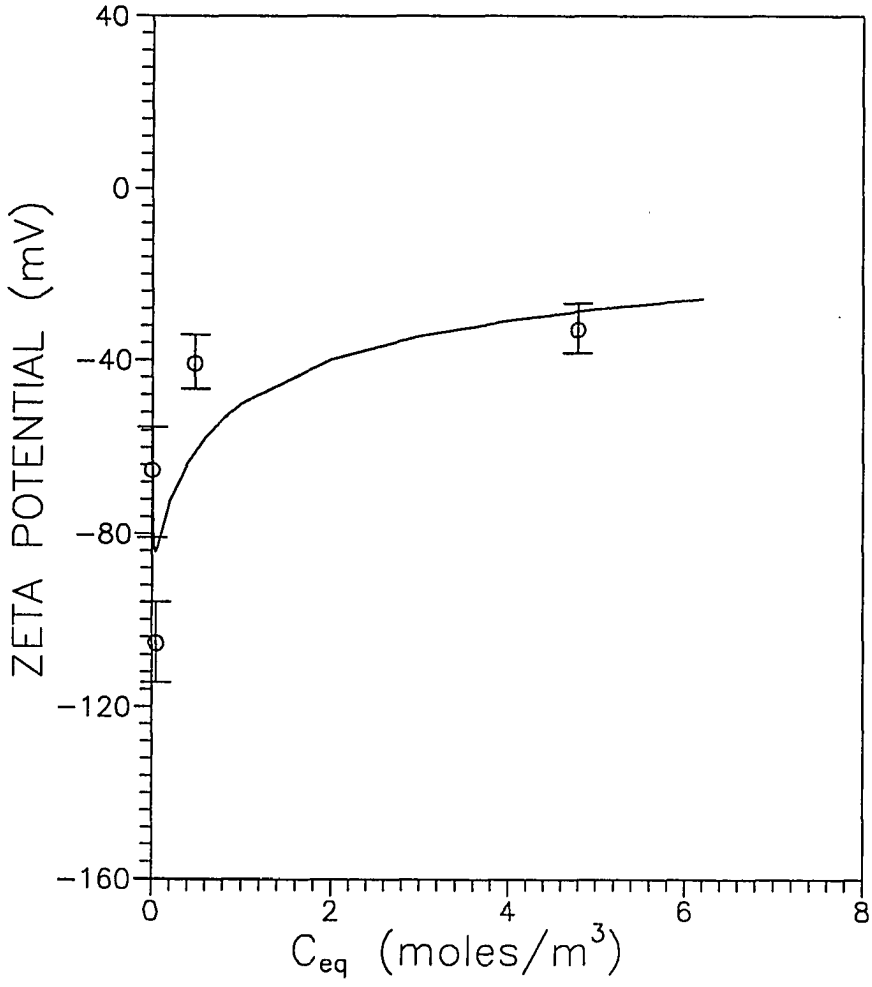

Figure 3–12. The zeta potential dependence on the charging agent concentration for dispersions of R100 (0.002 wt%) with OLOA 370 in cyclohexane. The solid line is from equation 3–21 (using the power fit in Figure 3–2 and Table 3–1) and the points are from the experimental results (Figure 3–4).

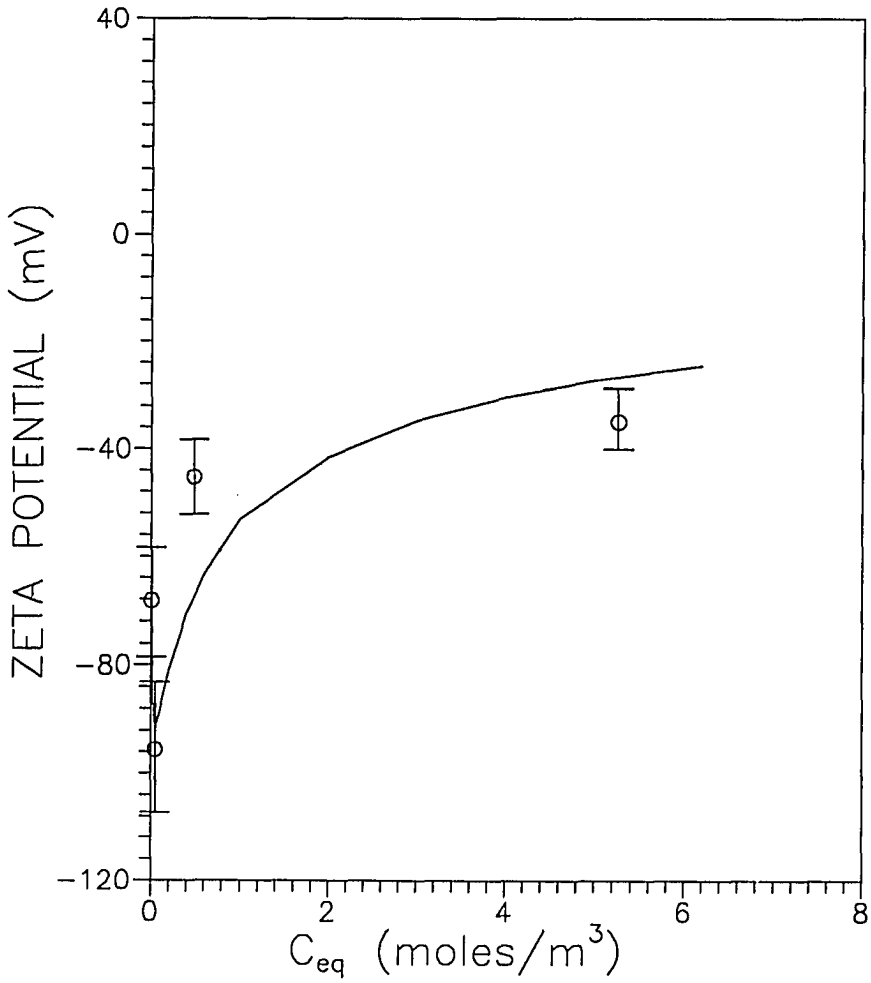

Figure 3–13. The zeta potential dependence on the charging agent concentration for dispersions of R901 (0.002 wt%) with OLOA 370 in cyclohexane. The solid line is from equation 3–21 (using the power fit in Figure 3–2 and Table 3–1) and the points are from the experimental results (Figure 3–4).

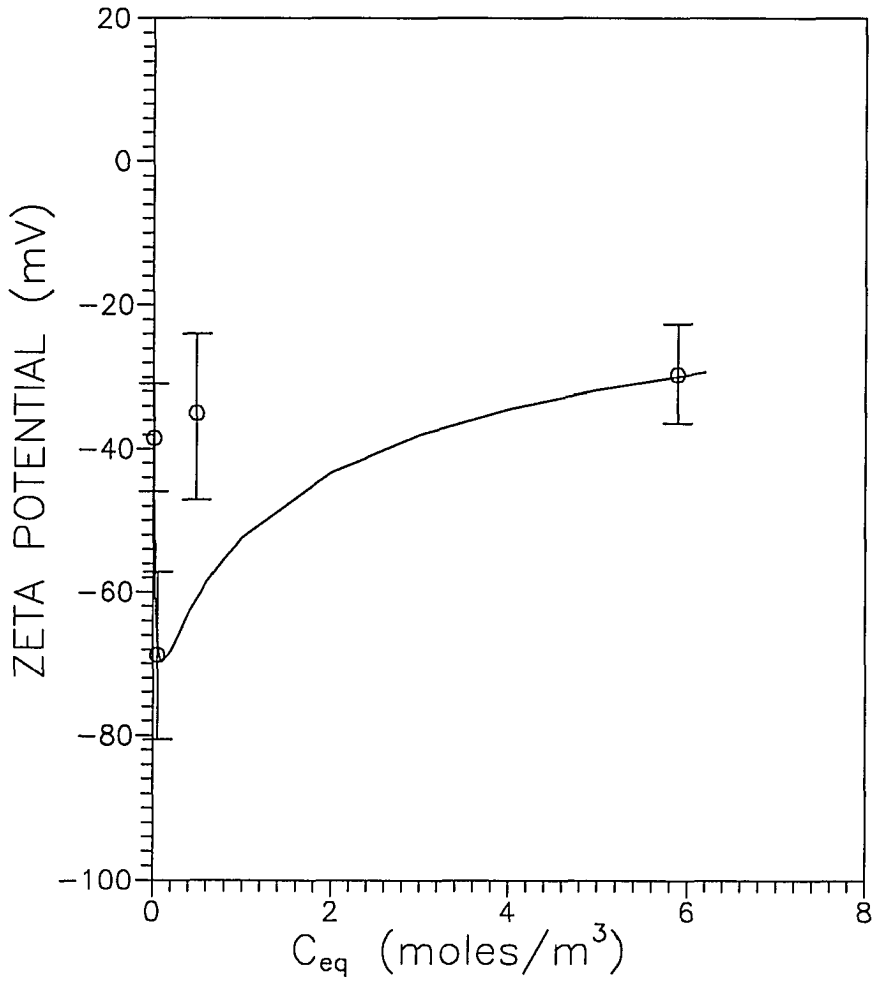

Figure 3–14. The zeta potential dependence on the charging agent concentration for dispersions of Al5 (0.002 wt%) with OLOA 370 in cyclohexane. The solid line is from equation 3–21 (using the power fit in Figure 3–2 and Table 3–1) and the points are from the experimental results (Figure 3–4).

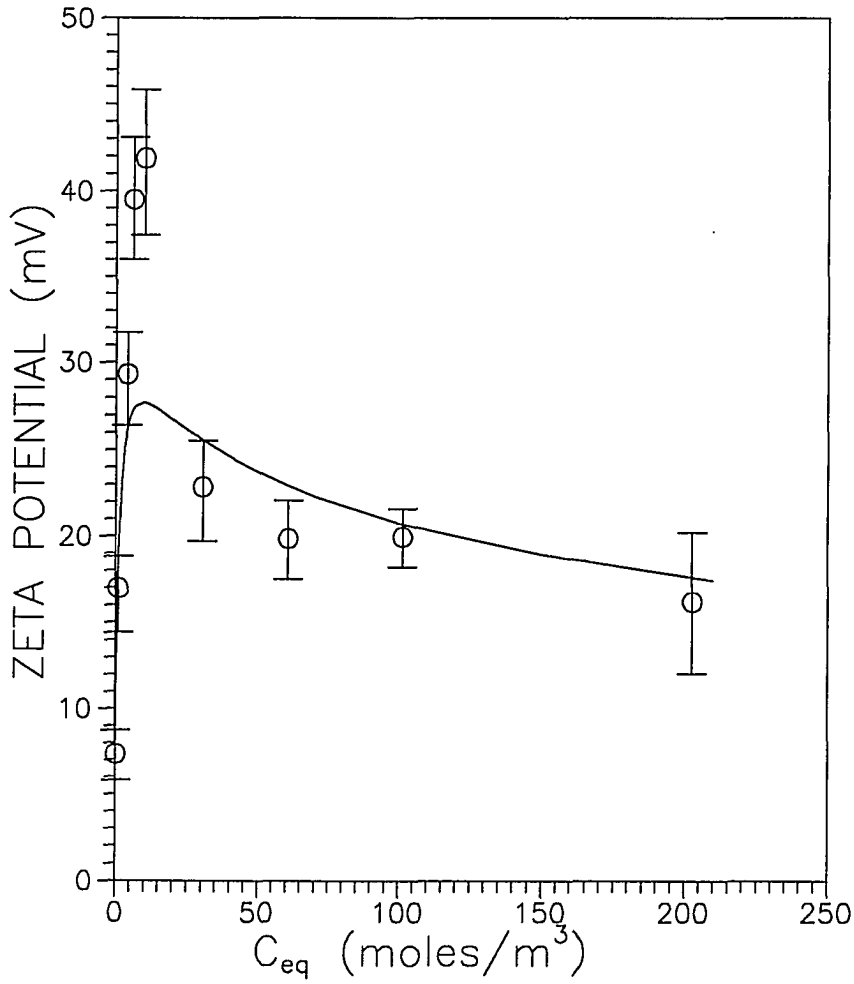

Figure 3–15. The zeta potential dependence on the charging agent concentration for dispersions of R100 (0.003 wt%) with RE410 in cyclohexane. The solid line is from equation 3–21 (using the power fit in Figure 3–3 and Table 3–1) and the points are from the experimental results (Figure 3–5).

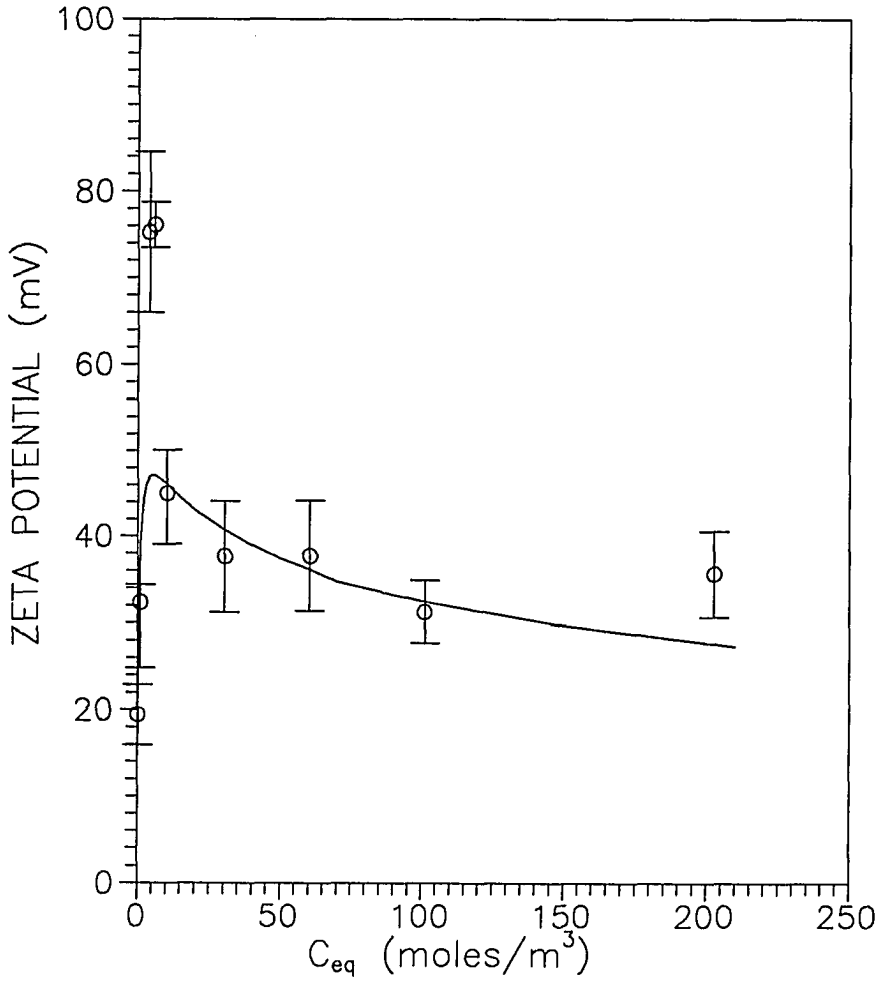

Figure 3–16. The zeta potential dependence on the charging agent concentration for dispersions of R901 (0.003 wt%) with RE410 in cyclohexane. The solid line is from equation 3–21 (using the power fit in Figure 3–3 and Table 3–1) and the points are from the experimental results (Figure 3–5).

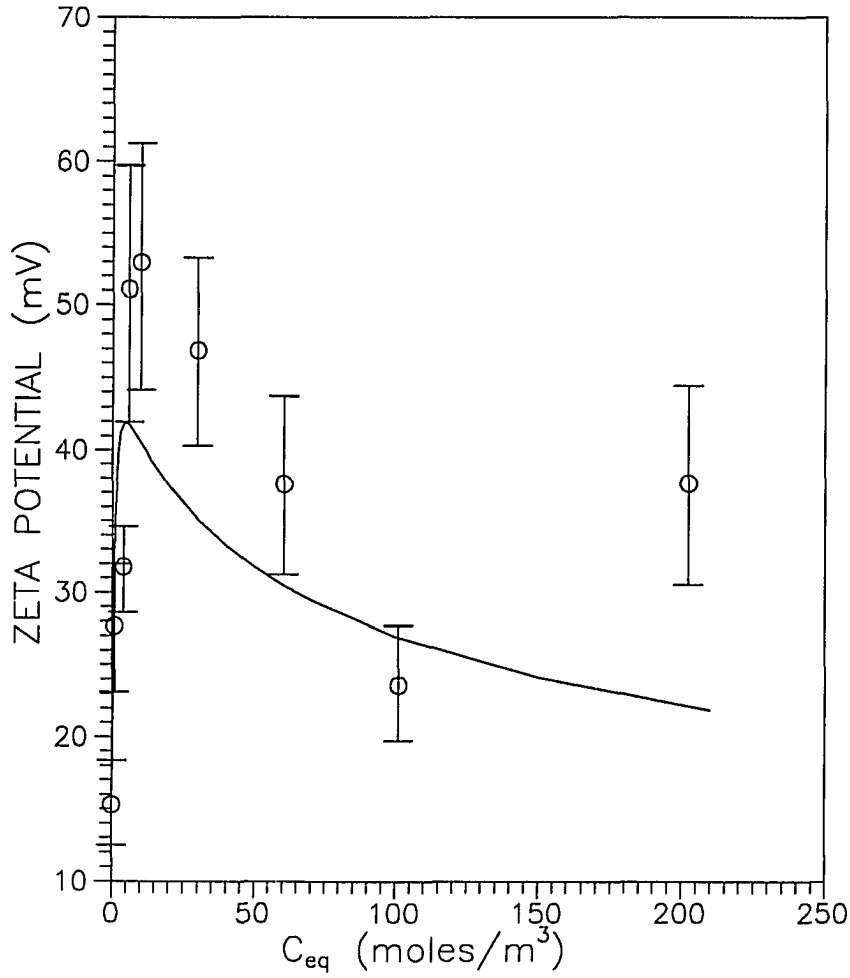

Figure 3–17. The zeta potential dependence on the charging agent concentration for dispersions of Al5 (0.003 wt%) with RE410 in cyclohexane. The solid line is from equation 3–21 (using the power fit in Figure 3–3 and Table 3–1) and the points are from the experimental results (Figure 3–5).

One more point needs to be discussed about the Fowkes model, which can also be argued through Equation 3-21. When the Debye length approaches infinity the surface charge is approximately proportional to the zeta potential times a constant (Equation 3-8) and Equation 3-21 would be written as:

$$\zeta = \left\{ \frac{C_{eq}[s_0]K_2}{k_p k_s\{1/K_1 + C_{eq}\}} \right\}^{1/2} \qquad 3\text{-}22$$

This equation predicts that the zeta potential would reach a plateau limit as an adsorption isotherm does. It would not predict the decrease observed after a maximum as the concentration of charging agent is increased. The term $\kappa a + 1$, most notably κ, is responsible for the zeta potential decrease. As the concentration of charging agent is increased so is the concentration of counter-ions, corresponding to an increase in the electrical conductivity of the dispersion. An increase in conductivity will decrease the Debye length, so as ultimately to make the second term in Equation 3-21 even more important in reducing the magnitude of the zeta potential. The importance of this term can be explained in more detail by looking at a rearranged version of Equation 3-8:

$$\zeta = \frac{Q}{4\pi\epsilon a(\kappa a + 1)} \qquad 3\text{-}23$$

As Q approaches some upper limit (as would be expected if a particle reached its maximum charge) only an increase in the term $\kappa a + 1$ would be available to decrease the zeta potential.

Equation 3-23 is intuitively satisfying because it enables the Fowkes mechanism to be reconciled to the experimental results and follow Le Châtelier's principle. Le Châtelier's principle applied to the Fowkes acid-base model would predict a saturation of charge as the concentration of charging agent is increased, since the finite number of sites would all eventually become charged. This agreement essentially implies that the reduction in the zeta potential is due to either an increase in counter-ion concentration and thus a decrease in the Debye length, and not to a decrease in the surface charge.

3-5 Conclusions

The dispersions covered in this dissertation all had low dielectric constant media which enable certain assumptions, such as substitution of the zeta potential for surface potential and the use of Equation 3-8. These two assumptions, combined with the equilibrium equation (3-1) which describes the Fowkes acid-base mechanism, led to the development (by the author) of an equation which describes the zeta potential-charging agent concentration phenomenon. This description is at least semi-quantitative in nature and yields equilibrium constants that support the Fowkes mechanism. The importance of the model described by Equation 3-21 is that it explains the concentration dependence behavior of the zeta potential and yet obeys

the Le Châtelier principle as applied to Equation 3-1. In addition, this expression suggests that both the surface charge and Debye length are responsible for the magnitude of the zeta potential, a finding that is in line with the law of electroneutrality.

APPENDIX I.

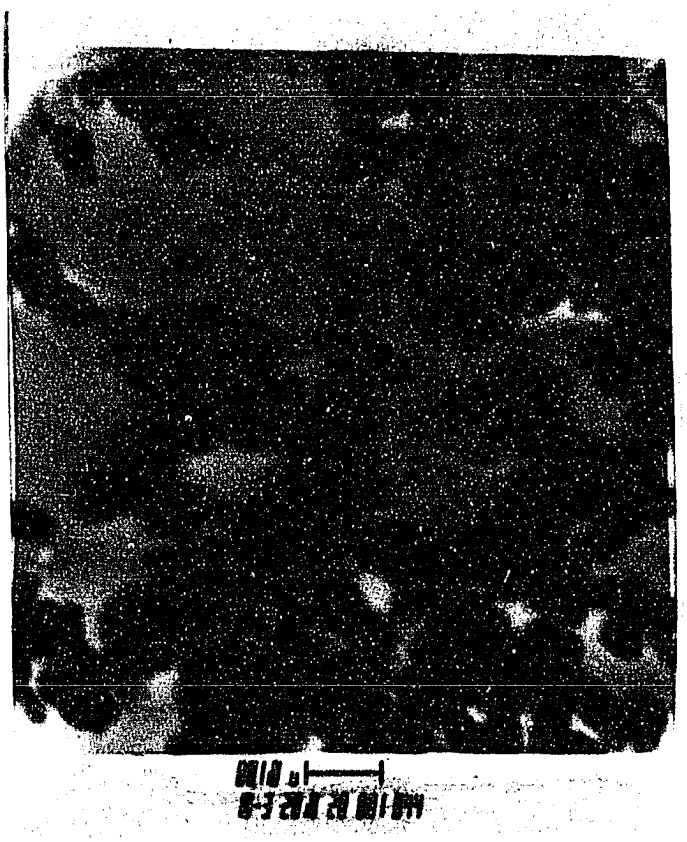

Figure A-1. R100 Pigments

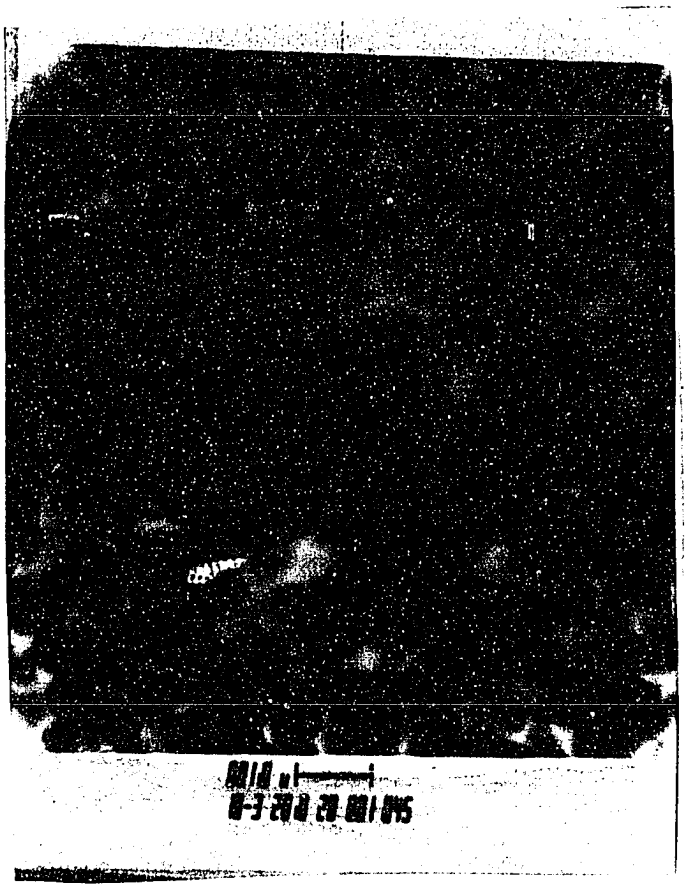

Figure A-2. R901 Pigments

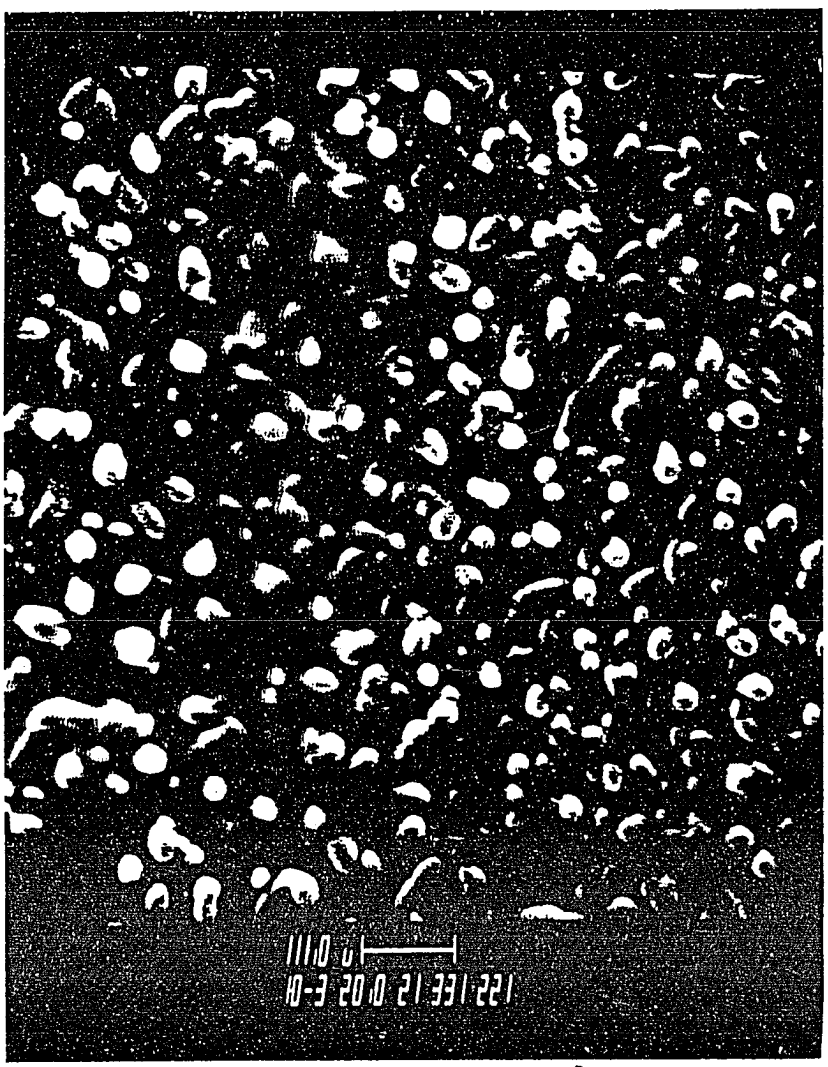

Figure A-3. A15 Pigments

APPENDIX II
(Evaluation of the constants k_p and k_s)

The constants k_p and k_s are required to evaluate the product GK_2, from Equation 3-20 as restated below:

$$GK_2 = \frac{k_p k_s}{n_o \text{ (intercept)}}$$

k_p from Equation 3-15 can be recast as:

$$\frac{k_p}{n_o} = \frac{4\pi\epsilon a}{eA_o V_d} \qquad \text{A2-1}$$

where all the constants were defined previously. The constant k_s, from Equation 3-13, can also be rewritten by substitution of n_o:

$$k_s = \frac{3\epsilon}{eA_o a^2 \rho A_{sp}} \qquad \text{A2-2}$$

where

$$n_o = \frac{3(m/\rho)}{4\pi a^3} \qquad \text{A2-3}$$

In the above equation n_o was calculated by dividing the total particle volume (m/ρ) by the volume of a single spherical particle. The quantities necessary to calculate k_p/n_o and k_s are listed in Table A2-1.

	R100	A15	R901
a(m)	$1.5x10^{-7}$	$1.5x10^{-7}$	$1.5x10^{-7}$
$V_d(m^3)$	$1x10^{-4}$	$1x10^{-4}$	$1x10^{-4}$
$A_{sp}(m^2/g)$	6.63	29.5	46.22
ϵ_r	2.036	2.036	2.036
ρ(g/ml)	4.10	4.03	3.68

Table A2-1.

For each dispersion series the quantities needed to calculate k_p/n_o and k_s in Table 2-1 will be the same (independent of the charging agent concentration), except for the dielectric constant. This constant is slightly dependent (2%) on the concentration of charging agent present (Figure 2-7). It is assumed that the concentration dependence is negligible and an average value of ϵ_r is used for all dispersions and constants. Therefore, only three values of k_s and one value of k_p/n_o (Table A2-2) are required to calculate the equilibrium product from the intercept results.

	$k_s \left\{ \frac{\text{C mole}}{\text{Nm}^3} \right\}$	$\frac{k_p}{n_o} \left\{ \frac{\text{C mole}}{\text{Nm}^4 \text{ Particle}} \right\}$
R100	9.10×10^{-10}	3.50×10^{-18}
R901	2.16×10^{-10}	3.50×10^{-18}
A15	1.45×10^{-10}	3.50×10^{-18}

Table A2-2.

REFERENCES

1. Novotny, V., Colloids and Surfaces, 24(1978) 361-375.

2. Hunter, R.J., "Zeta Potential in Colloid Science" Academic, London, 1981.

3. Ross, S.; Morrison, I.D. "Colloidal Systems and Interfaces", Wiley, New York, 1988.

4. Hunter, R.J. "Foundations of Colloid Science", Vol. 1; Clarendon Press: Oxford, 1987.

5. Bier, M., Ed.; "Theory, Methods, and Applications"; Academic Press: New York, 1967.

6. Fowkes, F.M., Disc. Faraday Soc., 1966, 42, 246.

7. Shaw, D.J.,"Electrophoresis"; Academic Press: New York, 1969.

8. Stern, D., Z. Elektrochm. Angew. Phys. Chem. 1924, 30, 508-516.

9. Hiemenz, P.C., "Principles of Colloid and Surface Chemistry", 2nd Edition, Marcel Dekker, Inc., New York, 1986.

10. Hirtzel, C.S.; Rajagopalan, R., "Colloidal Phenomena, Advanced Topics", Noyes Pub., Park Ridge, New Jersy, 1985.

11. Johnson, R.E.; Morrison, W.H., Adv. Ceramics, 21, 323(1987).

12. Kitahara, A., "Electrical Phenomena at Interfaces: Fundamentals, Measurements, and Applications" Kitahara, A.; Watanabe, A., (Eds.) Marcel Dekker, Inc., New York, 1984, P.119.

13. Fowkes, F.M.; Jinnai, H.; Mostafa, M.A.; Anderson, F.W.; Moore, R.J., "Colloid and Surfaces in Reprographic Technology", Hair, M.; Croucher, M., (Eds), ACS Symposium SERIES 200, 307(1981).

14. Novotny, V.J., "Colloids and Surfaces in Reprographic Technology", Hair, M; Croucher, M.D., (Eds), ACS Symposium SERIES 200, 1982, p 281.

15. Hückel, E., Physik. Z., 25, 204(1924).

16. DELSA Instrument Manual "Doppler Electrophorectic Light Scattering Analyzer"; Coulter Inc. 1988.

17. Ware, B.R.; Haas, D.D. "Fast Methods in Physical Biochemistry and Cell Biology" Shaafi, R.I.; Fernandez, S.M., (Eds), Elsevier, Amsterdam, p 173, 1983.

18. Goetz, P.J., United States Patent 4,154,669 May 15, 1979.

19. Goetz, P.J. "Automated Electrokinetic Analyzer"; Pen Kem Inc.

20. van Gils, G.E.; Kruyt, H.R., Kolloid Beil, 45, 60(1937).

21. Fowkes, F.M.; Chen, W.-J.; Fluck, D.J.; Hou, W., International Symposium on Surface Charge Characterization; The Twenty-First Meeting of the Fine Particle Society; 1990, p.14.

22. Huang, Y.C., Private Communication, Lehigh University, Bethlehem, PA.

23. Goetz, R., Ph.D. Dissertation, Lehigh University, October 1990.

24. van der Minne, J.L.; Hermanie, P.H., J. Colloids Sci. 1952, 7, 690.

25. Zettlemoyer, A.C., Micale, F.J., Preprints of 147th Meeting of the American Chemical Society, p.240 (April 1964).

26. Fowkes, F.M.; Chen, W.-J.; Fluck, D.J.; Johnson, R.E., "Comparison of Instrumentation for Electrophoretic Mobilities in Non-aqueous Media", ACS Book Abstracts, 195, 8-Coll.

27. Fairhurst, D., Private Communication, Pen Kem Inc., Bedford Hills, NY.

28. Marlow, B., Private Communication, Pen Kem Inc., Bedford Hills, NY.

29. Pohl, H.A.; "Dielectrophoresis"; Cambridge University Press: Cambridge, 1978.

30. Mann, R., Private Communication, Lehigh University, Bethlehem, PA.

31. Stutz, S., J. Colloid Interface Sci., 1978, 65, 118.

32. Israelachvilli, J.N., "Intermolecular and Surface Forces", Academic Press, New York, 1985.

33. Hamaker, H. C., Physica 1937, 4, 1068.

34. Kitahara, A., "Intermolecular Forces" John Wiley & Sons, New York (1976).

35. Lyklema, J., "Colloidal Dispersions" Goodwin, J.W. (Ed.), The Royal Society of Chemistry, London 1981.

36. Albers, W.; Overbeek, J. Th. G., J. Colloid Sci., 14, 510(1959).

37. Napper, D.H., J. Colloid Interface Sci., 58(2), 391, 1977.

38. Shaw, D. J., "Introduction to Colloid and Surface Chemistry", Butterworths, London, 1966, p. 211.

39. Pugh, R.J.; Matsunaga, T.; Fowkes, F.M., Colloids Surf., 1983, 7, 183.

40. Pecora, R. "Dynamic Light Scattering" Plenum, New York, 1985.

41. Coulter Instruments Inc. "N_4MD Instrument Manual" Hialeah, FL, 1987.

42. Provencher, S.W., Comp. Phys. Comm., 27, 213(1982).

43. Provencher, S.W., Comp. Phys. Commun., 27, 229(1982).

44. Fowkes, F.M.; "Surface and Colloid Science in Computer Technology" (Ed) Mittal, K.L. (Plenum Publishing Corporation (1987).

45. Fowkes, F.M., Adhesion and Adsorption of Polymers, Lee, L.-H. (Ed.) Part A, pp. 43-52, Plenum Press, New York (1980).

46. Lewis, G.N., "Valence and the structure of Atoms and Molecules", The Chemical Catalogue Co., New York, (1923) p.142.

47. Bockris, J.O'M.; Reddy, A.K.N., "Modern Electrochemistry", Plenum, New York, 1977, Vol. 1, p.414.

48. Fowkes, F.M.; Becher, D.Z.; Marmo, M.; Silebi, C.; Chao, C.C. "Micellazation, Solubilization, and Microemulsions" (Ed.) Mittal, K.L. (Plenum Press, NY 1977) II, 665-673.

49. Fowkes, F.M., "Solvent Propertiess of Surfactant Solutions" Ed. Shinoda, (Dekker, NY, 1967), 65-112.

50. Chen, W.-J., "Stabilization and Electrostatic Deposition of Aqueous and Non-aqueous Polymeric Colloids", Ph.D. Dissertation, Lehigh University, 1988.

51. Fowkes, F.M.; Fluck, D.J.; Lloyd, T.B., Confidential Company Report, Lehigh University, June 1987.

52. Cooper, W.D.; Wright, P., J. Chem. Soc. Faraday Trans. I, 70, 585(1974).

53. Kitahara, A.; Karasawa, S.; Yamada,H., J. Colloid Sci., 20 650 (1965).

54. Kitahara, A; Amano, M.; Kawasaki, S.; Kon-no, K., Colloid Polymer Sci., 255, 1118-1121(1977).

55. Joslin, S.T.; Fowkes, F.M., "Surface Acidity of Ferric Oxides Studied by Flow Microcalorimetry" IEC Prod R&D, 24, 369(1985).

56. Fowkes, F.M.; Jones, K.L.; Guozhen, L.; Lloyd, T.B., "Surface Chemistry of Coal by Flow Microcalorimetry" Energy & Fuels, 3, 97-105(1989).

57. Fowkes, F.M.; Huang, Y.C.; Shah, B.A.; Kulp, M.J.; Lloyd, T.B., Surface and Colloid Chemical Studies of Gamma Iron Oxides for Memory Media", Colloids Surfaces 29, 243-261(1988).

58. Fowkes, F.M., Rubber Chemistry Tech., 57(2), 1984.

59. Fluck, D.J.; Fowkes, F.M.; Lloyd, T.B., Confidential Company Report, 1988. (See author for authorization/information.)

60. Chen, W.-J.; Fluck, D.J., Unpublished Research, Lehigh University, December 1987.

61. Parkanyi-Berka, M.; Madi, I., Acta Chimica, Hungarica, 125(5) pp.695-703 (1988).

62. van Beelen, D.C.; Kruthof, K.J.H.; Mateboer, A., FATIPEC-Kongr., 1988, Vol. I, p.217-35.

63. Parfitt, G.D.; Willis, E., J. Colloid Interface Sci., 22, p.100-106 (1966).

64. Napper, D.H.; "Polymeric Stabilization of Colloidal Dispersions", Academic, New York, 1983.

65. Barrett, K.E.J., "Dispersion Polymerization In Organic Media", John Wiley & Sons, London, 1975.

66. Pugh, R.J.; Fowkes, F.M., Colloids Surf. 1084, 9, 33.

67. Gregory, J., Adv. Colloid Interface Sci., 1970, 2, 396.

68. Hamaker, H.C., Physica, 1937, 4, 1068.

69. Visser, J., Adv. Colloid Interface Sci., 3(1972) 331-363.

70. Parfitt, G.D.; Willis, E., J. Colloid Interface Sci.,22, 100-106(1966).

71. Fowkes, F.M.; Pugh, R.J., "Polymer Adsorption and Dispersion Stability", Goddard, E.D., Vincent, B. (Eds), ACS Symp. Ser. No. 240, pp.331-354(1984).

72. Casimir, H.B.G.; Polder, D. Phys. Rev., 73(1948), 360.

73. Overbeek, J. Th. G., "Colloid Science" Kruyt, H.R.(Ed), Vol. 1, Elsevier, Amsterdam, 1952, p.268.

74. Clayfield, E.J.; Lumb, E.C.; Mackey, P.H., J. Colloid Interface Sci., 1971, 37, 382.

75. Moelwyn-Hughs, E.A., "Physical Chemistry", 2nd ed., Pergamon, London, 1961, p.383.

76. Kauzmann, W., "Quantum Chemistry", Academic, New York, 1957, p.692.

77. Fowkes, F.M., Ind. Eng. Chem. 56,(12), 40(1964).

78. Deryagin, B. V., Landau, L. D., Acta Physico Chim USSR, 1941, 14, 633.

79. Klinkenburg, A., van der Minne, J. L., "Electrostatics in the Petroleum Industry", Elsevier, 1958, p.40.

80. Levine, I.N. "Physical Chemistry", 2nd Ed., New York, 1983.

81. Heller, W.; Pugh, T.L., J. Chem. Phys. 22, 1778(1954).

82. Napper, D.H., J. Colloid Interface Sci. 32, 106(1970).

83. Napper, D.H.; Hunter, R.J., MTP Int. Rev. Sci. Ser. 1, 7, 280(1972).

84. Napper, D.H., Trans Faraday Soc. 64, 1701(1964).

85. Evans, R.; Napper, D.H., J. Colloid Interface Sci. 52, 260(1975).

86. Evans, R.; Napper, D.H.; Ewald, A.J., J. Colloid Interface Sci. 51, 552(1975).

87. Elias, H-G.; Buhrer, I., "Polymer Handbook" (Brandup, J.; Immergut, E.H., Eds.) 2nd ed., p.IV-157. Wiley & Sons, New York, 1975.

88. Flory, P.J.; Krigbaum, W.R., J. Chem. Phys. 18, 1086(1950).

89. Jachel, K., Kolloid Z. Z. Polym. 197, 143(1964).

90. Fowkes, F.M.; Tischler, D.O.; Wolfe, J.A.; Lannigan, L.A.; Ademu-John, C.M.; Halliwell, M.J., J. Polym. Sci., Polym. Chem. Ed. 22, 547-566(1984).

91. Napper, D. H., Colloid Interface Sci., 1 (1977).

92. Napper, D. H., "Polymeric Stabilization of Colloidal Dispersions", (Ottevill, R. H., Rowell, R. L. eds.), Academic, New York 1983.

93. Tadros, T.F.; Krieger, "Industrial Rheology", Short Course, The Center for Professional Advancement, 144 Tices Lane, East Brunswick, NJ.

94. Fowkes, F.M., Private Communication, Lehigh University, 1989.

95. Smoluchowski, M., Z. Physik. Chem., Stoechiom. Verwandschaftsl. 1917, 92, 129-168.

96. Novich, B.E.; Ring, T.A., Clays & Clay Minerals, 32, 400(1984).

97. Barringer, E.A.; Novich, B.E.; Ring, T.A., J. Colloid Int. Sci. 100, 584(1984).

98. Chevron Environmental Health Center, Inc., P. O. Box 4054, Richmond, CA 94804-0054.

99. Fowkes, F.M.; Fluck, D.J.; Lloyd, T.B., Confidential Company Report, Lehigh University, 1987. (See author for authorization/information.)

100. Fowkes, F.M.; Dwight, D.W.; Lloyd, T.B.; Tischler, "Modification of Surface Acidity and Basicity of Glass Fillers", 40th Ann. Conf., Reinforced Plastics/Coposites Institute, Soc. Plastics Industry, 17E, 1-6(1985).

101. Chen, W.-J., "Stabilization and Electrostatic Deposition of Aqueous and Non-aqueous Polymeric Colloids", Ph.D. Dissertation, Lehigh University, 1988.

102. Pugh, R.J.; Matsunaga, T.; Fowkes, F.M., Colloids 7, 183, (1983).

103. Wiersema, P.H.; Loeb, A.L.; Overbeek, J.Th.G., J. Colloid Interface Sci., 22, 78(1966).

104. Chen, W.J., Personal Communication, Lehigh University, 1986.

105. Fowkes, F.M., Personal Communication, Lehigh University, 1986.

106. Fowkes, F.M., Fluck, D.J.; Lloyd, T.B., Confidential Company Report, Lehigh University, 1987. (See author for authorization/information.)

107. Fowkes, F.M., Private Communication, Lehigh University, Bethlehem, PA., 1989.

108. Rosen, M.J., "Surfactant and Interfacial Phenomena", John Wiley & Sons, New York 1978.

109. Pugh, R.J.; Fowkes, F.M., Colloids Surfaces 9, 33(1984).

110. Huang, Y.C.; Fowkes, F.M.; Lloyd, T.B., J. Adhesion Sci. Technol. 5(1), 1991, 39.

111. Huang, Y.C., Ph.D Dissertation, Lehigh University, June 1991.

112. Riddle, F.L.; Fowkes, F.M., J. Am. Chem. Soc., 112(9), 3259, 1988.

113. Dwight, D.W., Private Communication, Lehigh University, Bethlehem, PA, 1989.

114. Perkin-Elmer, Analytical Laboratory, Edison, NJ, 1989.

115. Miller, Alfred, Private Communication, Lehigh University, 1993.

116. Huang, Y.C.; Fowkes, F.M.; Lloyd, T.B.; Sanders,N.D., The proceedings of the 1991 TAPPI Coating Conference in Montreal, May 19th-22, 1991 page 123.

117. Klinkenberg, A. J. van der Minne, J. L., "Electrostatics in The Petroeum Industry", Elsevier, 1958, p. 40.

118. Vold, M.J., J. Colloid Sci. 16, 1(1961).

119. McCarthy, D.C., "Ph.D. Dissertation", Lehigh University, Bethlehem, PA.

120. Fowkes, F. M., Private Communication, Lehigh University, Bethlehem, PA., 1990.

121. Chen, W-J., Private Communication, Lehigh University, Bethlehem, PA, 1988.

VITA

David James Fluck was born in Abington, Pennsylvania on May 3, 1960. He was the fourth child of the late Ronald O. and Ethel K. Fluck. He was raised in Perkasie, Pennsylvania and graduated from Pennridge High School in 1978. From 1979 to 1981 he attended Bucks County Community College. In 1983 he graduated from Delaware Valley College of Science and Agriculture with a Bachelor of Science in Chemistry. He earned a Masters of Science degree in Chemistry from Villanova University in 1987. In 1986 he entered the Ph.D. program of the Department of Chemistry at Lehigh University, working under the direction of Dr. Frederick M. Fowkes. He joined Cabot Corporation, Cab-O-Sil Division at the Tuscola, Illinois Technical Center in May of 1992.